2020

Electric field control of fixed magnetic Skyrmions for energy efficient nanomagnetic memory

Dhritiman Bhattacharya

Electric field control of fixed magnetic Skyrmions for energy efficient nanomagnetic memory

A Dissertation submitted in partial fulfillment of the requirements for the degree of Doctor of Philosophy in Engineering at Virginia Commonwealth University.

by

Dhritiman Bhattacharya

Bachelor of Science, Electrical and Electronic Engineering,

Bangladesh University of Engineering and Technology, 2013

Advisor: Jayasimha Atulasimha, Ph.D.

Professor, Department of Mechanical and Nuclear Engineering

Virginia Commonwealth University

Richmond, Virginia

August 2020

This dissertation is dedicated to my parents and my sister for their love and support.

Abstract

To meet the ever-growing demand of faster and smaller computers, increasing number of transistors are needed in the same chip area. Unfortunately, Silicon based transistors have almost reached their miniaturization limits mainly due to excessive heat generation. Nanomagnetic devices are one of the most promising alternatives of CMOS. In nanomagnetic devices, electron spin, instead of charge, is the information carrier. Hence, these devices are non-volatile: information can be stored in these devices without needing any external power which could enable computing architectures beyond traditional von-Neumann computing. Additionally, these devices are also expected to be more energy efficient than CMOS devices as their operation does not involve translation of charge across the device. However, the energy dissipated in the clocking circuitry negates this perceived advantage and in practice CMOS devices still consume three orders of magnitudes less energy.

Therefore, researchers have been looking for nanomagnetic devices that could be energy efficient in addition to being non-volatile which has led to the exploration of several switching strategies. Among those, electric field induced switching has proved to be a promising route towards scalable ultra-low power computing devices. Particularly Voltage Control of Magnetic Anisotropy (VCMA) based switching dissipates ~1 fJ energy. However, incoherence due to thermal noise and material inhomogeneity renders this switching error-prone. This dissertation is devoted towards studying VCMA induced switching of a spin spiral magnetic state, magnetic skyrmions, which can potentially alleviate this issue.

Magnetic skyrmions has recently emerged as a viable candidate to be used in room temperature nanomagnetic devices. Most of the studies propose to utilize skyrmion motion in a magnetic track to implement memory devices. However, Magnetic Tunnel Junction (MTJ) devices based on skyrmions that are fixed in space might be advantageous in terms of footprint. To establish a new computing paradigm based on electrical manipulation of magnetization of fixed magnetic skyrmions we have studied:

i) Purely VCMA induced reversal of magnetic skyrmions using extensive micromagnetic simulations. This shows sequential increase and decrease of Perpendicular Magnetic Anisotropy (PMA) can result into toggling between skyrmionic and ferromagnetic states. We also demonstrate VCMA assisted Spin Transfer Torque (STT) induced reversal of magnetic skyrmions.

ii) Complete reversal of ferromagnets mediated by intermediated skyrmion state using rigorous micromagnetic simulation. We show that the switching can be robust by limiting the "phase space" of the magnetization dynamics through a controlled skyrmion state. Thus, the switching error can be lowered compared to conventional VCMA switching.

iii) Finally, we perform preliminary experiments on VCMA induced manipulation of skyrmions. We demonstrate that skyrmions can be annihilated when Perpendicular Magnetic Anisotropy of the system is increased by applying a negative voltage pulse and can be recreated by decreasing PMA by applying a positive voltage pulse. The experimental observations are corroborated using micromagnetic simulation.

Future research should focus on demonstrating reversal of skyrmions experimentally in MTJ like devices and study the downscaling of the proposed device. These can enable realization of energy efficient and robust nanomagnetic memory devices based on voltage control switching of fixed magnetic skyrmions as wells as other neuromorphic computing devices.

Acknowledgement

I would like to take this opportunity to express my sincere gratitude to my supervisor, Dr. Jayasimha Atulasimha. His expertise in different areas of spintronics and nanomagnetism has provided me the opportunity to learn and conduct research in several intriguing directions. He taught me valuable lessons towards being a successful researcher from the very basics of conducting a research project to writing grant proposals to funding agencies. Beyond research, he also supported me in difficult times during my early years at VCU for which I will be ever grateful to him.

I would like to extend my gratitude to the members of my dissertation committee, Dr. Ravi Hadimani, Dr. Hooman Tafreshi, Dr. Shiv Khanna and Dr. Supriyo Bandyopadhyay, who have given their valuable time to evaluate my research work and offered their critiques and advice along the way. Special thanks to Dr. Bandyopadhyay with whom I had the opportunity to work on several research projects. I would also like to thank my colleagues at Dr. Bandyopadhyay's lab, specially Dr. Ahsanul Abeed for the valuable discussions.

It was a pleasure sharing the last couple of years with my peers at the M3 lab who have extended their assistance and shared their knowledge with me at various times. I also offer my gratitude to scientists and staffs at Nano Characterization Center (NCC) and Virginia Microelectronics Center (VMC) for their help on my experiments; specially to Dr. Dmitry Pestov and Dr. Gary Atkinson for their valuable advice. I would like to thank my collaborators Dr. Caroline Ross, Dr. Damien Querlioz, Dr. Kang Wang and Seyed Armin Razavi. I am thankful for the academic and financial support provided by VCU College of Engineering and US National Science Foundation.

Finally, thanks to my mother Nilima Bhattacharya, my sister Debarati Bhattacharya, my nephew Srayash Talukder, my brother-in-law Surajit Talukder and my friends for their unconditional love and support throughout this endeavor. Thanks to my partner Jawata Afnan for her encouragement.

Table of Contents

List of Figures

List of Tables

Chapter 1: Introduction

Nanomagnetic devices have been investigated for their potential to replace CMOS based Random Access Memory and more recently envisioned to be utilized in neuromorphic computing application. This chapter begins with an overview of different nanomagnetic memory devices (1.1), followed by an overview of recent developments in one specific area of potential interest: magnetic skyrmions (1.2). Thereafter, we highlight the novelty and benefits of using fixed skyrmions and skyrmion mediated switching of perpendicular nanomagnets to implement memory devices (1.3).

1.1 Overview of nanomagnetic memory

The rapid development of computing technology was initiated by the invention of transistors in 1947. Since then, continuous miniaturization of transistors has paved way for revolutionizing the electronics industry. Numerous portable, handheld and implantable medical devices were enabled by accommodating increasing number of transistors in the same area of an electronic chip. This trend was envisioned by Gordon Moore, a co-founder of Intel Corporation, in the 1960's. He predicted that the number of transistors in a chip will continue to double in roughly every 18 months [1]. Unfortunately, this trend is now unlikely to continue. The amount of heat generated in a given area in a chip is likely to become unmanageable by current heat-sinking technology, if CMOS devices are further downscaled. Therefore, excessive heat generation is the primary threat to continued miniaturization of computing devices in accordance with Moore's law. To overcome this problem, many alternative low power computing strategies have been proposed.

Nanomagnet-based computing is an attractive alternative to traditional transistor-based electronics. A typical nanomagnetic device is usually based on Magnetic Tunnel Junctions (MTJs) as shown in *Figure 1-1*. An MTJ primarily consists of a free layer, a fixed layer and a tunnel barrier. There can be other layers such as synthetic antiferromagnetic layer, capping layer which are not shown in *Figure 1-1* for simplicity. To encode binary bits, the magnetization orientation of the free layer is switched between two stable magnetization orientations. The resistance of the MTJ is dependent on the relative angle between the free

and the fixed layer. This is called tunnel magnetoresistance or TMR [2-4]. Therefore, when the magnetization state of the free layer reverses, a change in resistance occurs as shown in *Figure 1-1* (b). To perform readout operation, a small current is passed through the MTJ and the voltage is indicative of whether the final magnetization state is parallel or antiparallel to the fixed layer.

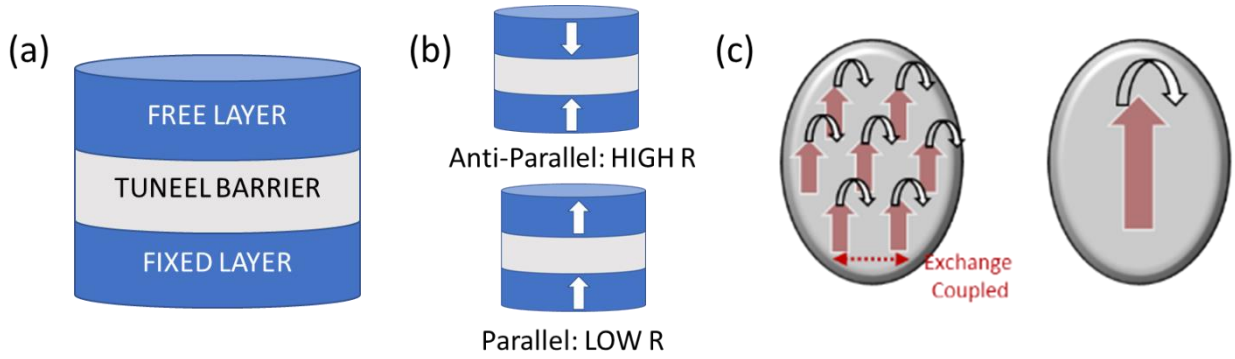

Figure 1-1 (a) Simplified sketch of a Magnetic Tunnel Junction (b) Parallel and anti-parallel states of MTJ which corresponds to high and low resistance states, (c) Equivalency between collective rotation of an ensemble of spins and rotation of a giant spin.

On the other hand, a transistor encodes two logic states or binary bits by the presence or absence of electrons in its channel. If N is the number of electrons in the transistor and p is the bit error probability (the probability that the bit being written in the transistor is the wrong bit), then the minimum energy dissipated in switching a transistor to write a bit at a temperature T is $Nk_BTln(1/p)$ [5,6]. As two different spin orientations encode the binary bit, information carriers in nanomagnetic switches are electrons spins rather than electron charge. While switching between bits, the spins can rotate together in unison due to exchange interaction [7]. This collective rotation of spins is equivalent to a giant spin rotating (*Figure 1-1* (c)). Therefore, in an ideal case, the minimum energy dissipated in a switching operation of a single domain nanomagnet is $\sim k_BTln(1/p)$ [6]. Hence, for the same bit error probability, a nanomagnetic switch should be N times more energy efficient compared to a transistor.

Although nanomagnetic computing appears to be highly energy efficient, the energy dissipated in the clock (the electrical signal that causes the nanomagnet's magnetization to switch) negates this perceived advantage. However, being "non-volatile" in nature is perhaps a more advantageous property of a

nanomagnet. To retain information in charge-based transistors, continuous refresh cycles are needed. Otherwise, charges leak, and the information is lost. Therefore, the information is "volatile". On the other hand, nanomagnets have an energy barrier that separates the two bistable states (easy axes of magnetization) which prevents it from flipping spontaneously to an undesired state. Therefore, information stored in the magnetization state of a nanomagnet does not leak.

An exemplary potential energy landscape is shown in *Figure 1-2* (b) where the two stable magnetization states are separated by an energy barrier E_b. The height of this energy barrier determines the stability of the nanomagnet. While subjected to thermal noise, the spins may overcome the energy barrier and flip to the other energy minima. Mean time between flips can be quantified as $\tau = \tau_a e^{E_b/k_B T}$, where τ_a is the inverse attempt frequency and k_B is the Boltzmann's constant [8]. By making the energy barrier $E_b \sim 60\ k_B T$ at room temperature by appropriately choosing the material, shape and volume, the bit encoded in either stable direction can be retained for $\tau \sim 3.62\times10^7$ years without being refreshed (i.e. when the device is switched off), considering $\tau_a = 1\times10^{-12}$ [9].

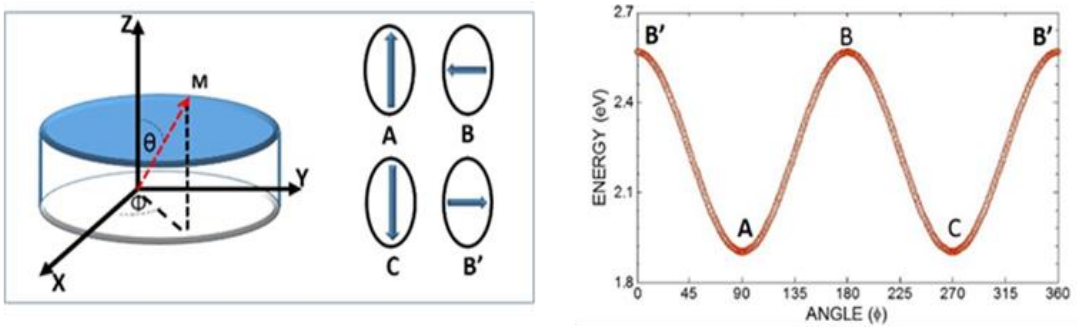

Figure 1-2 The magnetization vector and four different states A, B, C and B' defined by the magnetization orientation in a nanomagnet shaped like an elliptical disk. (b) Energy profile of a shape anisotropic nanomagnet (shaped like an elliptical disk) plotted as a function of the azimuthal angle. Reprinted with permission from [59], Copyright (2017), Institute of Physics.

Furthermore, non-volatility allows a switch to store the computed bit internally without having to store it in a remote memory device. Such a switch can perform both logic and memory functions at the same time thus eliminating the need for external memory. Novel computer architectures can be designed based on this unique property of nanomagnets such as non-von-Neumann type architectures where there is no physical partition between the processor and the memory [10, 11]. Nanomagnetic devices also has potential to be

used as the basis of neuromorphic computing [12]. Neuromorphic computing devices mimic the functionality of human brain: synapse and neurons. This type of computing can be advantageous in performing certain tasks such as pattern recognition, which are otherwise difficult to perform using Boolean algorithm.

These abovementioned advantages spurred investigations to stabilize and control magnetization in nanomagnetic memory devices. In Subsection 1.1.1, we will discuss two broad classes of nanomagnetic devices: single domain and domain wall based. In the next subsection, we will present different ways of controlling the magnetization of these nanomagnets.

1.1.1 Single domain and domain wall devices

Single domain devices: Single domain nanomagnetic devices have stable magnetization state where all the spins are oriented in the same direction. The magnetization direction is switched between two such states to encode binary bits. To achieve bistability, the free layer of an MTJ can be implemented using shape anisotropic elliptical nanomagnets or perpendicularly polarized nanomagnets. In elliptical nanomagnets, to minimize the demagnetization energy, the preferred magnetization direction or the easy axis coincide with the major axis of the ellipse (*Figure 1-3* a). On the other hand, easy magnetization direction is along ±z directions in perpendicularly polarized nanomagnets (*Figure 1-3* b).

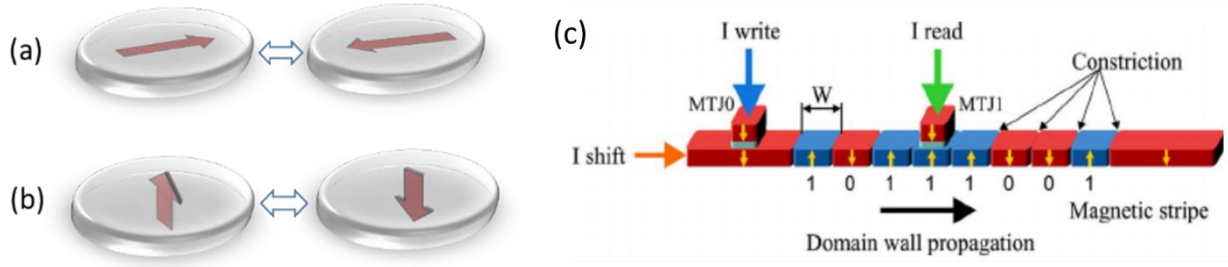

Figure 1-3 (a) Shape anisotropic elliptical nanomagnets, (b) Perpendicularly polarized nanomagnets, (c) Domain wall racetrack devices. Reprinted with permission from [16], Copyright (2012), IEEE.

The energy barrier between two bistable states is therefore determined by the lateral shape of the nanomagnet. This shape energy barrier $E_{shape} = \mu_o (Ms^2/2) \times (N_x \sin^2\theta \cos^2\varphi + N_y \sin^2\theta \sin^2\varphi + N_z \cos^2\theta) \times$ volume. Here, φ is the azimuthal angle and θ is the polar angle (see *Figure 1-2*). N_x, N_y, and N_z are

demagnetization factors which depend on the aspect ratio of the magnet. If the thickness<<lateral dimensions, $N_z \approx 1$. This forces $\theta \approx 90°$, or in other words, forces the magnetization to be in plane. The more elliptical a magnet is, the larger the barrier between two bistable states. To scale below 20 nm, small lithographic variation (typically 1-2 nm laterally) may degrade the stability significantly.

This issue can be addressed by using nanomagnets with easy magnetization direction perpendicular to plane easy axis. When a ferromagnetic layer is interfaced with a suitable material, surface anisotropy may exist. The surface anisotropy energy is given by $E_{surface} = -(k_{surf}/t) \times \cos^2\theta \times$volume. Here k_{surf} is surface anisotropy energy density per unit area and t is the thickness. In a circular thin magnet, $N_z \approx 1$ and $N_x = N_y \approx 0$. Therefore $E_{shape} = (\mu_o Ms^2/2) \times \cos^2\theta \times$ volume. If $k_{surf}/t > \mu_o Ms^2/2$, magnetization prefers $\theta=0°$ direction and points perpendicularly out of plane. In this case, two bistable states are ±z directions and therefore stability is not affected by lateral lithographic variation and scaling to smaller dimension becomes feasible. Due to scalability, perpendicular nanomagnets are now preferred for implementing nanomagnetic memory.

Domain wall based devices: In small nanomagnets, short-range exchange energy dominates, and uniform magnetic states are preferred. In larger nanomagnets, however, to minimize demagnetization energy, vortex states or multiple domain states are more prevalent. A domain wall separates two oppositely polarized magnetic domains. These domain walls can be moved by applying a current. Utilizing this phenomenon, domain wall based racetrack memory devices can be implemented [13, 14]. A domain wall racetrack device is shown in *Figure 1-3*c. In these devices, a train of domain walls in a magnetic nanowire represent the bits to write. MTJs are placed in several locations of the nanowire to readout the states. For speedy operation of racetrack devices, domain walls need to move rapidly. In this regard, extensive research has been performed [15, 16, 17] and domain walls in certain materials can be moved at ~1000 m/s [18]. Domain wall movement in a nanowire is also useful to implement neuromorphic devices [12].

However, domain wall easily gets pinned due to edge roughness and defects in the nanowire. This poses a challenge in controlling the position of the domain wall, which is a primary requirement for reliable

operation of racetrack memory devices. Recently, a new magnetic structure called skyrmion has shown the potential to efficiently implement racetrack like devices. These magnetic structures can easily be depinned from defects due to their special spin structure. Details of magnetic skyrmions and their potential use as nanomagnetic devices will be discussed later.

1.1.2 Methods of manipulating the magnetization in nanomagnetic devices

The potential of nanomagnetic devices has led to the investigation of several strategies to control magnetization. The very first and the most obvious is the use of electric current-generated magnetic field [19]. In hard drives, magnetic bits are still written using localized magnetic field. However, generating magnetic field is energetically costly. There are other techniques to manipulate magnetization which can be broadly divided into two categories: (i) spin current controlled, (ii) electric field controlled. We will discuss some prominent technics that are relevant to this thesis.

Spin Transfer Torque (STT): Electrical current usually carries same number of electrons with spin up and spin down orientation. The spins of the electrons carrying the current can be polarized. To distinguish between these two, we call the former charge current and the latter spin current. When spin current is passed through a nanomagnet, spin polarized electrons transfer their spin angular momentum to the spins of the nanomagnet [20-25]. This induces a torque, called spin transfer torque (STT), on the nanomagnet's magnetization. This STT can be utilized to switch a nanomagnet's magnetization to a desired orientation.

The switching mechanism is shown in *Figure 1-4*. While passing through the fixed layer, electrons get polarized parallel to the fixed layer's magnetization (*Figure 1-4*, Left). In other words, the fixed layer acts as the spin polarizer and injects spin polarized current into the free layer. The polarized spins transfer their momenta to the electrons in the free layer and ultimately align the spins along the fixed layer's magnetization direction. Thus, the magnetization direction of the free layer become parallel to the fixed layer. To align the magnetization directions antiparallel to each other, the polarity of the current direction is reversed. In this case, the free layer injects electrons into the fixed layer. Spins that are parallel to the fixed layer's magnetization gets preferentially transmitted by the fixed layer (*Figure 1-4*, Right).

Ultimately, spins that are antiparallel to the fixed layer's magnetization become majority spins in the free layer population as spins that are parallel to the fixed layer's magnetization deplete over the time. Hence, magnetization antiparallel to that of the fixed layer's magnetization is stabilized in the free layer.

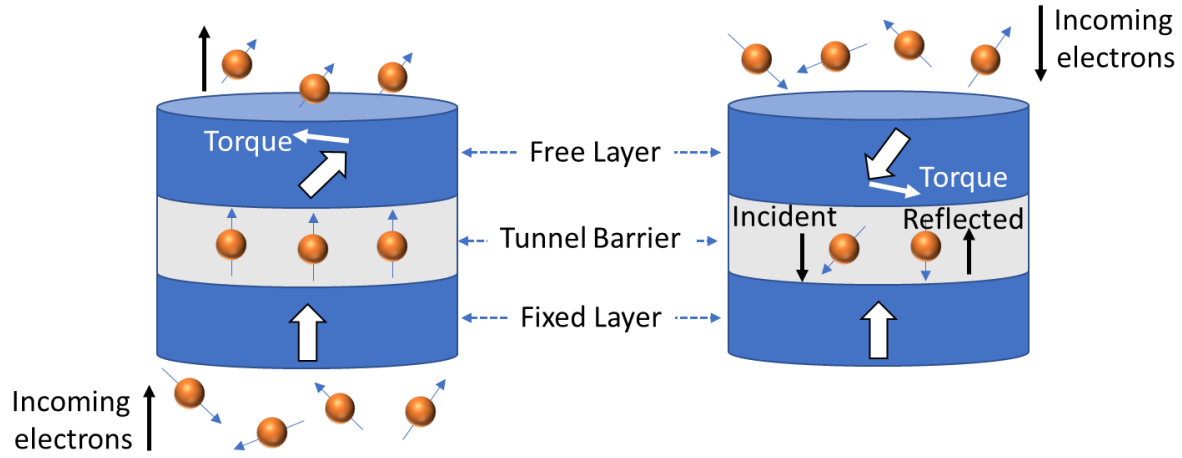

Figure 1-4 Mechanism of Spin Transfer Torque induced switching of the free layer. Left: Parallel to the fixed layer, Right: Antiparallel to the fixed layer

Following the above-mentioned strategy, one can write either bit 0 or bit 1 into the memory selectively by choosing the current direction. Switching of 11 nm MTJ structures has been demonstrated with write error as low as 10^{-10} [26]. However, STT induced switching is not particularly energy-efficient due to unavoidable I^2R loss. Energy dissipation was shown to be 100 fJ for 10 ns switching time in ref. [26] which is three orders of magnitude higher than CMOS based switching [27].

Spin Hall Effect (SHE): Spin hall effect is an alternative way to generate spin current which can reduce energy dissipation in switching a nanomagnet compared to STT induced switching [28-31]. When a charge current is injected in a thin slab of material with high spin orbit interaction, the electrons experience spin-dependent scattering. As a result, oppositely polarized spins populate the top and bottom edge of the material. This is shown in *Figure 1-5*. A charge current is injected in the y-direction and consequently +x-polarized spins are deflected to the bottom edge of the slab while –x-polarized spins are deflected to the top edge. If a ferromagnetic layer or an MTJ is delineated on top the slab, the spins diffuse into it, which results in a spin current. This spin current produces a torque that can ultimately rotate the magnetization of the

ferromagnet or the free layer of the MTJ. For the case shown in *Figure 1-5*, the magnetization of the soft layer will turn to the –x direction. For switching the magnetization of the soft layer to the +x-direction, simply reversing the polarity of the charge current (i.e. reversing the spin orientations at the two edges) is enough.

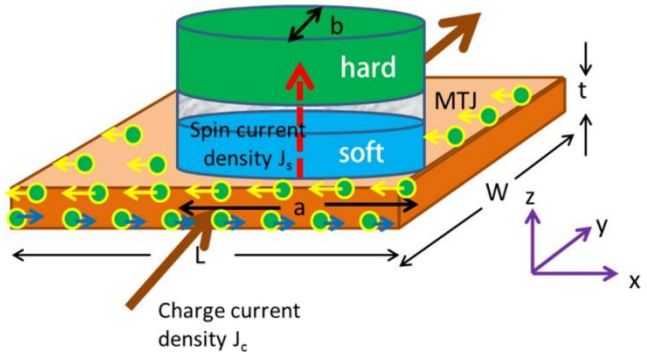

Figure 1-5 Spin Hall effect induced switching, Reprinted with permission from [58], Copyright (2018), Institute of Physics.

SHE based switching is much more energy efficient compared to the STT based switching. The energy consumption has been shown to be ~1 fJ experimentally and can be further reduced by scaling the device geometry [31]. Another important parameter related to the efficiency of SHE based switching is spin current to charge current ratio (J_s/J_c), called spin hall angle. Recent studies focus on improving this parameter to make this approach more energy efficient [32, 33]. SHE based switching faces a problem in reversing a perpendicular magnet as the spin current can drive the magnetization to one of the in-plane directions. Therefore, without any external bias, deterministic switching is not feasible. Exchange bias magnets [34], switching in conjunction with STT [35] can be employed to alleviate this problem to some extent. Three terminal device structure of SHE based devices may also lead to larger footprint. In conclusion, further optimization in design strategy and improved spin hall angle are required to enable energy efficient SHE based devices with deterministic switching.

Voltage control of magnetic anisotropy (VCMA): Perpendicular anisotropy originates at a ferromagnet/oxide interface from the overlap between oxygen's p_z and ferromagnet's hybridized d_{xz} orbital [37]. Therefore, when the electron density at the interface is altered by employing a voltage pulse the perpendicular anisotropy present in the system consequently changes [38, 39]. This is shown in *Figure 1-6*(a). The change in perpendicular anisotropy is expressed through a linear relationship of the form, ΔPMA

= a E/t_{free}, where a is the so-called VCMA coefficient, E is the applied electric field. VCMA co-efficient is expressed as $a = \frac{\Delta PMA \times t_{free}}{\Delta V / t_{spacer}}$. If an applied voltage increases PMA, then the easy axis will become perpendicular to the nanomagnet's plane. On the other hand, if opposite polarity voltage is applied, all in-plane directions would be equally probable for a circular nanomagnet. Voltage control of magnetic anisotropy and its effect on magnetization have been demonstrated in several interfaces experimentally over the last decade such as FeCo/MgO, CoFeB/MgO, Fe/MgO etc [40-47]. It has been shown that VCMA induced magnetization switching can be accomplished in 1 ns with ~6 fJ energy dissipation [48].

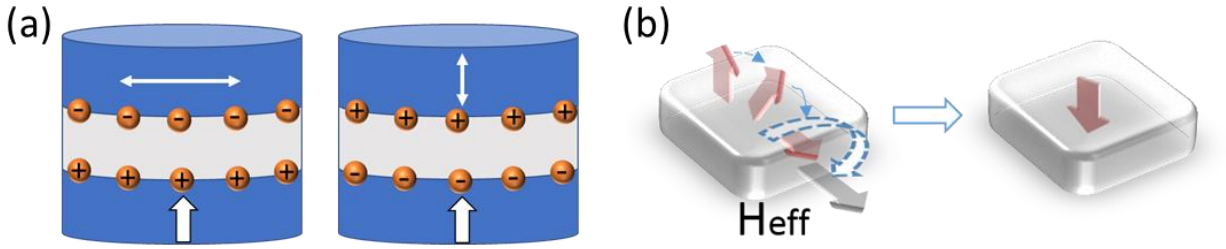

Figure 1-6 (a) Change of electron density and consequently PMA, (b) Mechanism of VCMA induced switching

If we start form a perpendicular state, application of a voltage pulse that reduces PMA results in magnetization rotation towards the in-plane direction. When the voltage pulse is withdrawn, the magnetization has an equal probability of ultimately settling in any of the two bistable perpendicular orientations. However, deterministic and complete 180° magnetization reversal is desired to induce a high magnetoresistance change as well as to ensure nonvolatile operation. An in-plane magnetic field is utilized to achieve this. Upon application of a voltage pulse, the magnetization rotates to the planar orientation while also precessing about the magnetic field (*Figure 1-6* (b)). Complete reversal can be achieved by designing the magnetic field strength and the voltage pulse duration appropriately. The VCMA voltage pulse duration is adjusted to approximately one-half of the precession period, which means that the voltage is withdrawn when the magnetization vector approaches the opposite normal-to-plane orientation (180° rotation). Since the normal-to-plane orientation coincides with the easy axis in the absence of the voltage, the magnetization will settle into this orientation at the end of the voltage pulse, completing the 180° rotation [49].

Unfortunately, this mode of switching is not very reliable at room temperature. In the presence of thermal noise and material inhomogeneity, the speed at which the magnetization precess around the magnetic field vary, which leads to switching error. Furthermore, the external in-plane bias magnetic field required in this switching mechanism is undesirable to incorporate on a chip.

VCMA co-efficient: To beat an energy barrier of 40 k_BT or 1 eV in a 45 nm diameter circular nanodisk of 1 nm thickness (i.e. volume=1.59×10^{-25} m^3), required change in PMA energy density ΔPMA = 40k_BT/ Volume = 1×10^5 J/m^3. This translates into VCMA co-efficient required $a = \frac{\Delta PMA \times t_{free}}{E}$= 100 μJ/$m^2$ per V/nm considering E=1 V/nm (MgO breakdown field 1-2 V/nm). Typically, experimentally measured VCMA co-efficient is in the range of 30-100 μJ/m^2 per V/nm [40-46]. However, if the device is scaled down to 20 nm diameter, required value of VCMA co-efficient goes up to 500 μJ/m^2 which is higher than that observed in those experiments. Therefore, improvement in VCMA co-efficient is needed for scaling. Recent theoretical studies show that the VCMA co-efficient can be 1800 μJ/m^2 per V/nm in Au/FeCo/MgO heterostructures [50].

Magnetoelastic switching: When a material is subjected to a mechanical stress, the magnetization of the material reorients itself. This is also called the Villari effect or inverse magnetostriction [51]. The magnetoelastic energy produced by stress $E = -3/2\ \lambda_s \sigma cos^2\theta$. uniaxial stress σ acting upon a magnetization that subtends an angle ($\theta°$) with the stress's direction, and λ_s is the saturation magnetostriction. Strain induced switching of nanomagnets and magnetoelectric memory have been studied both theoretically and experimentally [36, 52-60].

To implement a magnetoelastic or straintronic memory device, a nanomagnet is deposited on top of a piezoelectric layer (*Figure 1-7*a). If the nanomagnet is a shape anisotropic elliptical nanomagnet, initially the magnetization points along one of the major axes (state A or state C). When an electric field is applied, the energy landscape alters due to the magnetoelastic energy. If a uniaxial compressive (tensile) stress along the major axis for a magnet with positive (negative) magnetostriction (λs) is applied, the magnetization

rotates away from the major axis toward the minor axis. The magnetization rotates completely to the minor axis if this magnetoelastic energy or stress anisotropy energy exceeds the shape anisotropy barrier. The energy landscape for such a scenario is drawn in *Figure 1-7* (b). Clearly, the easy axis of magnetization (the magnetization orientation that corresponds to the energy minimum) is along the minor axis of the ellipse (state B or state B') in the stressed state. The maximum possible rotation that can be induced in magnetostrictive nanomagnets by strain is thus 90°.

When the stress is released, the magnetization can rotate from the minor axis toward either of the stable states along the major axis with 50% probability. This scenario is similar to SHE or VCMA induced switching. To achieve a complete 180° magnetization rotation (switching the magnetization from one orientation along the major axis to the antiparallel orientation along the major axis), precisely timed application and withdrawal of stress [58], dipole coupling with a neighboring nanomagnet [57], or sequential application of stress along different directions (with the aid of carefully designed electrode configuration) [60] can be employed.

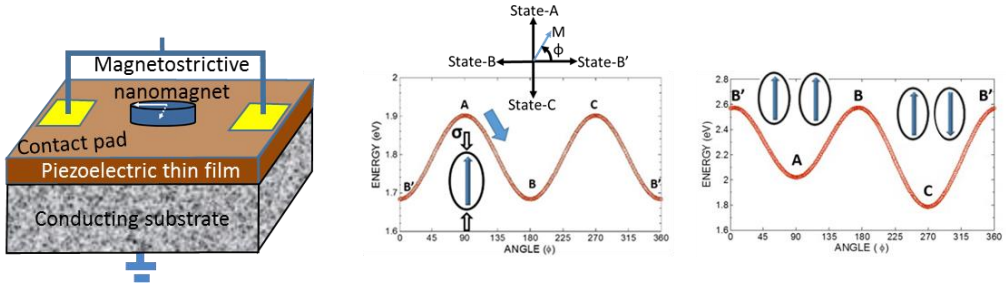

Figure 1-7 (a) Schematic of a straintronic switching device, (b) modified energy profile plotted as a function of the azimuthal angle with uniaxial compressive stress along the major axis for a magnet with positive magnetostriction (the same would be true for uniaxial tensile stress along the major axis for a magnet with negative magnetostriction), (c) introduction of asymmetry in the energy landscape due to dipole coupling plotted as a function of the azimuthal angle. Reprinted with permission from [59], Copyright (2017), Institute of Physics.

Another class of magnetoelastic memory uses surface acoustic wave to control magnetization. In these devices, alternative tensile and compressive stress cycle acts on the magnetization to reorient it. SAW induced magnetization rotation in thin films and nanomagnets have been demonstrated experimentally [61-65]. High frequency SAW can trigger ferromagnetic resonance [66-67]. These resonant dynamics can assist spin torque-based switching and reduce energy consumption [68-69].

1.2 Overview of Magnetic Skyrmions

Various competing interaction exists in a ferromagnetic material that lead to stabilization of a variety of magnetization orientation in a nanomagnet such as domain wall, vortices and perpendicular/in-plane uniform magnetization state. In previous sections, we have discussed single domain and domain wall based devices and several strategies to manipulate magnetization to implement such devices. Recently, Dzyaloshinskii-Moriya Interaction (DMI) has been extensively studied due to its ability to stabilize interesting magnetic states such as magnetic skyrmions. In this section, we will introduce skyrmions (1.2.1), discuss stabilization (1.2.2) and motion (1.2.3) of these magnetic objects.

1.2.1 Introduction to magnetic skyrmions

Dzyaloshinskii-Moriya Interaction (DMI) exists in inversion symmetry broken systems such as non-centrosymmetric bulk ferromagnetic materials or at the interface of a ferromagnet with a material with high spin orbit coupling [70,71]. It was first described by Dzyaloshinskii to explain weak ferromagnetism [70] while Moriya discovered its connection to spin orbit coupling [71]. DMI energy between two spins is given by $E_{DMI} = \vec{D}_{ij}.(\vec{S}_i \times \vec{S}_j)$. Hence, this interaction favors a perpendicular orientation between neighboring spins. The direction of DMI vector depends on the nature of asymmetry. *Figure 1-8* shows the direction of DMI vector for bulk and interfacial DMI. While it is parallel to the line joining the atomic sites in the bulk case, the direction is perpendicular in the interfacial case. Thus, the nature of chirality becomes different. First principle calculation shows that, DMI in a Heavy Metal/Ferromagnet system can be as large as 12 mJ/m^2 [54]. Moreover, Ferromagnet/Oxide interface can significantly contribute to enhance the total DMI. In Co/Pt/MgO structures, 1.6 times increment of DMI value over Co/Pt/Vacuum is observed in experiments (2.1 mJ/m^2 vs 1.5 mJ/m^2) [55] and confirmed via first principles calculations (8 mJ/m^2 vs 5 mJ/m^2) [56]. DMI value was experimentally measured to be 2.1 mJ/m^2 in Pt/CoFe/MgO [57].

On the other hand, exchange interaction energy between two spins is given by $E = -J(\vec{S}_i.\vec{S}_j)$. Therefore, depending on the sign of the exchange stiffness, neighboring spins preferentially align parallelly or anti-parallelly in a ferromagnetic system. Due to competition between exchange interaction and DMI canting between two spins can emerge. Ultimately, this can arrange the overall magnetic structure in different spiral orientations. Magnetic skyrmion is specifically important among these spiral states due to its potential application and non-trivial topology.

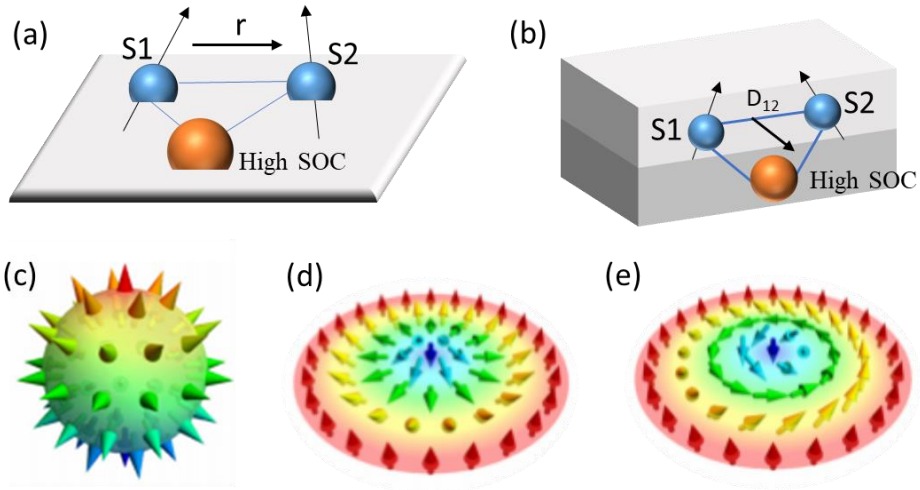

Figure 1-8 (a) Bulk DMI, (b) Interfacial DMI, (c) Neel skyrmion wrapped around a sphere, (d) Stereographic projection of (c), (e) a Bloch skyrmion. (c-e) Reprinted with permission from [76], Copyright (2018), American Physical Society.

Skyrmions were first described by particle physicist Tony Skyrme to describe elementary particles [72]. In magnetic systems, such a state was predicted theoretically in thin films and multilayers [73, 74]. The spins in the center of a magnetic skyrmion is opposite to the spins at the periphery. Depending on how the spins rotate from z=+1 at the center to z=-1 at the periphery, skyrmions can be classified into two types namely Bloch and Neel skyrmions. These are shown in *Figure 1-8* (c-e). Stabilization of Bloch vs Neel skyrmion depends on the direction of the DMI vector. If DMI vector is perpendicular to the vector that joins the two spin sites, Neel skyrmions are formed. On the other hand, if these vectors are parallel to each other Bloch skyrmions form. In bulk system, DMI vector direction prefers Bloch skyrmions while interface driven DMI prefers Neel skyrmions. The handedness of the chirality originates from the sign of the DMI vector.

The specialty of skyrmion lies in its unique topology which can be described in terms of skyrmion number or topological number which is given as $S = \frac{1}{4\pi}\int dx\, dy\, m.(\partial_x m \times \partial_y m)$. This gives us the number of times a skyrmion can be wrapped around a unit sphere. Converting to spherical co-ordinates, one can show, $S = \frac{1}{4\pi}\int_0^{\pi} \sin(\theta)\, d\theta \int_0^{2\pi} d\emptyset = \frac{-1}{4\pi}[cos\theta]_0^{\pi}\,[\emptyset]_0^{2\pi} = 1$ considering spins at the center pointing in the +z direction and spins at the boundary pointing in the -z direction [75]. We note that, in a mathematical system, transformation between two topologically distinct system is prohibited. However, unlike a continuous mathematical object, a magnetic system is discrete due to spins residing at different atomic lattice point. Therefore, transformation between topologically distinct objects can be accomplished if energy barrier between these two states is overcome [76].

1.2.2 Stabilization of skyrmions

Skyrmion formation was first observed in bulk MnSi after a decade of the theoretical prediction [77]. Using neutron scattering, a lattice phase, named A-phase, with hexagonal symmetry was observed in between helical and paramagnetic phase, which occupied a small window in the temperature-magnetic field phase diagram (*Figure 1-9*a). This state was argued to be the skyrmion lattice from mean field theory calculation. Later, an additional component in the hall measurements was found that could be attributed to the topology of skyrmions [78]. This provides more evidence that the A-phase is indeed skyrmion lattice. Real-space observation of magnetic skyrmions using Lorentz transmission electron microscopy in FeCoSi was performed by Yu et al [79]. In these initial studies, skyrmions only existed at very low temperatures. Huang et al [80] and Yu et al [81] showed, in epitaxial FeGe films, skyrmions could exist near room temperature. Skyrmions were then observed in thin film Fe layer interfaced with heavy metal Ir layer [82]. This means skyrmions were stabilized by interfacial DMI. These skyrmions were atomically small (*Figure 1-9*b). However, they were stabilized at very low temperatures.

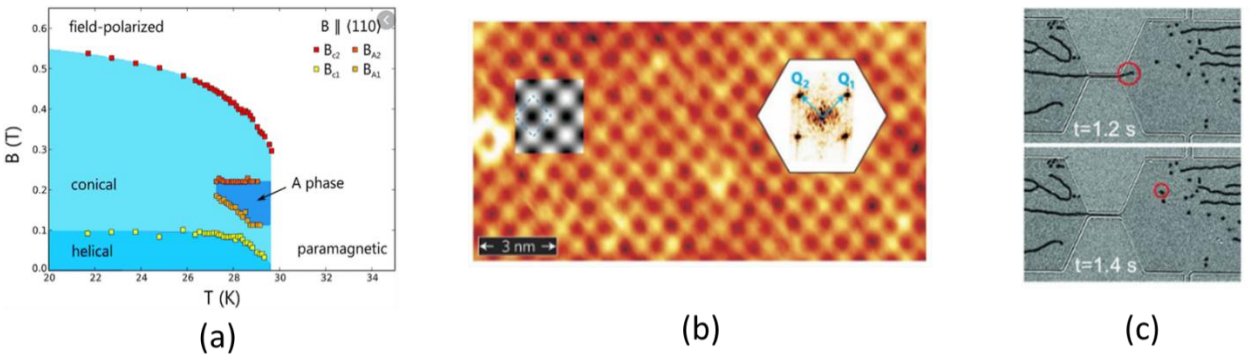

Figure 1-9 (a) First observation of skyrmion which is denoted by the A-phase, Reprinted with permission from [77], Copyright (2009), American Association for the Advancement of Science, (b) Atomic scale skyrmion in Fe/Ir bilayer at low temperature, Reprinted with permission from [82], Copyright (2011), Springer Nature. (c) Blowing skyrmion bubbles (right) from chiral domains(left), Reprinted with permission from [84], Copyright (2015), American Association for the Advancement of Science.

In a PdFe bilayer interfaced with Ir, controlled skyrmion creation and annihilation was demonstrated at 4.2 K [83]. This was achieved by depositing energy into the system by injecting high energy electrons utilizing a Spin Polarized Scanning Tunneling microscope (SP-STM) tip. Current induced manipulation of chiral domain walls was used to create skyrmions by introducing a geometrical constriction [84]. Using a small magnetic field first sparse domain walls are created. After passing a current, the chiral domain wall moves under the constriction and experience an inhomogeneous current distribution along one direction that breaks the stripes into circular domains. This is shown in *Figure 1-9* (c). Around same time, small skyrmion stabilization was shown by Moreau-Luchaire et al [85] and Boulle et el [86]. In [85], enhanced DMI was found by sandwiching the magnetic material between two heavy metal layers that lead to additive interfacial chiral interaction due to opposite DMI for Co on Ir and Co on Pt. The effective DMI value was around 2 mJ/m^2 and the skyrmions were sub 100 nm. Skyrmion creation with spin orbit torque at natural or artificial defect was demonstrated by Buttner et al [87].

1.2.3 Skyrmion motion and its application

Skyrmion motion driven by spin torque was first studied in MnSi [88] and FeGe [89] systems. Rotational and translational motion of skyrmion were observed. The threshold current needed for skyrmion motion was found to be less than 100 A/cm^2. This can be attributed to efficient Berry-phase coupling between conduction electrons and the spin structure and weak coupling to defects owing to the nature of the spiral spin structure. In domain walls, threshold current value to initiate motion is in the order of 10^5-10^7 A/cm^2.

A device operating with such high current values suffers from Joule heating issues. On the other hand, as skyrmion motion can be initiated with current that is 3-4 orders of magnitudes lower than that of domain walls, skyrmions were deemed promising to replace DW in racetrack memory devices.

In the initial studies, skyrmion motion in the creep regime was investigated and therefore skyrmion speed was only micrometers per second. In the last couple of years, many material systems, primarily thin ferromagnetic layer interfaced with a heavy metal layer, have been investigated [84-87, 90-94] and room temperature high speed skyrmion motion (~100 m/s) was demonstrated [86, 92, 94]. Recently, skyrmion stabilization of ferrimagnetic material have been demonstrated [95-97], which is particularly promising as ultrasmall ~10 nm skyrmion can be stabilized. Additionally, at angular momentum compensation point, DW velocities were shown to be very high [95] and skyrmion motion is also expected to be very fast which makes ferrimagnetic materials further promising.

Skyrmion motion based devices: Skyrmion motion can be utilized to implement logic and memory devices. Particularly, it has potential to replace domain walls in racetrack memory devices. Precise control of domain wall, which is necessary for implementation of racetrack memory, is difficult to achieve as DWs get pinned easily. Due to its spin structure, the skyrmions have very low depinning current and can overcome this problem. Therefore, skyrmion motion is investigated in different material systems although for similar

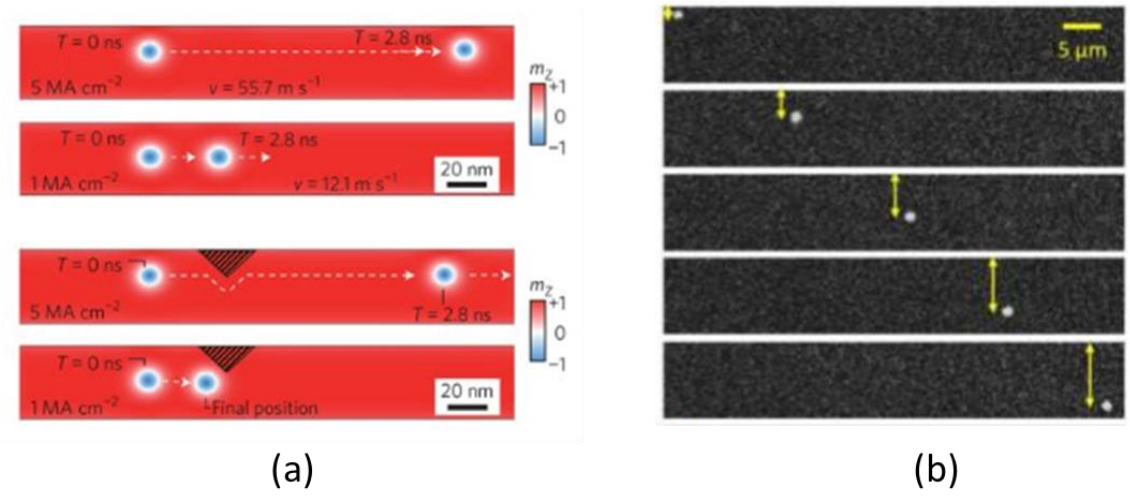

Figure 1-10 . (a) Skyrmion motion on a racetrack, Reprinted with permission from [98], Copyright (2013), Springer Nature, (b) Skyrmion hall effect. Reprinted with permission from [107], Copyright (2017), Springer Nature.

velocities required currents are similar [98]. Using micromagnetic simulation, strategy to design efficient racetrack memory device was proposed [98-101]. An exemplary racetrack device is shown in *Figure 1-10* (a). Using patterned nanowires, skyrmion motion can also be utilized to perform logic operations [102, 103]. Gyrotropic skyrmion motion of skyrmions can be used to implement nano-oscillators [104, 105]. Experimentally, proof-of-concept skyrmion shift device have been demonstrated by Yu et al [90].

Skyrmion Hall effect: Another important implication of skyrmion topology is skyrmion hall effect. This phenomenon is referred to as the SkHE. In ordinary hall effect, charged particles bend in the presence of a magnetic field due to Lorentz force. Magnetic skyrmions, when driven by a current, bend due to magnus force, which is a consequence of its topology. Therefore, skyrmions have both transverse and longitudinal component of velocity (*Figure 1-10*b). Skyrmion hall angle is defined as $\tan^{-1}(V_{trans}/V_{long})$. This was first theoretically predicted by Kong et al. [106]. Recent experimental studies [94, 107] also confirmed this phenomenon. While this is interesting from a physics point of view, this creates a problem in racetrack memory implementation. Due to this hall effect, skyrmion can go towards the edge and gets annihilated [108]. There exist several strategies, such as using antiferromagnetic skyrmions where two opposite polarity skyrmion sublattice can cancel hall angle and therefore skyrmion can be driven in a straight line [109, 110].

1.3 Fixed magnetic skyrmions in confined geometry (contribution of this thesis)

Skyrmion motion based racetrack memory faces multiple challenges that needs to be overcome for successful operation:

(1) Controlled skyrmion capture at specific location is necessary for racetrack devices. Domain walls are captured at geometric notches fabricated in the racetrack structure. However, skyrmions interact weakly with notches. This gives it the advantage of low threshold current but affects controllability.

(2) Skyrmion hall angle needs to be eliminated. This can be achieved utilizing antiferromagnetic skyrmions. Although, a reduction of skyrmion Hall angle was experimentally shown in partially

compensated sub-lattices of ferrimagnetic GdFeCo [96], complete suppression of spin hall effect is yet to be demonstrated.

(3) Skyrmion motion is generally induced by a current pulse. To achieve high velocity, required current is similar to that of domain walls. Therefore, it may suffer from the same Joule heating issues as DW based racetrack devices.

We propose to utilize fixed magnetic skyrmions that are confined in the free layer of an MTJ to implement memory devices. Therefore, this proposed device does not suffer from issues related to skyrmion motion (i.e. hall angle and controllability). To manipulate these skyrmions, we propose to use electric field, in particular VCMA which reduces energy dissipation. Hence, this proposed strategy can potentially address the issues mentioned above.

Fixed Magnetic Skyrmions: Magnetic skyrmions (*Fig 1-11 c*) can exhibit bistable and degenerate magnetic states at room temperature: core pointing "up" and core pointing "down". These two bistable states in a skyrmions are analogous to the two bistable "up" and "down" states of a shape anisotropic elliptical nanomagnet or a perpendicular nanomagnet where the magnetization points along the long axis or out of plane direction as shown in *Figure 1-11* (a) and (b). Therefore, the ability to switch deterministically and reliably between two stable skyrmionic states as well as detect ("read out") these states could lead to an energy efficient paradigm for the realization of nanomagnetic memory and computing devices. The readout

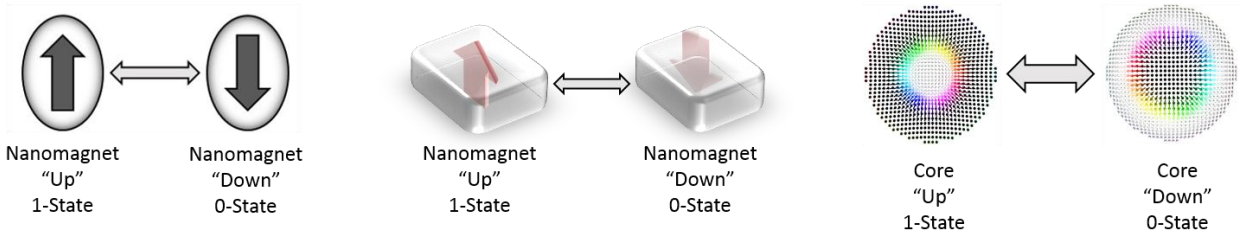

Figure 1-11 Bistable states in (a) shape anisotropic elliptical nanomagnets, (b) nanomagnets with perpendicular anisotropy, (c) magnetic skyrmions.

of the states can be performed using a vertically integrated magnetic tunneling junction (MTJ), which could result in high density memory elements.

Voltage control of magnetic anisotropy (VCMA) offers an extremely energy efficient route for manipulating magnetization. Previous schemes for switching nanomagnets with perpendicular magnetic anisotropy (PMA) using VCMA could only achieve a maximum of 90° magnetization rotation (from out of plane to in-plane) and an external magnetic field is required to achieve complete magnetization reversal. However, in one of our studies, we showed with rigorous micromagnetic simulation that core reversal of a magnetic skyrmion can be achieved employing an electric field only (i.e. without requiring any external field). Furthermore, we can switch reversibly between two skyrmionic states and two ferromagnetic states, i.e. skyrmion states with the magnetization of the core pointing down/up and periphery pointing up/down, and ferromagnetic states with magnetization pointing up/down, by applying a bipolar voltage pulse (i.e. sequential increase and decrease of the perpendicular magnetic anisotropy). Therefore, this switching strategy can provide functionality of a four-state memory element. Additionally, the energy dissipation can be as low as 100 aJ which is orders of magnitude lower than other competing technologies. This is further described in chapter 2.

Reduction of the switching current can be achieved by employing methods to reduce perpendicular magnetic anisotropy, which temporarily depresses the energy barrier between the “up” and “down” state during spin current induced switching. This can improve the energy-efficiency and switching speed without compromising the thermal stability. In chapter 3, we examine such a hybrid scheme for reversal of skyrmions where application of a small voltage can reduce the threshold current needed, present rigorous micromagnetic simulation to explain the underlying physics of the reversal process and quantify improvements in terms of dissipated energy.

In chapter 4, we propose and show preliminary simulations of memory devices based on complete ferromagnetic reversal mediated by skyrmions. Our work demonstrates that the presence of Dzyaloshinskii-Moriya Interaction (DMI) can create alternative route for magnetization reversal that obviates the need for

utilizing precessional magnetization dynamics as well as a bias magnetic field that are employed in traditional voltage control of magnetic anisotropy (VCMA) based switching of perpendicular magnetization. We further study dynamic error due to the presence of thermal noise in these devices and show with extensive micromagnetic simulation, in the presence of thermal noise, that the proposed skyrmion mediated VCMA switching mechanism is robust at room temperature leading to extremely low error switching.

In chapter 5, we demonstrate experimental switching of skyrmions. To demonstrate VCMA induced manipulation of skyrmions, we fabricate antiferromagnet/ferromagnet/oxide heterostructure films where skyrmions can be stabilized without any external magnetic field due to the presence of exchange bias. These isolated skyrmions were annihilated by applying a voltage pulse that increased PMA. On the other hand, decreasing PMA promoted formation of more skyrmions. Furthermore, skyrmions can be created from chiral domains by increasing PMA of the system.

Finally, in the concluding chapter, we present future research directions. We discuss challenges in scaling our proposed device structure to 20 nm diameter which is competitive to existing STT-MRAM devices. We further show some promising application of skyrmions beyond memory application that can guide and motivate future research.

References:

[1] G. E. Moore 1965 Cramming more components onto integrated circuits Electronics Magazine page 4.

[2] T. Valet and A. Fert, “Theory of the perpendicular magnetoresistance in magnetic multilayers,” Phys. Rev. B, 48(10), 7099-7113(1993).

[3] J. S. Moodera, Lr Kinder, TM Wong, R. Meservey, “Large magnetoresistance at room temperature in ferromagnetic film tunnel junctions,” Phys. Rev. Lett., 74(16), 3273-3276(1995).

[4] T. Miyazaki and N. Tezuka, “Giant magnetic tunneling effect in Fe/Al2O3/Fe junction,” Journal of magnetism and magnetic materials, 139(3), L231-L234(1995).

[5] R Landauer 1961 Irreversibility and Heat Generation in the Computing Process IBM J. 183–91

[6] S. Salahuddin and S. Datta, “Interacting systems for self-correcting low power switching,” Appl. Phys. Lett. 90, 093503(2007).

[7] R. P. Cowburn, D. K. Koltsov, A. O. Adeyeye, M. E. Welland and D. M. Tricker, “Single-Domain Circular Nanomagnets,” Phys. Rev. Lett., 83 1042–5(1999).

[8] W. F. Brown, “Thermal fluctuations of a single-domain particle,” Phys. Rev. 130, 1677–86(1963).

[9] P. Gaunt, “The frequency constant for thermal activitation of a ferromagnetic domain wall,” J. Appl. Phys. 48, 3470–4(1977).

[10] S. Khasanvis, M. Y. Li, M. Rahman, A. K. Biswas, M. Salehi-Fashami, J. Atulasimha, S. Bandyopadhyay and C. A. Moritz, “Architecting for causal intelligence at nanoscale,” COMPUTER 48, 54-64(2015).

[11]. S. D. Manasi, M. M. Al Rashid, J. Atulasimha, S. Bandyopadhyay and A. R. Trivedi, “Straintronic magneto-tunneling junction based ternary content-addressable memory (Parts I and II),” IEEE Trans. Elec. Dev. 64, 2835(2017).

[12] J. Grollier, D. Querlioz, K. Y. Camsari, K. Everschor-Sitte, S. Fukami, M. D. Stiles, “Neuromorphic spintronics,” Nature Electronics 3, 360-370(2020).

[13] S. S. P. Parkin, M. Hayashi and L. Thomas, “Magnetic domain-wall racetrack memory,” Science 320, 190-194(2008).

[14] D. A. Allwood, G. Xiong, C. C. Faulkner, D. Atkinson, D. Petit and R. P. Cowburn, “Magnetic domain wall logic,” Science 309, 1688-1692(2005).

[15] M. Yamanouchi, D. Chiba, F. Matsukura and H. Ohno, “Current-induced domain wall switching in a ferromagnetic semiconductor structure,” Nature 428, 539-542(2004).

[16] W. S. Zhao et al., “Magnetic domain-wall racetrack memory for high density and fast data storage,” IEEE 11th International Conference on Solid-State and Integrated Circuit Technology, Xi'an, 2012, pp. 1-4 (2012).

[17] Kim et al, “Fast domain wall motion in the vicinity of the angular momentum compensation temperature of ferrimagnets,” Nature Materials 16, 1187–1192(2017).

[18] Avci et al, “Interface-driven chiral magnetism and current-driven domain walls in insulating magnetic garnets,” Nature Nanotechnology 14, 561–566(2019).

[19] M. T. Alam, M. J. Siddiq, G. H. Bernstein, M. Niemier, W. Porod and X. S. Hu, “On-chip clocking for nanomagnet logic devices,” IEEE Trans. Nanotechnol. 9, 348–51(2010).

[20] J. C. Slonczewski, “Current-driven excitation of magnetic multilayers,” J. Magn. Magn. Mater. 159 L1(1996).

[21] L. Berger, “Emission of spin waves by a magnetic multilayer traversed by a current,” Phys. Rev. B 54, 9353(1996)

[22] J. Z. Sun, “Spin-current interaction with a monodomain magnetic body: a model study,” Phys. Rev. B 62, 570(2000).

[23] D. C. Ralph and M. D. Stiles, “Spin transfer torques,” J. Magn. Magn. Mater. 320, 1190-1216(2008).

[24] J. C. Sankey, Y. -T. Cui, J. Z. Sun, J. C. Slonczewski, R. A. Buhrman and D. C. Ralph, “Measurement of the spin transfer torque vector in magnetic tunnel junctions,” Nat. Phys. 4, 67-71(2008).

[25] H. Kubota et al, “Quantitative measurement of voltage dependence of spin-transfer torque in MgO-based magnetic tunnel junctions,” Nat. Phys. 4, 37(2008).

[26] Nowak et al, “Dependence of Voltage and Size on Write Error Rates in Spin-Transfer Torque Magnetic Random-Access Memory,” IEEE Magnetics Letters 7, 3102604(2016).

[27] K. L.Wang and P. Khalili-Amiri, “Nonvolatile spintronics: perspectives on instant-on non-volatile nanoelectronic systems,” Spin 2, 1250009(2012).

[28] L. Liu, C. -F. Pai, Y. Li, H. W. Tseng, D. C. Ralph and R. A. Buhrman, “Spin-torque switching with the giant spin Hall effect of tantalum,” Science 336, 555(2012).

[29] C. -F. Pai, L. Liu L, Y. Li, H. W. Tseng, D. C. Ralph and R. A. Buhrman, “Spin transfer torque devices utilizing the giant spin Hall effect of tungsten,” Appl. Phys. Lett. 101, 122404(2012).

[30] J. E. Hirsch, “Spin Hall Effect,” Phys. Rev. Lett. 83, no. 9,1834–1837(1999).

[31] D. Bhowmik, L. You and S. Salahuddin, “Spin Hall effect clocking of nanomagnetic logic without a magnetic field,” Nat. Nanotechnol. 9, 59(2014).

[32] S. Sayed, V. -Q. Diep, K. Y. Camsari and S. Datta, “Spin funneling for enhanced spin injection into ferromagnets,” Sci. Rep. 6, 28868(2016).

[33] Y. Niimi, Y. Kawanishi, D. H. Wei, C. Deranlot, H. X. Yang, M. Chshiev, T. Valet, A. Fert and Y. Otani, “Giant spin Hall effect induced by skew scattering from bismuth impurities inside the thin film CuBi alloys,” Phys. Rev. Lett. 109, 156602(2012).

[34] Brink et al, “Field-free magnetization reversal by spin-Hall effect and exchange bias,” Nature Communications 7, 10854 (2016).

[35] Wang et al, “Field-free switching of a perpendicular magnetic tunnel junction through the interplay of spin–orbit and spin-transfer torques,” Nature Electronics 1, 582–588(2018).

[36] D. Bhattacharya, S. Bandyopadhyay and J. Atulasimha, “Review: Voltage induced strain control of magnetization: computing and other applications”, Multifunct. Mater. 2 032001 (2019).

[37] H. X. Yang, M. Chshiev, B. Dieny, J. H. Lee, A. Manchon, and K. H. Shin, “First-principles investigation of the very large perpendicular magnetic anisotropy at Fe|MgO and Co|MgO interfaces,” Phys. Rev. B - Condens. Matter Mater. Phys. 84, no. 5(2011).

[38] M. K. Niranjan, C. G. Duan, S. S. Jaswal, and E. Y. Tsymbal, “Electric field effect on magnetization at the Fe/MgO (001) interface,” Appl. Phys. Lett. 96, no. 22(2010).

[39] Juan G Alzate, Thesis: Voltage-Controlled Magnetic Dynamics in Nanoscale Magnetic Tunnel Junctions, UCLA

[40] S. Miwa, K. Matsuda, K. Tanaka, Y. Kotani, M. Goto, T. Nakamura and Y. Suzuki, “Voltage controlled magnetic anisotropy in Fe/MgO tunnel junctions studied by x-ray absorption spectroscopy,” Appl. Phys. Lett. 107, 162402(2016).

[41] M. Endo, S. Kanai, S. Ikeda, F. Matsukura and H. Ohno, “Electric field effects on thickness dependent magnetic anisotropy of sputtered MgO/Co4OFe4OB2O/Ta structures,” Appl. Phys. Lett. 96, 212503(2010).

[42] W. -G. Wang, M. Li, S. Hageman and C. L. Chien, “Electric-field-assisted switching in magnetic tunnel junctions,” Nat. Mater. 11, 64(2012)

[43] A. Rajanikanth, T. Hauet, F. Montaigne, S. Mangin and S. Andrieu, “Magnetic anisotropy modified by electric field in V/Fe/MgO (001)/Fe epitaxial magnetic tunnel junction,” Appl. Phys. Lett. 103, 062402(2013).

[44] T. Nozaki, Y. Shiota, M. Shiraishi, T. Shinjo and Y. Suzuki, “Voltage-induced perpendicular magnetic anisotropy change in magnetic tunnel junctions,” Appl. Phys. Lett. 96, 022506(2010).

[45] S. Kanai, M. Yamanouchi, S. Ikeda, Y. Nakatani, F. Matsukura and H. Ohno, "Electric field induced magnetization reversal in a perpendicular-anisotropy CoFeB-MgO magnetic tunnel junction," Appl. Phys. Lett. 101, 122403(2012).

[46] Y. Shiota, T. Nozaki, F. Bonell, S. Murakami, T. Shinjo and Y. Suzuki, "Induction of coherent magnetization switching in few atomic layers of FeCo using voltage pulses," Nat. Mater. 11, 39(2012).

[47] P. K. Amiri and K. L. Wang, "Voltage-controlled magnetic anisotropy in spintronic devices," Spin 2, 1240002(2012).

[48] C. Grezes, F. Ebrahimi, J. G. Alzate, X. Cai, J. A. Katine, J. Langer, B. Ocker, P. K. Amiri and K. L. Wang K L, "Ultra-low switching energy and scaling in electric-field-controlled nanoscale magnetic tunneling junctions with high resistance-area product," Appl. Phys. Lett. 108, 012403(2016).

[49] J. Stöhr, H. C. Siegmann, A. Kashuba and S. J. Gamble, "Magnetization switching without charge or spin currents," Appl. Phys. Lett. 94, 072504(2009).

[50] P. V. Ong, N. Kioussis, P. K. Amiri and K. L. Wang, "Electric-field-driven magnetization switching and nonlinear magnetoelasticity in Au/FeCo/MgO heterostructures," Sci. Rep. 6, 29815(2016).

[51] E. Villari, "Change of magnetization by tension and by electric current", Annual Review of Physical Chemistry, vol. 126, pp. 87– 122 (1865).

[52] N. Tiercelin, Y. Dusch, A. Klimov, S. Giordano, V. Preobrazhensky and P. Pernod, "Room temperature magnetoelectric memory cell using stress-mediated magnetoelastic switching in nanostructured multilayers," Appl. Phys. Lett. 99(2011).

[53] N. D'Souza et el, "Energy-efficient switching of nanomagnets for computing: straintronics and other methodologies," Nanotechnology 29 442001 (2018).

[54] T. Brintlinger, S. H. Lim, K. H. Baloch, P. Alexander, Y. Qi, J. Barry, J. Melngailis, L. Salamanca-Riba, I. Takeuchi and J Cumings, “In situ observation of reversible nanomagnetic switching induced by electric fields,” Nano Lett. 10, 1219–23(2010).

[55] T. Wu, A. Bur, K. Wong, P. Zhao, C. S. Lynch, P. K. Amiri, K. L. Wang and G. P. Carman, “Electrical control of reversible and permanent magnetization reorientation for magnetoelectric memory devices,” Appl. Phys. Lett. 98(2011).

[56] N. A. Pertsev and H. Kohlstedt, “Magnetic tunnel junction on a ferroelectric substrate,” Appl. Phys. Lett. 95(2009).

[57] N. D’Souza N, M S Fashami, S Bandyopadhyay and J. Atulasimha, “Experimental Clocking of Nanomagnets with Strain for Ultralow Power Boolean Logic,” Nano Lett. 16, 1069–75(2016).

[58] K. Roy, S. Bandyopadhyay and J. Atulasimha, “Binary switching in a “symmetric” potential landscape,” Sci. Rep. 3, 3038(2013).

[59] D. Bhattacharya, M. M. Al-Rashid, N. D’Souza, S. Bandyopadhyay and J. Atulasimha, “Incoherent magnetization dynamics in strain mediated switching of magnetostrictive nanomagnets,” Nanotechnology 28 (1), 015202 (2016).

[60] A. K. Biswas, S. Bandyopadhyay and J. Atulasimha, “Energy-efficient magnetoelastic nonvolatile memory,” Appl. Phys. Lett. 104(2014).

[61] J. Tejada, E. M. Chudnovsky, R. Zarzuela, N. Statuto, J. Calvo-De La Rosa, P. V.Santos and A. Hernández-Mínguez, “Switching of magnetic moments of nanoparticles by surface acoustic Waves,” Epl 118(2017).

[62] V. Sampath, N. D’Souza, D. Bhattacharya, G. M. Atkinson, S. Bandyopadhyay and J. Atulasimha, “Acoustic-Wave-Induced Magnetization Switching of Magnetostrictive Nanomagnets from Single-Domain to Nonvolatile Vortex States,” Nano Lett. 16, 5681–7(2016).

[63] S. Mondal, M. A. Abeed, K. Dutta, A. De, S. Sahoo, A. Barman and S. Bandyopadhyay, "Hybrid Magnetodynamical Modes in a Single Magnetostrictive Nanomagnet on a Piezoelectric Substrate Arising from Magnetoelastic Modulation of Precessional Dynamics," ACS Appl. Mater. Interfaces 10, 43970–7(2018).

[64] L. Thevenard, J. -Y. Duquesne, E. Peronne, H. J. von Bardeleben, H. Jaffres, S. Ruttala, J. -M. George, A. Lemaître and C. Gourdon, "Irreversible magnetization switching using surface acoustic Waves," Phys. Rev. B 87, 144402(2013).

[65] S. Davis, A. Baruth and S. Adenwalla, "Magnetization dynamics triggered by surface acoustic Waves," Appl. Phys. Lett. 97(2010).

[66] M. Weiler, L. Dreher, C. Heeg, H. Huebl, R. Gross, M. S. Brandt and S. T. B. Goennenwein, "Elastically driven ferromagnetic resonance in nickel thin films," Phys. Rev. Lett. 106(2011).

[67] L. Thevenard, C. Gourdon, J. Y. Prieur, H. J. Von Bardeleben, S. Vincent, L. Becerra, L. Largeau and J. Y. Duquesne, "Surface-acoustic-wave-driven ferromagnetic resonance in (Ga,Mn)(As,P) Epilayers," Phys. Rev. B - Condens. Matter Mater. Phys. 90(2014).

[68] A. Roe, D. Bhattacharya, J. Atulasimha, "Resonant acoustic wave assisted spin-transfer-torque switching of nanomagnets," Applied Physics Letters 115 (11), 112405(2019).

[69] W. A. Misba, M. M. Rajib, D. Bhattacharya, J. Atulasimha, "Acoustic-Wave-Induced Ferromagnetic-Resonance-Assisted Spin-Torque Switching of Perpendicular Magnetic Tunnel Junctions with Anisotropy Variation," Phys. Rev. Applied 14, 014088(2020).

[70] I. Dzyaloshinsky, "A thermodynamic theory of 'weak' ferromagnetism of antiferromagnetics," J. Phys. Chem. Solids 4, no. 4, 241–255(1958).

[71] T. Moriya, "Anisotropic superexchange interaction and weak ferromagnetism," Phys. Rev. 120, no. 1, 91–98(1960).

[72] T. H. R. Skyrme, “A unified field theory of mesons and baryons,” Nucl. Phys. 31, 556 (1962).

[73] A. Bogdanov and A. Hubert, “Thermodynamically stable magnetic vortex states in magnetic crystals,” J. Magn. Magn. Mater. 138, 255(1994).

[74] U. K. Rössler, A. Bogdanov, and C. Pfleiderer, “Spontaneous skyrmion ground states in magnetic metals.,” Nature 442, no. 7104, 797–801(2006).

[75] N. Nagagosa and Y. Tokura, “Topological properties and dynamics of magnetic skyrmions”, Nature Nanotechnology volume 8, 899–911(2013).

[76] K. Everschor-Sitte, J. Masell, R. M. Reeve, and M. Kläui, “Perspective: Magnetic skyrmions—Overview of recent progress in an active research field”, Journal of Applied Physics 124, 240901 (2018).

[77] S. Mühlbauer, B. Binz, F. Jonietz, C. Pfleiderer, A. Rosch, A. Neubauer, R. Georgii, P. Böni, “Skyrmion Lattice in a Chiral Magnet,” Science 80, 915–920(2009).

[78] A. Neubauer, C. Pfleiderer, B. Binz, A. Rosch, R. Ritz, P. G. Niklowitz, and P. Böni, “Topological Hall Effect in the A Phase of MnSi,” Phys. Rev. Lett. 102, 186602(2009).

[79] X. Z. Yu, Y. Onose, N. Kanazawa, J. H. Park, J. H. Han, Y. Matsui, N. Nagaosa, and Y. Tokura, “Real-space observation of a two-dimensional skyrmion crystal,” Nature 465, 901(2010).

[80] S. X. Huang and C. L. Chien, “Extended Skyrmion Phase in Epitaxial FeGe (111) Thin Films Phys,” Rev. Lett. 108, 267201(2012).

[81] Yu et al, “Near room-temperature formation of a skyrmion crystal in thin-films of the helimagnet FeGe,” Nature Materials 10, 106–109 (2011).

[82] S. Heinze, K. Von Bergmann, M. Menzel, J. Brede, A. Kubetzka, R. Wiesendanger, G. Bihlmayer, and S. Blügel, “Spontaneous atomic-scale magnetic skyrmion lattice in two dimensions,” Nat. Phys. 7, 713 (2011).

[83] N. Romming, C. Hanneken, M. Menzel, J. E. Bickel, B. Wolter, K. Von Bergmann, A. Kubetzka, and R. Wiesendanger, "Writing and Deleting Single Magnetic Skyrmions," Science 341, 636 (2013).

[84] Jiang et al, "Blowing magnetic skyrmion bubbles," Science 349, Issue 6245, 283-286(2015).

[85] Moreau-Luchaire, C. Moutafis, N. Reyren, J. Sampaio, C. A. Vaz, N. Van Horne, K. Bouzehouane, K. Garcia, C. Deranlot, P. Warnicke, P. Wohlhüter, J. M. George, M. Weigand, J. Raabe, V. Cros, and A. Fert, "Additive interfacial chiral interaction in multilayers for stabilization of small individual skyrmions at room temperature," Nat. Nanotechnol. 11, 444 (2016).

[86] O. Boulle, J. Vogel, H. Yang, S. Pizzini, D. De Souza Chaves, A. Locatelli, T. O. Mente, A. Sala, L. D. Buda-Prejbeanu, O. Klein, M. Belmeguenai, Y. Roussigné, A. Stashkevich, S. Mourad Chérif, L. Aballe, M. Foerster, M. Chshiev, S. Auffret, I. M. Miron, and G. Gaudin, "Room-temperature chiral magnetic skyrmions in ultrathin magnetic nanostructures," Nat. Nanotechnol. 11, 449 (2016).

[87] Buttner et al., "Field-free deterministic ultrafast creation of magnetic skyrmions by spin–orbit torques," Nature Nanotechnology 12, 1040–1044 (2017).

[88] Jonitez et al., "Spin Transfer Torques in MnSi at Ultralow Current Densities," Science 330, Issue 6011, 1648-1651(2010).

[89] X. Z. Yu et al., "Skyrmion flow near room temperature in an ultralow current density," Nat. Commun. 3, 988 (2012).

[90] Yu et al., "Room-Temperature Skyrmion Shift Device for Memory Application," Nano Lett. 17, 1, 261-268(2017).

[91] W. Legrand et al., "Room-temperature current-induced generation and motion of sub-100 nm skyrmions," Nano. Lett. 17, 2703–2712 (2017).

[92] S. Woo et al., "Observation of room-temperature magnetic skyrmions and their current-driven dynamics in ultrathin metallic ferromagnets," Nat. Mater. 15, 501–506 (2016).

[93] A. Hrabec et al., “Current-induced skyrmion generation and dynamics in symmetric bilayers,” Nat. Commun. 8, ncomms15765 (2017).

[94] K. Litzius, I. Lemesh, B. Krüger, P. Bassirian, L. Caretta, K. Richter, F. Büttner, K. Sato, O. A. Tretiakov, J. Förster, R. M. Reeve, M. Weigand, I. Bykova, H. Stoll, G. Schütz, G. S. Beach, and M. Klaüi, “Skyrmion Hall effect revealed by direct time-resolved X-ray microscopy,” Nat. Phys. 13, 170 (2017).

[95] Caretta et al., “Fast current-driven domain walls and small skyrmions in a compensated ferrimagnet,” Nature Nanotechnology 13, 1154–1160(2018).

[96] Woo et al., “Current-driven dynamics and inhibition of the skyrmion Hall effect of ferrimagnetic skyrmions in GdFeCo films,” Nature Communications 9, 959 (2018).

[97] J. Brandão, D. A. Dugato M. V. Puydinger dos Santos J. C. Cezar, “Evolution of Zero-Field Ferrimagnetic Domains and Skyrmions in Exchange-Coupled Pt/CoGd/Pt Confined Nanostructures: Implications for Antiferromagnetic Devices,” ACS Appl. Nano Mater. 2, 12, 7532-7539(2019).

[98] A. Fert, V. Cros and J. Sampaio., “Skyrmion on the track,” Nature Nanotechnology, 8, 152-156(2013).

[99] R. Tomasello, E. Martinez, R. Zivieri, L. Torres, M. Carpentieri, and G. Finocchio, “A strategy for the design of skyrmion racetrack memories”, Sci. Rep. 4, 6784 (2014).

[100] X. Zhang, G. P. Zhao, H. Fangohr, J. P. Liu, W. X. Xia, J. Xia, and F. J. Morvan, “Skyrmion-skyrmion and skyrmion-edge repulsions in skyrmion-based racetrack memory”, Sci. Rep. 5, 7643 (2015).

[101] D. D. Cortés-Ortuño, W. Wang, M. Beg, R. A. Pepper, M. A. Bisotti, R. Carey, M. Vousden, T. Kluyver, O. Hovorka, and H. Fangohr, “Thermal stability and topological protection of skyrmions in nanotracks,” Sci. Rep. 7, 4060 (2017).

[102] X. Zhang, M. Ezawa, and Y. Zhou, “Magnetic skyrmion logic gates: conversion, duplication and merging of skyrmions,” Sci. Rep. 5, 9400 (2015).

[103] S. Luo, M. Song, X. Li, Y. Zhang, J. Hong, X. Yang, X. Zou, N. Xu, and L. You, “Reconfigurable Skyrmion Logic Gates,” Nano Lett. 18, 1180 (2018).

[104] S. Zhang, J. Wang, Q. Zheng, Q. Zhu, X. Liu, S. Chen, C. Jin, Q. Liu, C. Jia, and D. Xue, “Current-induced magnetic skyrmions oscillator,” New J. Phys. 17, 023061 (2015).

[105] F. Garcia-Sanchez, J. Sampaio, N. Reyren, V. Cros, and J. V. Kim, “A skyrmion-based spin-torque nano-oscillator,” New J. Phys. 18, 075011 (2016).

[106] L. Kong and J. Zang, “Dynamics of an Insulating Skyrmion under a Temperature Gradient,” Phys. Rev. Lett. 111, 067203(2013).

[107] Jiang et al., “Direct observation of the skyrmion Hall effect,” Nature Physics 13, 162–169(2017).

[108] M. -W. Yoo, V. Cros, and J.-V. Kim, “Current-driven skyrmion expulsion from magnetic nanostrips,” Phys. Rev. B 95, 184423(2017).

[109] J. Barker and O. A. Tretiakov, “Static and Dynamical Properties of Antiferromagnetic Skyrmions in the Presence of Applied Current and Temperature” Phys. Rev. Lett. 116, 147203 (2016),

[110] X. Zhang, Y. Zhou, and M. Ezawa, “Antiferromagnetic Skyrmion: Stability, Creation and Manipulation,” Sci. Rep. 6, 24795 (2016).

Chapter 2: Modeling and Experimental Imaging of Nanomagnetic Devices and Magnetic Skyrmions

This chapter deals with modeling of magnetization dynamics inside a nanomagnet as well as several experimental characterization technics to image magnetization states of nanomagnets. We will first discuss modeling of nanomagnets in section 2.1. Modeling can be performed at different scales starting from quantum mechanical modeling that deals with electronic structure to macrospin assumption in which the whole magnet is considered as a giant spin. We particularly focus our discussion to describing micromagnetic simulation framework where a magnetic structure is divided into smaller cells and magnetization dynamics is solved for each of them. In section 2.2, we introduce a variety of instruments that are used to image magnetization states in magnetic materials. We describe Magnetic Force Microscopy (MFM) in detail which was used to image magnetic skyrmions in our experiments.

2.1 Micromagnetic Modeling of Magnetization Dynamics

In the Micromagnetic framework, the magnetization dynamics is simulated using the Landau Lifshitz Gilbert (LLG) equation:

$$\frac{\partial \vec{m}}{\partial t} = \vec{\tau} = \left(\frac{-\gamma}{1+\alpha^2}\right)\left(\vec{m} \times \vec{H}_{eff} + \alpha\left(\vec{m} \times \left(\vec{m} \times \vec{H}_{eff}\right)\right)\right) \quad (1)$$

where $\vec{m}$ is the reduced magnetization ($\vec{M}/M_s$), M_s is the saturation magnetization, γ is the gyromagnetic ratio and α is the Gilbert damping coefficient. The quantity H_{eff} is the effective magnetic field, which is given by,

$$\vec{H}_{eff} = \vec{H}_{demag} + \vec{H}_{exchange} + \vec{H}_{anisotrpy} + \vec{H}_{thermal} \quad (2)$$

Here, $\vec{H}_{demag}$ is the demagnetization (or magnetostatic) field, $\vec{H}_{exchange}$ is the effective field due to Heisenberg exchange coupling and DMI interaction, $\vec{H}_{anisotrpy}$ is the effective field due to uniaxial anisotropy and $\vec{H}_{thermal}$ is the random thermal field. These are evaluated in the Micromagnetic framework in the manner described in Ref. 1 and Ref. 2.

The effective field term for uniaxial anisotropy is given by,

$$\vec{H}_{anis} = \frac{2K_{u1}}{\mu_0 M_{sat}}(\vec{u}.\vec{m})\vec{u} + \frac{4K_{u2}}{\mu_0 M_{sat}}(\vec{u}.\vec{m})^3\vec{u} \quad (3)$$

where, K_{u1} and K_{u2} are first and second order uniaxial anisotropy constants, M_{sat} is the saturation magnetization and $\vec{u}$ is the unit vector in the direction of the anisotropy. For $K_{u2} = 0$, Equation (3) reduces to

$$\vec{H}_{anis} = \frac{2K_{u1}}{\mu_0 M_{sat}}(\vec{u}.\vec{m})\vec{u} \quad (4)$$

VCMA effectively modulates the anisotropy energy density, which is given by ΔPMA = aE. Here a and E are respectively the coefficient of electric field control of magnetic anisotropy and the applied electric field. The resultant change in uniaxial anisotropy due to VCMA is incorporated by modulating K_{u1} while keeping K_{u2} = 0.

To determine strain mediated magnetization dynamics, we incorporate the effect of stress using uniaxial anisotropy, facilitated by their equivalent contribution to the effective field as the micromagnetic frameworks lack any inbuilt functionality to directly accomplish this. The effective field due to an external uniaxial stress can be expressed as

$$\vec{H}_{stress} = \frac{3\lambda_s \sigma}{\mu_0 M_{sat}}(\vec{s}.\vec{m})\vec{s} \quad (5)$$

where, $(3/2)\lambda_s$ is the saturation magnetostriction, σ is the external stress (Pa) and $\vec{s}$ is the unit vector in the direction of the applied stress. Comparing Equations (4) and (5),

$$K_{u1} = \frac{3\lambda_s \sigma}{2} \quad (6)$$

this equation was used to find the value of K_{u1} to simulate the effect for a given uniaxial stress σ applied in the same direction as the uniaxial anisotropy.

The effect of thermal noise is incorporated by adding an equivalent field to the total effective field

$$\vec{H}_{thermal} = \vec{\eta}(step)\sqrt{\frac{2\alpha k_B T}{\mu_0 M_s \gamma \Delta\sigma \Delta t}} \quad (7)$$

Where $\vec{\eta}(step)$ a random vector from a standard normal distribution whose value is changed after every time step, $\Delta\sigma$ is the cell volume, Δt the time step and k_B the Boltzmann constant.

Magnetic skyrmions are stabilized due to the presence of The Dzyaloshinskii-Moriya interaction which has been introduced in an atomic description as

$$E_{DMI} = \sum_{i,j} \vec{D}_{ij}.(\vec{S}_i \times \vec{S}_j) \quad (8)$$

where $\vec{D}_{ij}$ is the DM interaction vector for the atomic bond ij (in Joule), S_i the atomic moment unit vector, and the summation is performed on the neighbor pairs <i, j>.

The DMI contribution to the effective exchange field is given by:

$$\vec{H}_{DMI} = \frac{2D}{\mu_0 M_s}\left[(\vec{\nabla}.\vec{m})\hat{z} - \vec{\nabla}m_z\right] \quad (9)$$

where m_z is the z-component of magnetization and D is the continuous effective DMI constant.

The torque due to spin current is given by,

$$\tau_{STT} = \gamma\beta\left(\vec{m} \times \left(\vec{m} \times \vec{m}_p\right)\right) \quad (10)$$

$$\beta = \frac{h}{2\pi}\,\frac{PJ}{2\mu_0 e M_s L} \quad (11)$$

Here, $\vec{m}_p$ is the unit vector of spin polarization direction, h is Planck's constant, P is the degree of spin polarization, J is the current density, μ_0 is vacuum permeability, e is the electron charge, L is the thickness of the free layer.

2.2 Experimental approaches to characterize magnetic skyrmions

In the very first experiment that reported observation of magnetic skyrmions, small angle neutron scattering was used to identify skyrmions from the scattering pattern [1]. Later, topological hall effect arising due to emergent electrodynamics of the spiral spin structure of magnetic skyrmion was used to confirm this prediction [2]. Following this, experiments with a goal to realize real space observation of skyrmions were performed. skyrmion crystal was first observed in FeCoSi using Lorentz Transmission Electron Microscope [3]. Several technics have been used since this seminal study. In section 2.2.1, we will briefly survey some of these technics. In the next section, we will describe the operating principle of magnetic force microscopy which we used to study skyrmions in our experiments.

2.2.1 Different imaging technics

Lorentz Transmission Electron Microscope (Lorentz-TEM): In a TEM, electrons are transmitted through a very thin film and information about the sample, such as crystalline structure, chemical composition etc. are obtained from different electron-sample interactions. Electrons passing through a ferromagnetic material experience Lorentz force and therefore gets deflected. This interaction is used to form an image of the magnetization of the sample. Amount of deflection depends on the magnetization direction and therefore, contrast appears in the image when electrons pass through oppositely polarized magnetic domains. Lorentz-TEM was used in the very first real space observation of skyrmion [3]. This is shown in *Figure 2-1 (a).* Other examples can be found in reviews [4,5].

Spin Polarized-Scanning Tunneling Microscope (SP-STM): In a STM, a conducting tip is used to scan the surface. When a bias voltage is applied, electrons tunnel between the surface and the tip. This tunneling current is used to characterize a sample's surface which depends on tip to sample distance, applied voltage etc. If a magnetized tip is used, tunneling current depends on the electron spin due to tunnel magnetoresistance. The spins that are parallel to the magnetization of the tip now have a higher probability to tunnel. Thus, information about surface magnetization can be obtained. In Ref [6], SP-STM was used to both image the skyrmions and create and destroy them by applying spin polarized current using the tip.

Several other studies also used SP-STM to image magnetic skyrmions [7-9]. One example of SP-STM imaging of skyrmions is shown in *Figure 2-1 (b)* where the blue and the read area mean high and low current.

X-ray Magnetic Circular Dichroism (XMCD): Interaction between polarized X-ray and magnetic moment is dichroic in nature; absorption of X-ray is different depending on polarization of the X-ray (i.e. left vs right circular polarization) and the magnetization direction. The magnetic property of transition metals depends on the 3d electrons and there exists an imbalance between spin up and spin down electrons in the 3d orbital. Therefore, to probe magnetic characteristics, X-ray absorption at L-edge (i.e. 2p to 3d transition) is performed. The imbalance can be measured using polarized X-rays. Right circularly polarized X-ray photons transfer the opposite momentum to the electron compared to left circularly polarized photons. Therefore, depending on the difference in number of spin up and spin down electrons in the 3d orbital, one of the X-rays is absorbed more than the other [10]. This gives rise to difference in the absorption spectra between left and right circularly polarized X-Ray absorption spectra, from which magnetization information can be interpreted. This is shown in *Figure 2-1 (c)*.

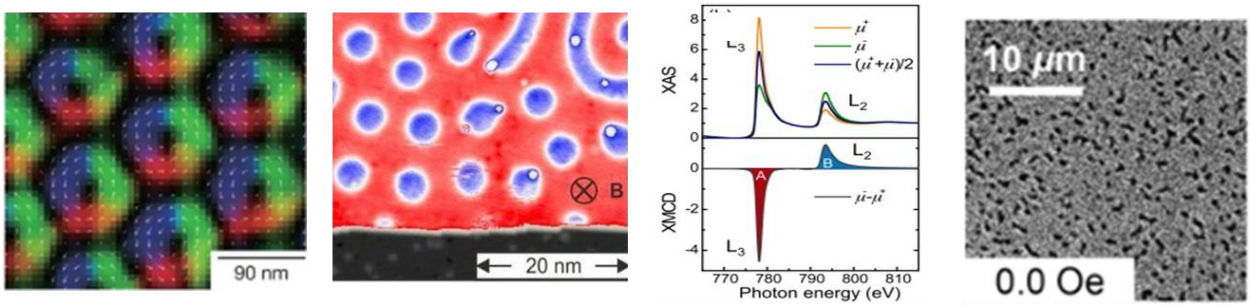

Figure 2-1 (a) Lorentz TEM image of skyrmions, Reprinted with permission from [3], Copyright (2013), Springer Nature, (b) SP-STM image of skyrmions, Reprinted with permission from [9], Copyright (2015), American Physical Society, (c) Difference in X-ray absorption due to different polarization, Reprinted with permission from [10], Copyright (2014), Elsevier, (d) MOKE microscopy image of skyrmions, Reprinted with permission from [16], Copyright (2018), American Chemical Society.

In transmission X-ray microscopy such as Scanning Transmission X-ray Microscopy (STXM), Magnetic transmission X-ray microscopy (MTXM), X-rays are transmitted through the sample and detected using a charge coupled device. Another kind of XMCD based device collects secondary electrons emitted in the 2p

to 3d electron transition process via X-ray absorption. This is called XMCD-PEEM (Photoelectron Emission Microscopy). Examples of XMCD based imaging of skyrmions can be found in Ref. [11-14].

Magneto Optical Kerr Effect (MOKE): When polarized light is reflected from a magnetized surface, the polarization and the intensity of the reflected light can change. Sample magnetization modulates the permittivity tensor differently in different direction by adding off-diagonal components to the tensor. Thus, circularly polarized light gets converted to elliptically polarized light. Depending on relative direction between magnetization and the plane of light incidence MOKE can be divided into three classes. Polar MOKE is particularly relevant to our discussion as it probes samples with out-of-plane magnetization. MOKE microscopy is used widely to image skyrmions [15-17] as it does not require vacuum and image collection is instantaneous. However, resolution of MOKE microscopy is limited by wavelength of light and typically ~1 μm (*Figure 2-1 d*). As smaller skyrmions are more desirable, other high-resolution technics described above could be more useful in future.

2.2.2 Magnetic Force Microscopy

Magnetic force microscopy is based on Atomic force microscopy (AFM) which is one of the prominent examples of scanning probe microscopy. This imaging technic became popular as it does not require vacuum and any cryogenic chambers. Also, the resolution is not limited by diffraction and can be as high as 25 nm laterally. One drawback is slow data collection the probe needs to scan the whole sample area to be imaged. In this section, we will discuss the basic operating principle of AFM and MFM.

Atomic Force Microscopy (AFM) Instrumentation:

Configuration of an AFM is shown in *Figure 2-2*(a). A sharp tip that interacts with the sample is attached to the free end of a cantilever which is mounted on a probe holder. This probe holder is attached to a piezo scanner that controls its position. A laser is reflected from the back of the cantilever to a series of photodiodes. When the tip deflects, the position of the laser in the photodiode changes. Thus, the change in position is recorded as an electrical signal. This information is sent to a controller which produces a

feedback signal to the piezo scanner that controls the tip location in the next step. AFM can be operated in constant height mode or constant force mode. This mode determines the feedback signal that changes the tip height such that either the tip sample distance or the force exerted on the tip by the sample always remains the same.

Operating Mode: Primary technics used in AFM operation is contact mode and tapping mode. In contact mode, the probe comes in close contact with the sample. This applies a repulsive force on the tip. When the topographic features change, this repulsive force changes. This is compared against a set value. To keep the force constant and equal to the set value, a feedback signal drives the piezo to change the probe-sample distance. This feedback signal therefore is a measure of the sample topography. In contact mode, the sample or the tip is often damaged as the tip is dragged along the surface of the sample. Adhesion, electrostatic charges etc can also cause problem in imaging.

In tapping mode, the tip intermittently touches the surface. To achieve this, the cantilever is oscillated near its resonant frequency, which is typically 50-500 KHz, with a vertical displacement amplitude of 20-200 nm. During the downswing, the tip lightly touches the surfaces. When there is attractive (repulsive) force between tip and the sample, the resonant frequency is decreased (increased). An example of resonant behavior of AFM cantilever and its change due to interaction is shown in *Figure 2-2* (b). This change in resonance frequency can be detected in three ways: (i) measuring the phase of the cantilever oscillation relative to the excitation signal (phase detection) (ii) measuring the variation in oscillation amplitude due to tip-sample interaction (amplitude detection) (iii) measuring the shift in resonant frequency (frequency detection). Thus, sample tip interaction is measured. As the tip is not always in contact with the sample, problems regarding damage, adhesion etc. can be minimized.

Basic principles of MFM: In MFM, the magnetic interaction between the sample and the tip is detected. Usually, regular AFM tips are coated with a magnetic material to be used in MFM. The coercivity and moment of the coating depends on the application (e.g. nature of the sample to be probed). The tip is magnetized axially. To decouple the magnetic signal from the topographic signal, interleave mode is used.

This is a two pass technique. In the first pass, the topography of the sample is measured. Then, the probe is lifted vertically to a user-defined height, which is typically 10-100 nm. At this height, all other forces but magnetostatic force is minimized as magnetostatic energy is a long range energy. Therefore, the magnetic signal and the topographic signal can be separated using interleave mode.

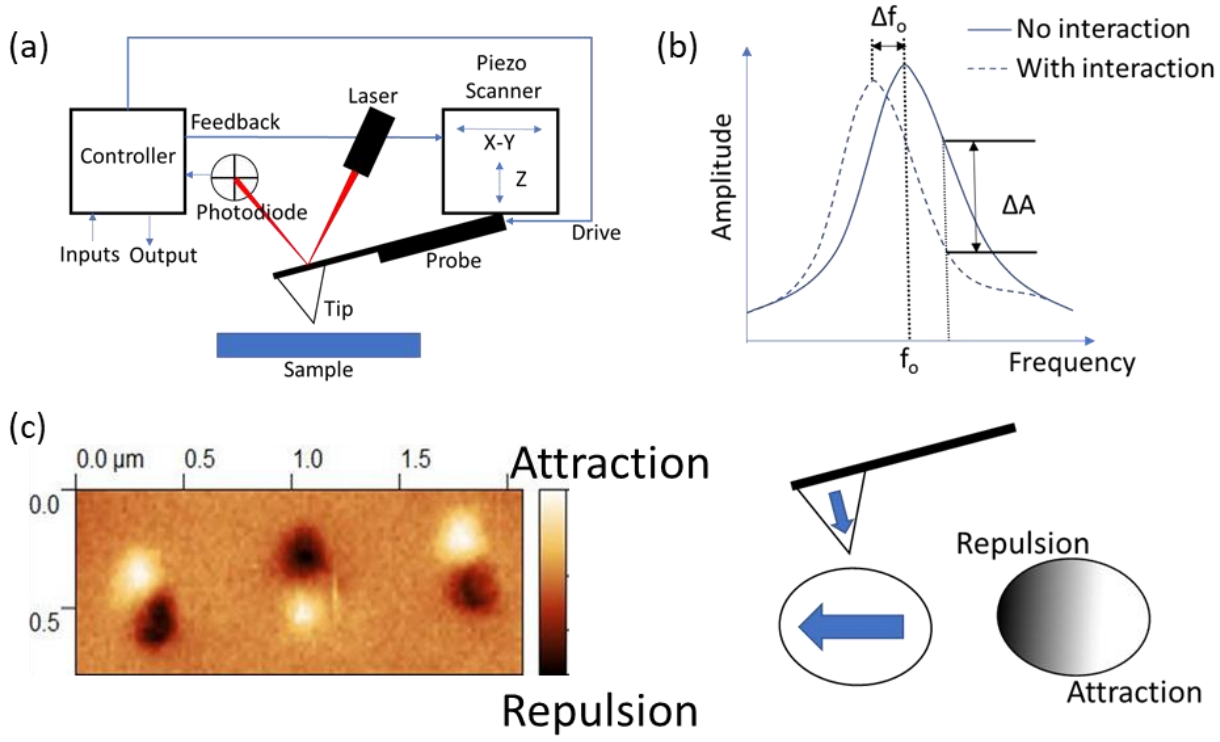

Figure 2-2 (a) Block diagram of an Atomic Force Microscope, (b) Resonant frequency of a cantilever and it's shift due to interaction, (c) Appearance of dark and bright contrast in an MFM image. Left: MFM image of single domain elliptical Cobalt nanomagnets. Right: Illustration of attractive and repulsive forces on the tip due to sample magnetization.

Tip-sample interaction in MFM is rather convoluted due to complex nature of stray field and its interaction with different areas of the tip. However, simplification of the interaction can be made by considering the tip to be a point dipole oriented along z-axis and its only sensitive to the sample magnetization along the z-axis. The force on the tip and change in resonant frequency due to the sample in this case:

$$F = \mu_0 m_{z,tip} . \frac{\partial H_{z,sample}}{\partial z}$$

$$\Delta\omega = -\frac{\omega_0 \mu_0}{2k} m_{z,tip} . \frac{\partial^2 H_{z,sample}}{\partial^2 z}$$

In these equations, μ_0 is the vacuum permeability, $m_{z,tip}$ and $H_{z,sample}$ is respectively the tip and the sample magnetization in z direction, ω_0 is the initial resonant frequency, k is the spring constant of the cantilever. This change is detected through measuring change in phase due to better signal to noise ratio. In the MFM image this shows up as dark and bright contrast. Example of MFM images are shown in *Figure 2-2*(c). Note that, this can only give us a qualitative picture of the magnetization of the sample. Quantitative imaging using MFM is also possible but requires ultra-high vacuum to ensure high-Q resonant behavior [21, 22].

The resolution of MFM depends on several factors. Lateral resolution is primarily dependent on the sharpness of the tip and usually this ranges between 25-50 nm. Vertical resolution depends on electronic, thermal and vibrational noise, tip sample distance, moment of the tip and the sample. If the tip sample distance is low, crosstalk with topographic information can corrupt the magnetic signal. On the other hand, if the distance is very high, signal strength decreases. If tip moment is very high, the signal level increases but it can disturb the sample magnetization. Low moment tip is preferable to minimize tip perturbation, but signal level decreases. The thinner the sample, the harder it becomes to detect any signal. Finally, optimizing scanning parameters such as amplitude setpoint, feedback gain can help to achieve higher resolution.

References:

[1] C. Pfleiderer, A Rosch, A Neubauer, and R. Georgii, "Skyrmion Lattice in a Chiral Magnet," *Science 80*, 915–920(2009).

[2] A. Neubauer, C. Pfleiderer, B. Binz, A. Rosch, R. Ritz, P. G. Niklowitz, and P. Böni, "Topological Hall Effect in the A Phase of MnSi," Phys. Rev. Lett. 102, 186602(2009).

[3] X. Z. Yu, Y. Onose, N. Kanazawa, J. H. Park, J. H. Han, Y. Matsui, N. Nagaosa, and Y. Tokura, "Real-space observation of a two-dimensional skyrmion crystal," Nature 465, 901(2010).

[4] Kovacs et al., “Lorentz microscopy and off-axis electron holography of magnetic skyrmions in FeGe,” Resolution and Discovery, 1, 2-8 (2016).

[5] Tang et al., “Lorentz transmission electron microscopy for magnetic skyrmions imaging,” Chinese Physics B 28, Number 8(2019).

[6] N. Romming, C. Hanneken, M. Menzel, J. E. Bickel, B. Wolter, K. Von Bergmann, A. Kubetzka, and R. Wiesendanger, “Writing and Deleting Single Magnetic Skyrmions,” Science 341, 636 (2013).

[7] S. Heinze, K. Von Bergmann, M. Menzel, J. Brede, A. Kubetzka, R. Wiesendanger, G. Bihlmayer, and S. Blügel, “Spontaneous atomic-scale magnetic skyrmion lattice in two dimensions,” Nat. Phys. 7, 713 (2011).

[8] P. -J. Hsu, “Electric-field-driven switching of individual magnetic skyrmions,” Nature Nanotechnology 12, 123–126(2017).

[9] Romming et al., “Field-Dependent Size and Shape of Single Magnetic Skyrmions,” Phys. Rev. Lett. 114, 177203(2015).

[10] G. van der Laan, A. I. Figueroa, “X-ray magnetic circular dichroism—A versatile tool to study magnetism,” Coordination Chemistry Reviews, Volumes 277–278, Pages 95-12 (2014).

[11] O. Boulle, J. Vogel, H. Yang, S. Pizzini, D. De Souza Chaves, A. Locatelli, T. O. Mente, A. Sala, L. D. Buda-Prejbeanu, O. Klein, M. Belmeguenai, Y. Roussigné, A. Stashkevich, S. Mourad Chérif, L. Aballe, M. Foerster, M. Chshiev, S. Auffret, I. M. Miron, and G. Gaudin, “Room-temperature chiral magnetic skyrmions in ultrathin magnetic nanostructures,” Nat. Nanotechnol. 11, 449 (2016).

[12] S. Woo et al., “Observation of room-temperature magnetic skyrmions and their current-driven dynamics in ultrathin metallic ferromagnets,” *Nat. Mater*. 15, 501–506 (2016).

[13] K. Litzius, I. Lemesh, B. Krüger, P. Bassirian, L. Caretta, K. Richter, F. Büttner, K. Sato, O. A. Tretiakov, J. Förster, R. M. Reeve, M. Weigand, I. Bykova, H. Stoll, G. Schütz, G. S. Beach, and M. Klaüi, "Skyrmion Hall effect revealed by direct time-resolved X-ray microscopy," Nat. Phys. 13, 170 (2017).

[14] Woo et al., "Current-driven dynamics and inhibition of the skyrmion Hall effect of ferrimagnetic skyrmions in GdFeCo films," Nature Communications 9, 959 (2018).

[15] Jiang et al., "Blowing magnetic skyrmion bubbles," Science 349, Issue 6245, 283-286(2015).

[16] Yu et al., "Room-Temperature Skyrmions in an Antiferromagnet-Based Heterostructure," Nano Lett. 18, 2, 980–986 (2018).

[17] Jiang et al., "Direct observation of the skyrmion Hall effect," Nature Physics 13, 162–169(2017).

[18] W. Legrand et al., "Room-temperature current-induced generation and motion of sub-100 nm skyrmions." *Nano. Lett.* 17, 2703–2712 (2017).

[19] A. Hrabec et al., "Current-induced skyrmion generation and dynamics in symmetric bilayers," Nat. Commun. 8, ncomms15765 (2017).

[20] J. Brandão, D. A. Dugato M. V. Puydinger dos Santos J. C. Cezar, "Evolution of Zero-Field Ferrimagnetic Domains and Skyrmions in Exchange-Coupled Pt/CoGd/Pt Confined Nanostructures: Implications for Antiferromagnetic Devices," ACS Appl. Nano Mater. 2, 12, 7532-7539(2019).

[21] H. J. Hug *et al*., "Quantitative magnetic force microscopy on perpendicularly magnetized samples," J. Appl. Phys 83, 5609 (1998).

[22] S. Vock *et al*., "Magnetic vortex observation in FeCo nanowires by quantitative magnetic force microscopy," Appl. Phys. Lett. 105, 172409 (2014).

Chapter 3: Voltage controlled core reversal of fixed magnetic skyrmions

In this chapter, we discuss two different strategies to achieve core reversal of a fixed magnetic skyrmion utilizing Voltage Control of Magnetic Anisotropy (VCMA). Using micromagnetic simulations, we show that, skyrmion core can be reversed solely by modulating the perpendicular anisotropy with an electric field, i.e. without any external magnetic field (Section 3.1). Furthermore, VCMA can assist in STT induced switching of magnetic skyrmion core and reduce energy consumption (Section 3.2). These strategies can have potential for memory application where a relatively simple modification of the standard STT-RAM to include a heavy metal adjacent to the soft magnetic layer (as shown in Figure 3-1). Interfacial DMI originates at the free layer/heavy metal interface equips the free layer to host a skyrmion. One common pair of electrodes is used for application of both VCMA and spin current. With appropriate design of the tunnel barrier, this can lead to energy efficient and fast magnetic memory device based on the reversal of fixed skyrmions.

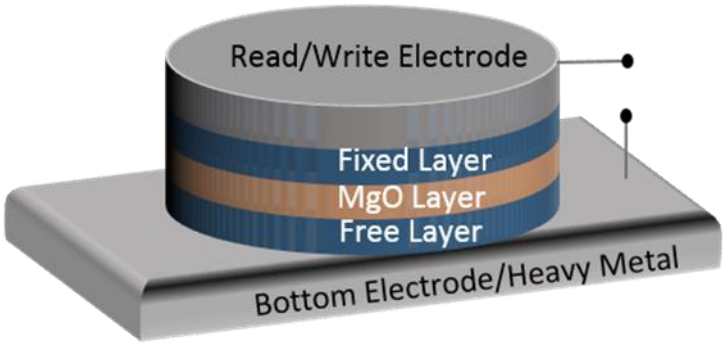

Figure 3-1 Proposed MTJ device, Reprinted with permission from [1], Copyright (2016), Springer Nature.

3.1 Core reversal of skyrmion using only VCMA

In this section, we demonstrate switching reversibly between two skyrmion states and two ferromagnetic states, i.e. skyrmion states with the magnetization of the core pointing down/up and periphery pointing up/down, and ferromagnetic states with magnetization pointing up/down, by sequential increase and decrease of the perpendicular magnetic anisotropy [1]. The switching between these states is explained by the fact that the spin texture corresponding to each of these stable states minimizes the sum of the magnetic

anisotropy, demagnetization, Dzyaloshinskii-Moriya interaction (DMI) and exchange energies. This mechanism along with micromagnetic magnetization states visited during the switching is discussed in section 3.1.1. In Section 3.1.2 we outline the energy efficiency of our proposed device.

3.1.1 Switching Mechanism

We simulate the magnetization dynamics in a perpendicular anisotropy CoFeB/MgO/CoFeB MTJ structure shown in *Figure 3-1* to demonstrate skyrmion core reversal. The bottom CoFeB layer is the free layer which is chosen to be a nanodisk with diameter of 80 nm and thickness of 1 nm. The reversal of the skyrmionic state is achieved through modulation of the perpendicular magnetic anisotropy by applying an electrical voltage. Modulation of the PMA initiates a change in the orientation of the spins and ultimately the equilibrium spin configuration is determined by minimizing the total energy of the system which includes exchange energy, DMI energy, magnetic anisotropy energy and demagnetisation energy. We note that the micromagnetic simulation describes the evolution of the magnetic configuration with time to reach this local minimum. The reversal is a two-step process. The voltage profile and anisotropy energy density change with time, the magnetic energies of the system at various states and configurations of different magnetic states visited during the switching process are shown in *Figure 3-2*(a), *Figure 3-2* (b) and *Figure 3-2*(c, d) respectively. Typical parameters for the CoFeB layer are listed in table 1 [2]. (This is for $Co_{20}Fe_{60}B_{20}$).

We start with a skyrmion whose core points down (*Figure 3-2* (c), state A). In the first step, a positive voltage is applied to the skyrmion which strengthens the perpendicular anisotropy. This forces more spins to point in the direction perpendicular to the x-y plane (i.e. in the direction ±z) to reduce the anisotropy energy. Minimization of curvature energy cost of the circular domain wall (i.e. the spin spiral) demands stabilization of a skyrmion with smaller core radius when PMA is increased. [3]. As a result, the diameter of the skyrmion core keeps reducing with increasing PMA (*Figure 3-2* (c), state B). This makes +z direction the preferred direction among the two possible perpendicular spin orientations (±z). Allowing the spins to relax under this condition would transform the magnetization to a complete ferromagnetic state. However,

once a sufficient number of spins are pointing in the downward (-z) direction (very small core diameter as can be seen in *Figure 3-2* (c), state B), exchange interaction can drive rest of the core spins downward and thus a ferromagnetic state can be achieved while reducing the applied voltage to zero (*Figure 3-2* (c), state C). Increase in the DMI and demagnetization energy due to this transformation (from state A to state C) is compensated by the reduction in anisotropy and exchange energy as shown in *Figure 3-2* (b). This ferromagnetic state is also stable (similar to the skyrmionic state A) and this is what makes it non-volatile. Note that, spins at the edge of a skyrmions confined in a nanodisk tilt in a plane containing the edge surface normal [3]. This can be seen by observing magnetization component in the z-direction of different points along the diameter in *Figure 3-2* (c). Therefore, geometric edge could enable continuous annihilation.

Table 3-1. Parameter values used in section 3.1

Parameters	Value
Saturation Magnetization ($M_{s)}$	1×10^6 A/m
Exchange Constant (A)	2×10^{-11} J/m
Perpendicular Anisotropy Constant ($K_{u)}$	8×10^5 J/m^3
Gilbert Damping (α)	0.03
DMI Parameter (D)	3 mJ/m^2

In the next step, a negative voltage is applied to lower the perpendicular anisotropy. When the perpendicular anisotropy is made sufficiently low by applying a large enough negative voltage, the DMI and demagnetization energies become dominant. The spins then rearrange themselves in this altered energy landscape and transforms from the complete ferromagnetic state to an incomplete skyrmion state as shown in *Figure 3-2* (c), state D. In this state, the spins in the core point up (+z) and the spins in the periphery are tilted downward (-z). Under these conditions, the spins finally stabilize as shown in *Figure 3-2* (c), state E,

forming an incomplete skyrmion with skyrmion number between 0.5 and 1. The tilting starts at the periphery of the disk because this results in a smaller penalty in terms of exchange energy than the tilting of the spins in the core. Finally, the applied voltage is removed, and the zero bias PMA is restored. The spins in the periphery of the nanodisk now rotates completely to the –z direction and the spins in the core retains their upward (+z) magnetization direction. As a result, a skyrmion state with core pointing up is formed as shown in *Figure 3-2* (c), state F. The skyrmion formed in state F is not at equilibrium but can

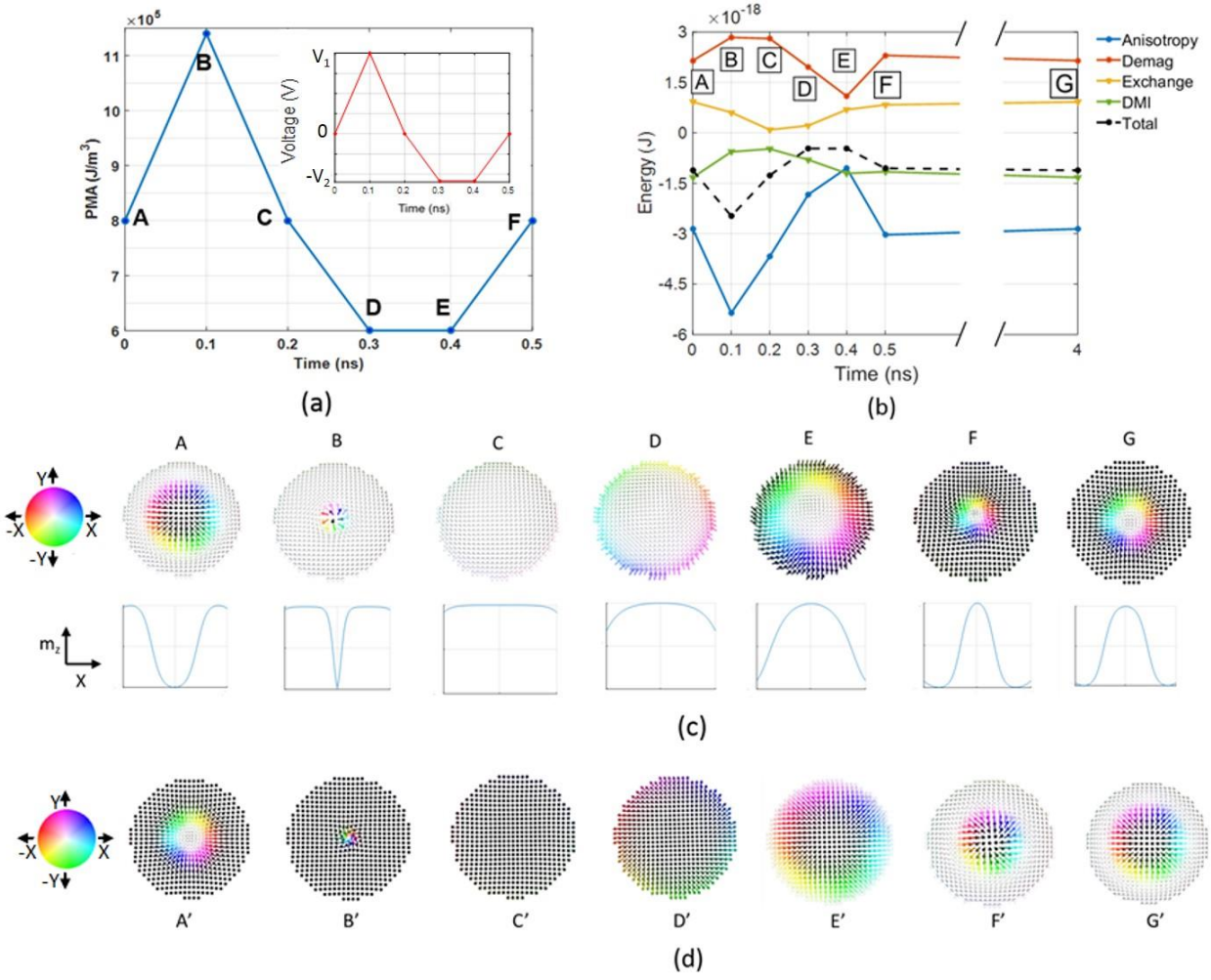

Figure 3-2 (a) Anisotropy energy density and voltage vs time, we considered the rise time and fall time of the electric field to be 100ps (to charge the capacitive MgO layer). This is typically idealized as a trapezoidal shaped voltage pulse with a dwell time between the rise and fall. However, a tent like (triangular) positive pulse is used to show that skyrmion-ferromagnetic transition can occur as fast as 0.2 ns. In other words, we can immediately remove the electric field once it reaches peak value. We could also use a usual symmetrical trapezoidal shaped positive pulse without affecting the switching physics. (b) Energies of different magnetic states at corresponding discrete point in time during the switching process (connecting lines between two points are for ease of visualization and do not represent actual energies as a function of time between these points), (c) spin states at different time and associated magnetization component in the z-direction of different points along the diameter, (d) Different magnetic sates during the reversal of a skyrmion with upward core. Reprinted with permission from [1], Copyright (2016), Springer Nature.

reach equilibrium without any external bias after some time as shown in *Figure 3-2* (c), state G. This is also non-volatile. Hence, we have bistable skyrmionic state "0" and "1". A similar voltage pulse can be applied immediately to the skyrmion in state F to switch to the initial magnetic state. Transition from state A to state F takes 0.5 ns. Therefore, a memory device with speed of 2 GHz can be realized.

We note that each equilibrium configuration (A, C, G) was attained by forming a magnetic configuration that corresponds to a local energy minimum closest to its prior state, i.e. the state from which this system evolves, and separated from other local minima by an energy barrier. Thus, when the system evolves from a state stabilized by high PMA due to VCMA with a positive voltage, it settles to the ferromagnetic state when the VCMA is reduced to zero. But, when the system evolves from a state stabilized by low PMA due to VCMA with a negative voltage, it settles to the skyrmion state when the VCMA is reduced to zero. But it cannot spontaneously switch between the skyrmion and ferromagnetic state due to the energy barrier separating them.

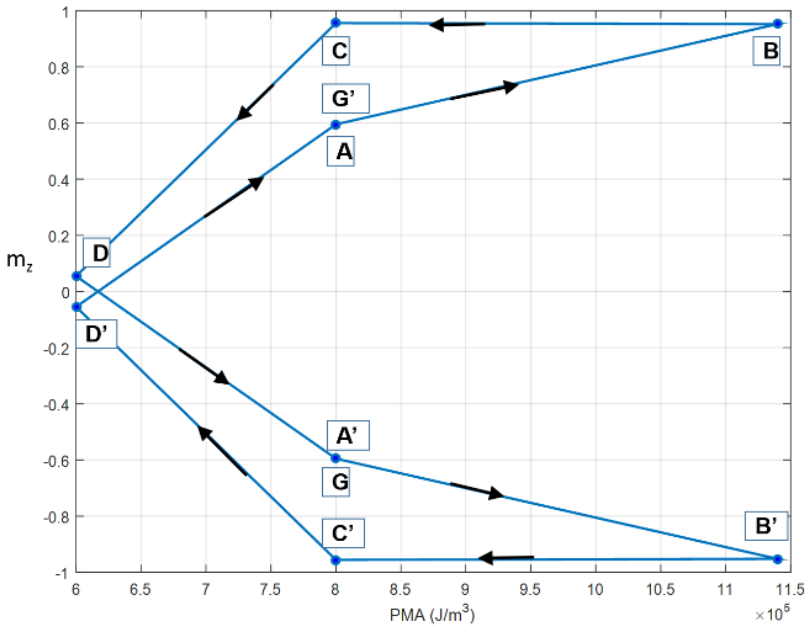

Figure 3-3 Normalized perpendicular magnetization (Mz vs. PMA). Reprinted with permission from [1], Copyright (2016), Springer Nature.

Switching of a skyrmion with upward core spins and downward periphery spins to a skyrmion with downward core spins and upward periphery spins can be achieved by applying the same voltage pulse as

shown *Figure 3-2* (a). The transition through the various magnetic states (from A' to G') during this switching process is shown in *Figure 3-2* (d). We note that the electrically controlled skyrmion core reversal is deterministic. With a sufficiently long positive (negative) voltage pulse, skyrmion-FM (FM-skyrmion) transition probability does not rely on precise pulse withdrawal as these states are stable and separated by an energy barrier. Consequently, reversible switching between all four states (two skyrmion and two ferromagnetic) is possible as can be seen in *Figure 3-3*. The ability to toggle between the possible states makes this device a viable memory element.

3.1.2 Energy Dissipation

We can estimate the energy dissipated in switching between the skyrmions states as follows: the modulation of the interface anisotropy energy is given by $J_{sa}=J_o + aE$, where a, E and J_0 are respectively the coefficient of electric field control of magnetic anisotropy, the applied electric field and the interface anisotropy energy at zero bias field. Now, coefficient of electric field control of magnetic anisotropy is defined as, $a = \frac{\Delta k \times t_{CoFeB}}{\Delta V / t_{MgO}}$. Reported value of "$a$" is ≈100 $\mu J/m^2$ per V/nm with appropriate iridium buffer [4]. Thus, with a 1 nm thick free layer and 1 nm thick MgO layer, $1\times10^5\ J/m^3$ change in the anisotropy energy density can be obtained per volt. Note that a thinner fixed layer would provide large PMA and ensure the magnetization of this fixed layer is not affected by the voltage applied. The required maximum and minimum PMA can be achieved by applying electrical voltages of V_1=3.4 V and V_2= -2 V respectively for the proposed device configuration. These values translate into an energy dissipation of ≈ 2.4 fJ per switching cycle at a switching speed of 2 GHz if all the energy required to charge the capacitive MgO layer (relative permittivity ≈ 7 [5], thickness ≈ 1nm, diameter ≈ 80 nm) is ultimately dissipated. Insertion of a Hafnium (Hf) monolayer between free and MgO layer can increase "a" by 5.2 times [6]. Such optimization can reduce energy dissipation to only ≈ 90 aJ which is five times less than the energy dissipated to switch a conventional CMOS device [7] of comparable speed. The diameter of the nanodisk forming the free layer can be scaled down to 40 nm to further reduce the energy dissipation. However, an advantage of the nanomagnetic element is its non-volatility. Further, substantial reduction of energy dissipation may be

achieved by lowering the electric field needed for the switching process if the coefficient of anisotropy energy change (a) is enhanced in future materials/interfaces. Moreover, we can switch between states in a few nanoseconds, which is competitive for computing applications, particularly given low energy dissipation and non-volatility.

A recent study reported modification of exchange stiffness by applying Electric field [8] which is not considered in our model. However, a positive (negative) electric field will increase (decrease) the exchange stiffness which will enable easy transformation from skyrmion-ferromagnetic (FM-Sk) state which can be understood from the energy profile plotted in *Figure 3-2*(b). We have simulated scenarios considering electric field induced modification of exchange stiffness and verified that switching occurs at lower electric field. Hence, the voltage estimates we present are conservative.

3.1.3 Additional Remarks

MTJ Design: The fixed layer can be designed to be thinner to have much higher PMA which will ensure a minimal effect of changing PMA. In other words, the PMA in this fixed layer can be designed to be strong so that any voltage induced change of magnetic anisotropy will not perturb the magnetization direction of this fixed layer. Additionally, the coefficient of electric field control of magnetic anisotropy in the fixed layer can be tailored to be low. For example, one such method could be not inserting the Hafnium monolayer between the MgO and the fixed layer which will make the coefficient of electric field control of magnetic anisotropy smaller in the fixed layer. Furthermore, one can use a synthetic antiferromagnetic (SAF) [9] layer to increase magnetic stability of the fixed layer and electric field induced magnetization rotation in the fixed layer will be further minimized. Hence, we ignore anti-symmetric modification effects in our model. The synthetic antiferromagnetic (SAF) layer offsets the dipolar interaction between the fixed and the free layer. Hence, we also ignore dipolar effects in our model.

Other ways to control magnetic anisotropy: In addition to directed voltage control of magnetic anisotropy one could modulate the magnetic anisotropy of magnetostrictive nanomagnets with acoustic waves or

voltage generated strain in a piezoelectric layer in elastic contact with the nanomagnet. However, assuming optimistically that ~100 MPa could be generated in a Terfenol-D nanomagnet with magnetostriciton ~ 1000 ppm [10] the effective change in magnetic anisotropy energy density ~10^5 J/m^3 can be achieved. This is about one order of magnitude smaller than the required change in anisotropy. Hence, strain mediated switching of skyrmion states could be feasible only if materials that have much larger magnetoelastic coupling and sufficient DMI (when interfaced with appropriate materials) to form skyrmions are developed.

3.2 Energy efficient and fast reversal of a fixed skyrmions with spin current assisted by voltage controlled magnetic anisotropy

Recent work [11, 12] suggests that ferromagnetic reversal with spin transfer torque (STT) requires more current in a system in the presence of DMI than switching a typical ferromagnet of the same dimensions and perpendicular magnetic anisotropy (PMA). However, DMI promotes stabilization of skyrmions and we report that when the perpendicular anisotropy is modulated (reduced) for both the skyrmion and ferromagnet, it takes much smaller current to reverse the fixed skyrmion than to reverse the ferromagnet in the same time, or the skyrmion reverses much faster than the ferromagnet at similar levels of current.

I^2R loss in spin current induced magnetization reversal can be considerably large. Reducing this loss requires reduction of the switching current, which can be achieved by employing methods to reduce perpendicular magnetic anisotropy (PMA), which temporarily depresses the energy barrier between the "up" and "down" state during spin current induced switching. This can improve the energy-efficiency and switching speed without compromising the thermal stability of the nanomagnet based computing device. Reduction in switching current utilizing VCMA has been shown for magnetization reversal of ferromagnets with uniform magnetization orientation [13, 14]. We show with rigorous micromagnetic simulations that the skyrmion switching proceeds along a different path at very low PMA which results in a significant reduction in the spin current required or time required for reversal. The presence of DMI in a skyrmion system is what distinguishes our current study from those performed on uniformly magnetized ferromagnetic systems. In the previous section, we showed skyrmion core reversal by sequential increase

and decrease of PMA using VCMA only (i.e. no spin current). In this study, while the basic memory operation relies on reversing skyrmion core; the underlying physics (spin wave excitation), the switching agent employed to reverse the core (spin current induced switching facilitated by VCMA) and the switching path between two stable skyrmionic states are completely different.

In this section, we demonstrate a hybrid scheme where application of a small voltage can reduce the threshold current needed for reversal of skyrmions (subsection 3.2.1), present rigorous micromagnetic simulation to explain the underlying physics of the reversal process, and quantify improvements in terms of dissipated energy and switching speed (subsection 3.2.2).

3.2.1 Operating Principle

A simplified Magnetic Tunnel Junction (MTJ) structure for the implementation of our proposed hybrid scheme for switching a magnetic skyrmion (free layer of the MTJ) is shown in *Figure 3-1*. Heavy Metal/Ferromagnet/Insulator trilayer can have epitaxial strain, which has been shown to give rise to a ∧-shaped electric field dependence of magnetic anisotropy [15, 16]. As a result, application of a voltage, regardless of the polarity, will reduce the PMA. However, the direction of the spin current will depend on the polarity of the applied voltage. Skyrmions can be reversed with a spin current when $\vec{m}_p.\vec{m}_c = 1$, where $\vec{m}_p$ is the polarity of spin current and $\vec{m}_c$ is the polarity of the skyrmion core [17]. This is very convenient since we can change the polarity of the applied voltage depending on the required direction of the spin polarized current for reversal and nevertheless achieve PMA reduction due to VCMA. Therefore, if we use a fixed layer with magnetization pointing up (down), we can reverse a skyrmion with core pointing up applying a positive (negative) voltage. Hence, this basic MTJ structure is sufficient to carry out our switching scheme given that an epitaxial strain and therefore a ∧-shaped electric field dependence of magnetic anisotropy is present in the structure. This is well suited to typical magnetic memory applications as this the structure is similar to existing spin transfer torque (STT) RAM and only requires appropriate design of the MgO layer thickness and addition of a heavy metal layer between the free layer and the substrate. Reversing the skyrmion will change the magnetoresistance of the ferromagnet (hard layer)/tunnel

barrier/skyrmion (soft later) MTJ structure appreciably, thereby allowing the skyrmion state to be read easily (more detail in supplement).

Table 3-2 Parameter values used in section 3.2 (Ref. 18, 19).

Parameters	Value
Saturation Magnetization ($M_{s)}$	1.3×10^6 A/m
Exchange Constant (A)	1×10^{-11} J/m
Perpendicular Anisotropy Constant (K_{u1})	1.1 MJ/m^3
Effective Perpendicular Anisotropy $(K_{eff} = K_{u1} - \frac{\mu_0}{2} {M_{sat}}^2)$	43570 J/m^3
Gilbert Damping (α)	0.01
DMI Parameter (D)	1.4 mJ/m^2
Degree of Spin Polarization (P)	0.4

In this study, current is assumed to be uniform along the diameter of the nanodisk. For the sake of simplicity, field like torque and Oersted field due to current flow is not included. This is described in detail in chapter 2. However, as these terms are consistently not considered for all the cases simulated, the key conclusions of this study will not change significantly even if these terms are considered. If the pinned ferromagnetic layer has a high enough PMA, the spin current or the VCMA will not be able to rotate its magnetization significantly. Therefore, modeling the magnetization dynamics in the pinned layer can be avoided without compromising the accuracy of the simulation (see supplementary section for further discussion). Hence, we only simulated the free layer of an MTJ, which was chosen to be a nanodisk of 100 nm diameter and 0.8 nm thickness. Our geometry was discretized into 2×2×0.8 nm^3 cells. We used typical material parameters

of CoFe for the free layer in our simulations listed in the table below compiled from Ref. 18 and Ref. 19. We used a fixed ferromagnetic layer with magnetization pointing up. All simulations were carried out at T=0 K, i.e. effect of thermal noise on magnetization dynamics was not included in this study. However, we note that skyrmion is stable in the presence of room temperature thermal noise.

3.2.2 Magnetization switching in various cases

For these material parameters, ferromagnetic state is the ground state. Skyrmion can be formed by applying a current pulse and emerges as a stable state once formed. We start with a skyrmionic state with spins in the core pointing upwards and spins in the periphery pointing downwards. As our fixed layer points upwards, a positive current will initiate reversal (as, $\vec{m}_p.\vec{m}_c = 1$). We inject a current pulse of 0.1 ns rise and 0.1 ns fall time (shown in *Figure 3-4*) and find the critical switching current and time required for reversal. *Figure 3-4* shows snapshot of magnetization dynamics during the switching process while a spin current of 1×10^{11} A/m^2 was employed. The spin current excites breathing mode of increasing amplitude.

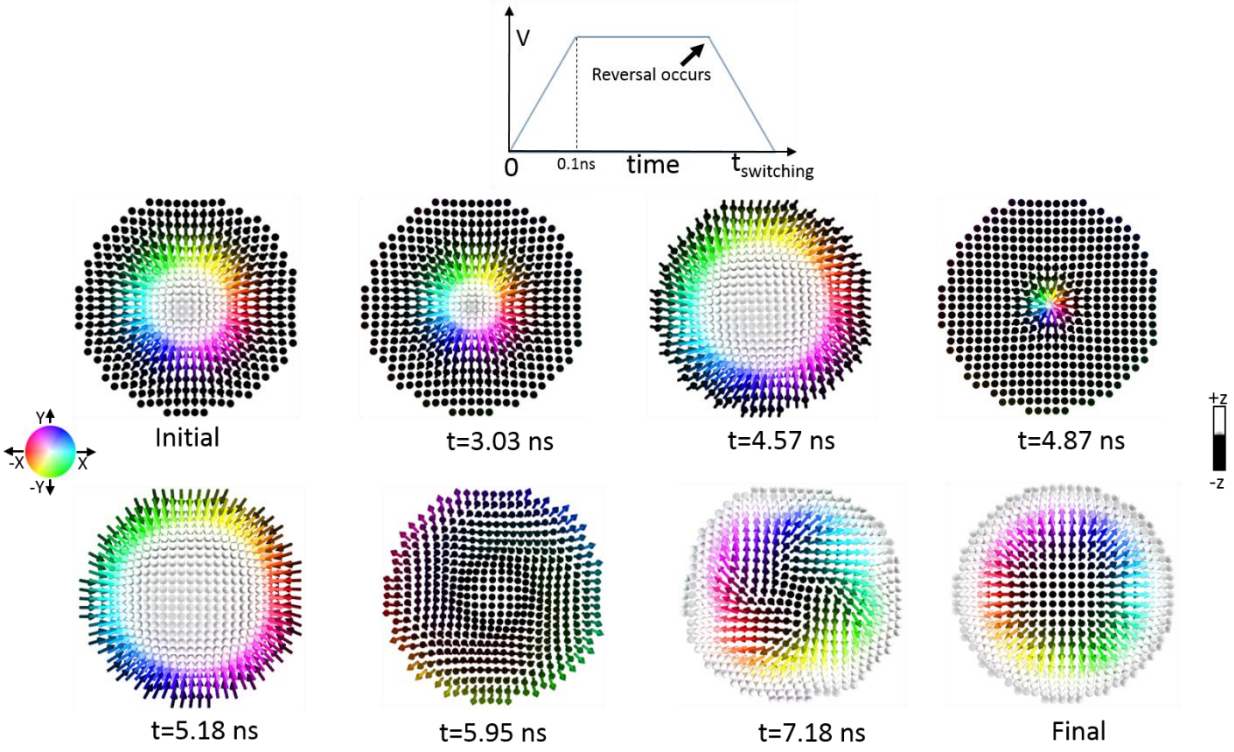

Figure 3-4 Snapshot of magnetization dynamics during the switching process with only spin current (1×10^{11} A/m^2). The voltage pulse is shown on top. Note that, the rotational motion of domain wall spins is not shown here for simplicity. Reprinted with permission from [23], Copyright (2018), Institute of Physics.

Also, the skyrmion texture continually alters between Néel (radial outward and inward) and Bloch (counterclockwise and clockwise) states [20, 21]. These two motions are synchronized. Thus, the breathing mode stabilizes the Néel skyrmion texture at the largest and the smallest core size and Bloch texture in between these Néel states. Due to this spin wave excitation, the skyrmion core expands and shrinks (*Figure 3-4*, t=3.03 ns, 4.57 ns, 4.87 ns, 5.18 ns, 5.95 ns) and eventually reverses. Once reversal occurs (t=7.18 ns) the torque induced by the spin current acts as a damping agent and skyrmion with opposite core polarity is stabilized (*Figure 3-4*, Final). The critical switching current density is found to be 6.5×10^{10} A/m^2 and takes 13.6 ns to complete the switching. The values of switching time and critical current are in line with the values reported in Ref. [17].

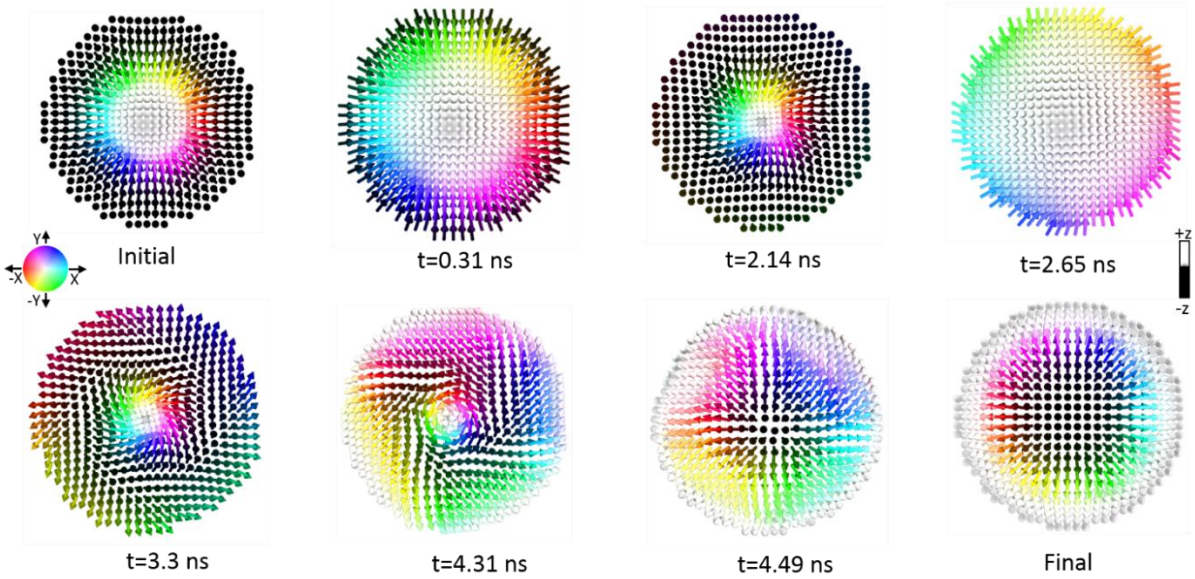

Figure 3-5 Snapshot of magnetization dynamics during the switching process with spin current (6×10^{10} A/m^2) and small ΔPMA (10%). Reprinted with permission from [23], Copyright (2018), Institute of Physics.

Next, we study the effect of reducing PMA on the switching behavior. Reduction in PMA creates alternative path for reversal. We studied two cases, 10% and 20% reduction in PMA (which we denote as ΔPMA=10% and ΔPMA=20%). This reduction in perpendicular anisotropy shifts the easy orientation from perpendicular to in plane with $K_{eff} = -66430\ \mathrm{J}/m^3$ for ΔPMA=10% and $K_{eff} = -176430\ \mathrm{J}/m^3$ for ΔPMA=20%. We assumed 0.1 ns rise and 0.1 ns fall time for both the pulses (i.e. spin current and perpendicular anisotropy

modulation). *Figure 3-5* corresponds to the case where ΔPMA=10%. This switching resembles the previous case where only spin current was used to reverse the skyrmion. The reversal stabilizes a skyrmion with opposite polarity, and after restoring the PMA a skyrmionic state exactly opposite to the initial state stabilizes (*Figure 3-5*, Final). Although the switching behavior remains same, the critical current density is reduced by ~1.6 times compared to the case where no VCMA is applied. The switching time vs. current density is discussed later in this paper.

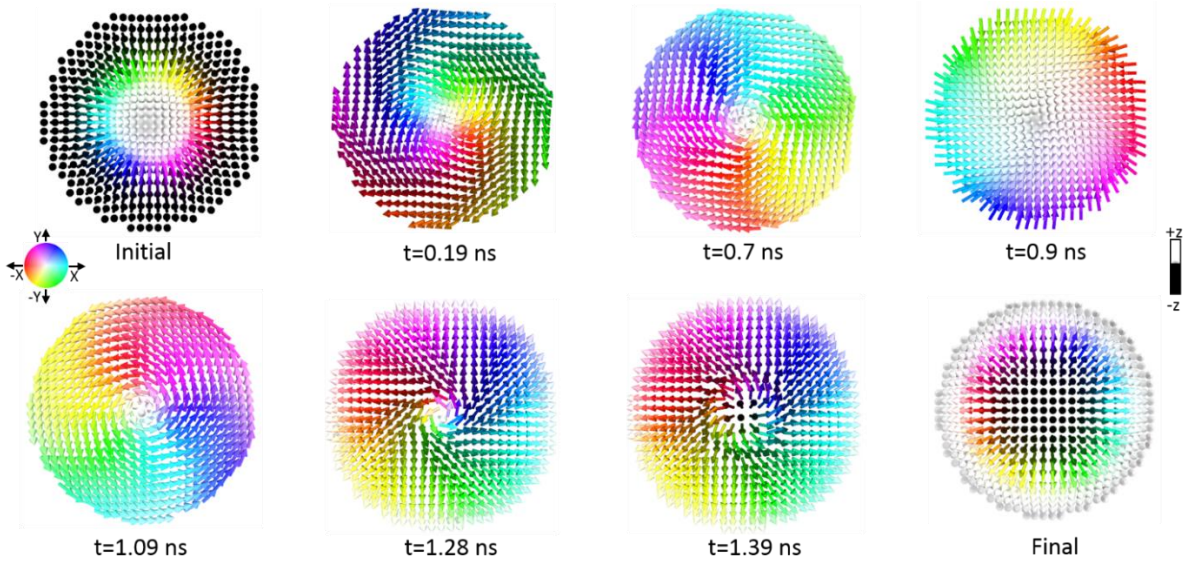

Figure 3-6 Snapshot of magnetization dynamics during the switching process with spin current (1.4×10^{10} A/m^2) and large ΔPMA (20%). Reprinted with permission from [23], Copyright (2018), Institute of Physics.

Interestingly, when PMA is reduced further (ΔPMA=20%), the switching follows a very different trajectory which is shown in *Figure 3-6*. At first, reduction in PMA pushes the peripheral spins to the x-y plane while the core still points upwards. (*Figure 3-6*, t=0.19 ns). The spin wave excitation alters the magnetic texture between circular (clockwise: *Figure 3-6*, t=0.7 ns and counter clockwise: *Figure 3-6*, t=1.09 ns) and radial vortex (*Figure 3-6*, t=0.9 ns) states [23] and ultimately reverses the core (*Figure 3-6*, t=1.39 ns). Therefore, a radial vortex state with core pointing downward is formed (*Figure 3-6*, t=1.39 ns). After reversal, restoring PMA pushes the peripheral spin upwards and thus a skyrmion with polarity opposite to the initial state is

stabilized (*Figure 3-6*, Final). Here, the critical current density is reduced by ~4.6 times compared to the case where no VCMA is applied along with a drastic reduction in switching time.

Figure 3-7 shows switching time vs. current density for the three cases discussed. The critical current and the switching time needed for reversal of the fixed skyrmion is substantially reduced in the latter two cases. Also, with similar level of current, reduction in PMA results in faster switching. We compare this reversal with ferromagnetic reversal in a system with same PMA but no DMI. When, only spin current (i.e. no VCMA is considered) induces reversal, the skyrmionic reversal takes longer time (*Figure 3-7*) than for the ferromagnet without DMI. Furthermore, critical current density is almost 4 times smaller for the ferromagnetic case (not shown in *Figure 3-7*).

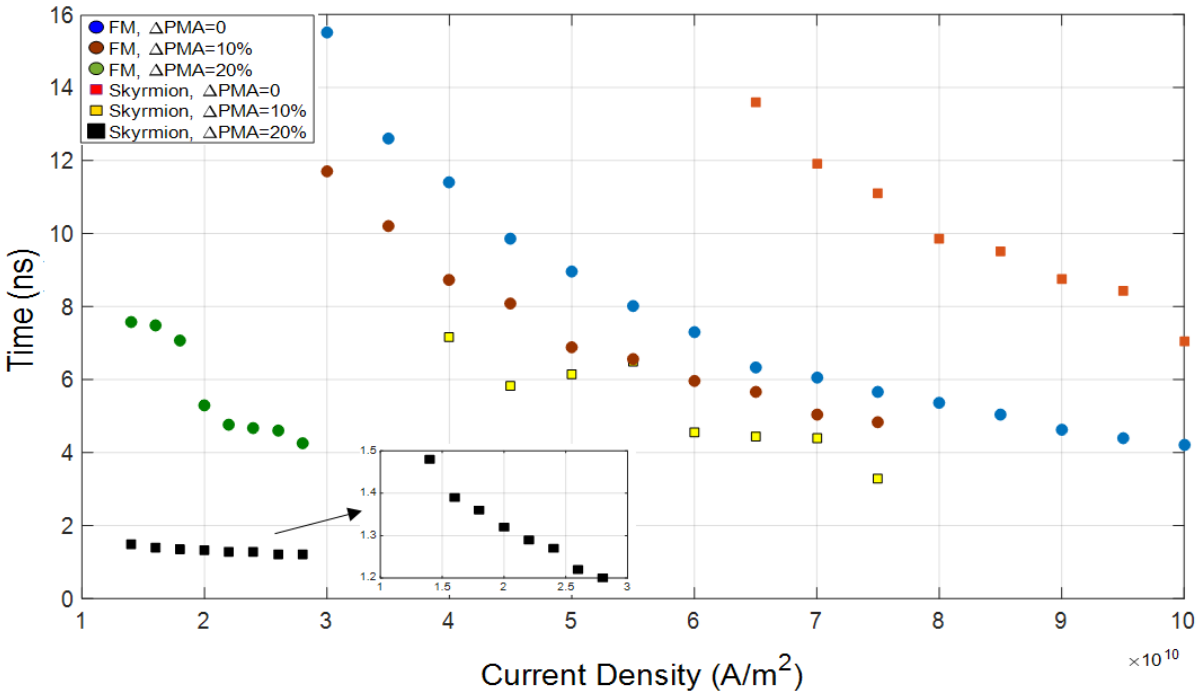

Figure 3-7 Switching time vs current density for ferromagnetic and skyrmion reversal. Reprinted with permission from [23], Copyright (2018), Institute of Physics.

However, the skyrmionic reversal shows an improved performance in the hybrid scheme. The skyrmion switching, in the case with highest VCMA (ΔPMA=20%), can take place approximately *five times faster* (1.5 ns vs. 7.7 ns) than the ferromagnetic reversal for current densities of 1.4×10^{10} A/m^2. For a fixed switching time ~1.5 ns the current density required to switch the skyrmion is *more than 10 times smaller*

than that required to switch the ferromagnet with the same VCMA (ΔPMA=20%) (not shown in *Figure 3-7*). The concomitant write energy (I^2R loss) would therefore show *two orders of magnitude improvement*. Hence, one could *write five times as faster* at the same current density or write with *two orders of magnitude less energy* for the same switching time.

Furthermore, if you consider conventional spin transfer torque (STT) devices without VCMA or DMI, then the current density to switch in ~ 1.5 ns is 3×10^{11} A/m^2 (not shown in *Figure 3-7*) while the corresponding current density to switch in 1.5 ns for the skyrmion with VCMA is ~1.4×10^{10} A/m^2. Thus, the best-case reduction in current density for switching in ~ 1.5ns is about 21 times which can result in ~441 times less energy dissipation.

The modulation of the interface anisotropy energy is given by ΔPMA = aE, where a and E are respectively the coefficient of electric field control of magnetic anisotropy and the applied electric field. The coefficient of electric field control of magnetic anisotropy is defined as, $a = \frac{\Delta k \times t_{CoFe}}{\Delta V / t_{MgO}}$. The theoretical reported value of "a" is 250 $\mu J/m^2$ per V/nm [16]. Thus, with a 0.8 nm thick free layer and 1 nm thick MgO layer, 20% change in the perpendicular anisotropy can be obtained by applying 0.7 volt. The energy required to charge the capacitive MgO layer (relative permittivity ≈ 7 [5], thickness ≈ 1 nm, diameter ≈ 100 nm) is 0.12 fJ which is negligible compared to the typical write energy is conventional spin transfer torque (STT) devices. Thus, the use of VCMA in conjunction with spin current to switch fixed skyrmion based memory devices could result in an order of magnitude smaller energy dissipation compared to switching conventional STT devices or voltage assisted reversal of ferromagnets.

In conclusion, we showed voltage assisted reversal process of skyrmionic state can significantly reduce the write energy over voltage assisted reversal of ferromagnets. Furthermore, comparing this with ferromagnetic switching, we found skyrmion switching induced by spin current can be faster while assisted by a small voltage induced change in perpendicular magnetic anisotropy. Moreover, our proposed device structure can be fabricated with very small modification to the existing spin transfer torque (STT) RAM

device. Hence, this work can contribute significantly towards implementing energy efficient non-volatile nanomagnetic memory devices based on existing spin transfer torque (STT) writing schemes.

References:

[1] D. Bhattacharya, M. M. Al-Rashid, J. Atulasimha, "Voltage controlled core reversal of fixed magnetic skyrmions without a magnetic field," *Sci. Rep.* 6, 31272(2016).

[2] R. Tomasello, E. Martinez, R. Zivieri, L. Torres, M. Carpentieri, and G. Finocchio, "A strategy for the design of skyrmion racetrack memories.," *Sci. Rep.* 4, 6784(2014), J. Torrejon *et al.*, "Interface control of the magnetic chirality in CoFeB/MgO heterostructures with heavy-metal underlayers," *Nat. Commun.*5, 4655(2014).

[3] S. Rohart and A. Thiaville, "Skyrmion confinement in ultrathin film nanostructures in the presence of Dzyaloshinskii-Moriya interaction," *Phys. Rev. B - Condens. Matter Mater. Phys.* 88, no. 18, 1–8(2013).

[4] W. Skowroński *et al.*, "Perpendicular magnetic anisotropy of Ir/CoFeB/MgO trilayer system tuned by electric fields," *Appl. Phys. Express* 8, no. 5(2015).

[5] I.-C. Ho, Y. Xu, and J. D. Mackenzie, "Electrical and optical properties of MgO thin film prepared by sol-gel technique," *J. Sol-Gel Sci. Technol.* 9, no. 3, 295–301(1997).

[6] T. Bonaedy, J. W. Choi, C. Jang, B.-C. Min, and J. Chang, "Enhancement of electric-field-induced change of magnetic anisotropy by interface engineering of MgO magnetic tunnel junctions," *J. Phys. D. Appl. Phys.*48, no. 22, 225002(2015).

[7] S. Datta, V. Q. Diep, and B. Behin-Aein, "What Constitutes a Nanoswitch? A Perspective," in *Emerging Nanoelectronic Devices*, 15–34(2015).

[8] T. Dohi, S. Kanai, A. Okada, F. Matsukura, and H. Ohno, "Effect of electric-field modulation of magnetic parameters on domain structure in MgO/CoFeB," *AIP Adv.* 6, no. 7(2016).

[9] S. Bandiera *et al.*, "Comparison of synthetic antiferromagnets and hard ferromagnets as reference layer in magnetic tunnel junctions with perpendicular magnetic anisotropy," *IEEE Magn. Lett.*, vol. 1, 1–4(2010).

[10] K. Ried *et al.*, "Crystallization behaviour and magnetic properties of magnetostrictive TbDyFe films," *Phys. Status Solidi a-Applied Res.* 167, no. 1, 195–208(1998).

[11] J. Sampaio *et al.*, "Disruptive effect of Dzyaloshinskii-Moriya interaction on the magnetic memory cell performance," *Appl. Phys. Lett.*108, no. 11(2016).

[12] P. H. Jang, K. Song, S. J. Lee, S. W. Lee, and K. J. Lee, "Detrimental effect of interfacial Dzyaloshinskii-Moriya interaction on perpendicular spin-transfer-torque magnetic random access memory," *Appl. Phys. Lett.* 107, no. 20(2015).

[13] Y. Shiota, T. Nozaki, F. Bonell, S. Murakami, T. Shinjo and Y Suzuki, "Induction of coherent magnetization switching in a few atomic layers of FeCo using voltage pulses," Nat. Mater. 11, 39(2012).

[14] W. Wang, M. Li, S. Hageman & C. L. Chien, "Electric-field-assisted switching in magnetic tunnel junctions," Nat. Mater. 11, 64(2012).

[15] Y. Hibino *et al.*, "Peculiar temperature dependence of electric-field effect on magnetic anisotropy in Co/Pd/MgO system," *Appl. Phys. Lett.* 109, no. 8(2016).

[16] P. V. Ong, N. Kioussis, D. Odkhuu, P. Khalili Amiri, K. L. Wang, and G. P. Carman, "Giant voltage modulation of magnetic anisotropy in strained heavy metal/magnet/insulator heterostructures," *Phys. Rev. B - Condens. Matter Mater. Phys.* 92, no. 2(2015).

[17] Y. Liu, H. Du, M. Jia, and A. Du, "Switching of a target skyrmion by a spin-polarized current," *Phys. Rev. B - Condens. Matter Mater. Phys.* 91, no. 9, 1–6(2015).

[18] S. Emori, U. Bauer, S.-M. Ahn, E. Martinez, and G. S. Beach, "Current-driven dynamics of chiral

ferromagnetic domain walls," Nat. Mater. 12, 611(2013).

[19] M. Belmeguenai *et al.*, "Brillouin light scattering investigation of the thickness dependence of Dzyaloshinskii-Moriya interaction in Co0.5Fe0.5 ultrathin films," *Phys. Rev. B* 93, no. 17, 174407(2016).

[20] M. Carpentieri, R. Tomasello, R. Zivieri, and G. Finocchio, "Topological, non-topological and instanton droplets driven by spin-transfer torque in materials with perpendicular magnetic anisotropy and Dzyaloshinskii-Moriya Interaction.," *Sci. Rep.* 5, 16184(2015).

[21] R. H. Liu, W. L. Lim, and S. Urazhdin, "Dynamical Skyrmion State in a Spin Current Nano-Oscillator with Perpendicular Magnetic Anisotropy," *Phys. Rev. Lett.* 114, no. 13(2015).

[22] G. Siracusano *et al.*, "Magnetic Radial Vortex Stabilization and Efficient Manipulation Driven by the Dzyaloshinskii-Moriya Interaction and Spin-Transfer Torque," *Phys. Rev. Lett.* 117, no. 8, 87204(2016).

[23] D. Bhattacharya, M. M. Al-Rashid, J. Atulasimha, "Energy efficient and fast reversal of a fixed skyrmion two-terminal memory with spin current assisted by voltage controlled magnetic anisotropy." Nanotechnology 28 (42), 425201 (2017).

Chapter 4: Skyrmion mediated voltage controlled switching of ferromagnets for reliable and energy efficient 2-terminal memory

In this chapter, we discuss a two terminal nanomagnetic memory element based on magnetization reversal of a perpendicularly magnetized nanomagnet employing a unipolar voltage pulse that modifies the perpendicular anisotropy of the system [1]. Our work demonstrates that the presence of Dzyaloshinskii-Moriya Interaction (DMI) can create alternative route for magnetization reversal that obviates the need for utilizing precessional magnetization dynamics as well as a bias magnetic field that are employed in traditional voltage control of magnetic anisotropy (VCMA) based switching of perpendicular magnetization. We show with extensive micromagnetic simulation, in the presence of thermal noise, that the proposed skyrmion mediated VCMA switching mechanism is robust at room temperature leading to extremely low error switching while also being potentially 1-2 orders of magnitude more energy efficient than state of the art spin transfer torque (STT) based switching. In Section 4.1, we discuss the device structure and magnetization dynamics of our proposed mechanism. In section 4.2 and 4.3 we respectively analyze the switching error rate and switching energy dissipation.

4.1 Device Structure and magnetization dynamics:

Our proposed structure is shown in *Figure 4-1*. PMA and DMI arise due to symmetry breaking at the oxide/free layer and free layer/heavy metal interfaces. We simulated the free layer of the MTJ structure in micromagnetic framework MuMax3. The free layer was chosen to be nanodisk of 100 nm diameter and 1 nm thickness. We only simulated the free layer of our device. This does not affect our results as voltage induced change in the fixed layer PMA and dipolar interaction between the free and the fixed layer can both be negligible when a pinning synthetic antiferromagnetic layer is used on top of the fixed layer. Additionally, in the fixed layer, the coefficient of electric field control of magnetic anisotropy can be tailored to be low and PMA can be designed to be strong to further ensure the magnetization direction of fixed layer is not perturbed due to application of a voltage pulse.

Recent studies reported modification of exchange stiffness by applying Electric field [2] which are not considered in our model. However, increase (decrease) in the exchange stiffness due to a positive (negative) electric field will assist skyrmion-ferromagnetic (ferromagnetic-skyrmion) transformation. We verified this by simulating scenarios considering electric field induced modification of exchange stiffness and found that switching occurs at lower ΔPMA. Hence, the estimated voltage or energy dissipation in this study can be considered conservative.

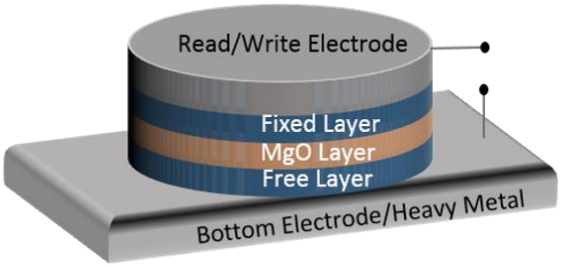

Figure 4-1 (a) Simple schematic representation of a magnetic tunnel junction, Reprinted with permission from [1], Copyright (2018), American Chemical Society.

The material parameters used in the simulations are: saturation magnetization M_s=1.3× 10^6 A/m, perpendicular anisotropy K_{u1} = 1.1 MJ/m^3, exchange stiffness A_{ex}=25 pJ/m and Gilbert damping coefficient α=0.01 which are commonly found values for ferromagnets. Effective perpendicular anisotropy, $K_{eff} = K_{u1} - \frac{1}{2}\mu_0 {M_s}^2$=4.5× 10^4 J/m^3 without considering barrier reduction due to DMI. In our simulations, we choose DMI parameter D=1.2 mJ/m^2. This DMI value is less than the critical value ($D_{crit} = \frac{4}{\pi}\sqrt{AK_{eff}}$ =1.35 mJ/m^2) needed to form a skyrmion at this PMA. Hence, (quasi)ferromagnetic state emerges as the only stable state where the spins at the periphery slightly tilt towards the x-y plane.

Next, we study the behavior of the nanomagnet when PMA in the system is reduced through VCMA from 1.1 MJ/m^3 to 0.94 MJ/m^3. The magnetization dynamics is shown in *Figure 4-2*(a). We take a quasi-FM state with spins tilting slightly at the disk edge (*Figure 4-2*b, 0 ns) as our initial state found by relaxation of an upward ferromagnetic state for 5 ns. When the PMA in the system is reduced, peripheral spins start to tilt more in the planar direction and undergo 180° rotation. The amount of rotation is smaller for the spins that are closer to the core and spins at the core do not budge from their initial position. Therefore, we find

a state where the spins at the core point up (+z) and the spins at the periphery are tilted downward (-z) and a core-up Neel skyrmion is formed (*Figure 4-2*b, 0.6 ns). Once the skyrmion is formed, breathing mode is excited due to which the skyrmion core expands and shrinks. Hence, the magnetization state of the system alternatively visits the skyrmionic and the quasi ferromagnetic state (*Figure 4-2*b). During this transition, clockwise and counterclockwise incomplete Bloch skyrmions appear as intermediate states (*Figure 4-2*b, 0.4 ns and 0.8 ns).

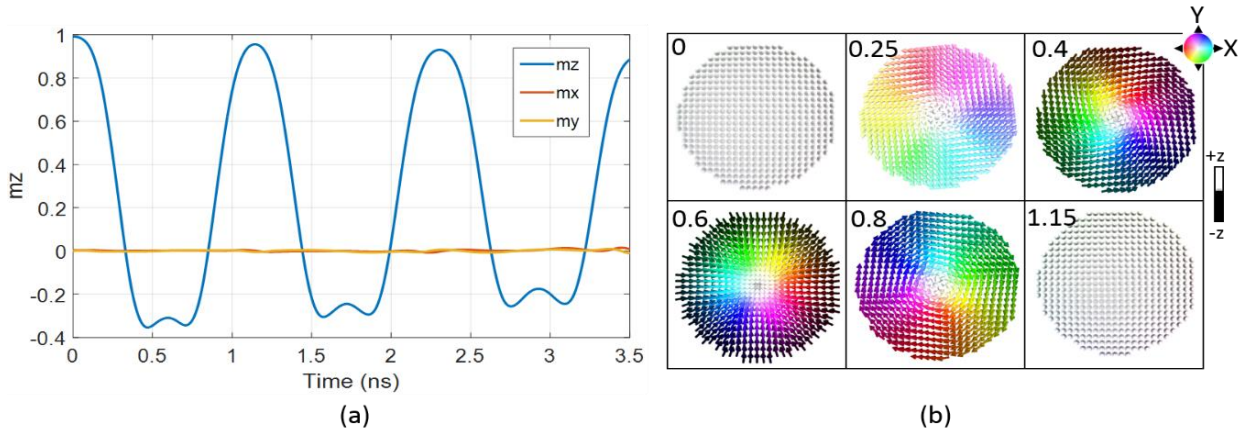

Figure 4-2 (a) Change in magnetization due to reduction in PMA, (b) Magnetization states visited during the first cycle of breathing mode, top left corner shows time in nanosecond. Reprinted with permission from [1], Copyright (2018), American Chemical Society.

When the voltage pulse is withdrawn, the perpendicular anisotropy in the system is restored. To reduce the anisotropy energy, spins are forced to point in the direction perpendicular to the x-y plane, i.e. along the z-axis. Therefore, restoration of PMA makes the up or down directions (i.e. ±z directions) the preferred orientations. Depending on the pulse width (PW) of the applied voltage pulse, the magnetization can be driven to upward or downward oriented ferromagnetic state. Magnetization dynamics for five different pulse width are shown in *Figure 4-3*. The magnetization reversal cannot take place if the pulse width is smaller than the time it takes to form a skyrmion (*Figure 4-3*, PW=0.4 ns) or if the pulse withdrawal time coincides with the expansion of skyrmion (*Figure 4-3*, PW=1.1 ns). Successful switching can be accomplished only if the pulse withdrawal coincides with skyrmion inbreathing (i.e. shrinking) motion (*Figure 4-3*, PW=0.5-0.7 ns) as restoration of PMA by withdrawing the voltage pulse when the skyrmion

is breathing in promotes further shrinkage of the core. Therefore, the skyrmionic state annihilates and transforms into a downward ferromagnetic state. As previously mentioned, while breathing, Bloch skyrmions appear as intermediate states. During the annihilation through continual reduction of core size, skyrmion remains as Bloch type (*Figure 4-3*).

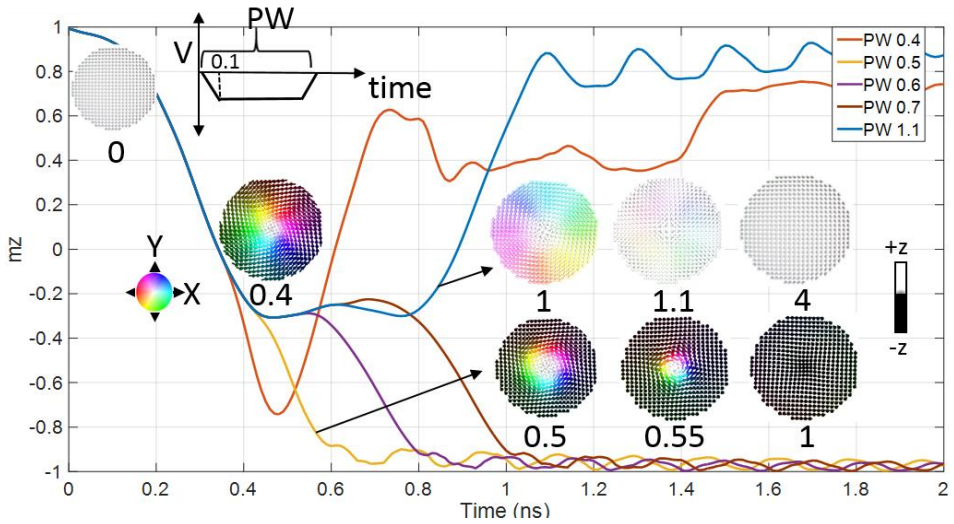

Figure 4-3 Magnetization dynamics in response to voltage pulse of different pulse width. The voltage pulse is shown on the top left corner. The time to reach maximum voltage is taken to be 0.1 ns. Magnetization states visited due to the application of voltage pulse of PW=1.1 ns (top) and PW=0.5 ns (bottom) are shown to elaborate the dependence of pulse width on the final magnetization state. (NOTE: No thermal noise included here). Reprinted with permission from [1], Copyright (2018), American Chemical Society.

We note that, in a magnetic system, strict topological protection does not exist and micromagnetic energy balance plays an important role in addition to topology in its stability. Hence, transition between distinct topological states can be achieved by overcoming an energy barrier and skyrmion can be annihilated when subjected to external stimuli such as thermal perturbation, spin polarized current etc. [3,4]. Additionally, spins at the edge of a skyrmion confined in a nanodisk tilt in a manner that they have a magnetization component along the x-y plane. This geometric edge effect could enable continuous annihilation. To further elucidate the switching mechanism, we analyze the temporal evolution of topological charge (*Figure 4-4*). Three distinct regions can be identified from the *Figure 4-4*. During the formation of the skyrmion from the ferromagnetic state, topological charge increases from 0 to 1. After the formation, the PMA is restored

and the skyrmion radius continually decreases. While shrinking, the topological nature is retained and therefore the topological charge remains unchanged. A sharp transition is observed when the skyrmion is annihilated. Annihilation ensures formation of a topologically trivial ferromagnetic state. Hence, the topological charge vanishes to zero.

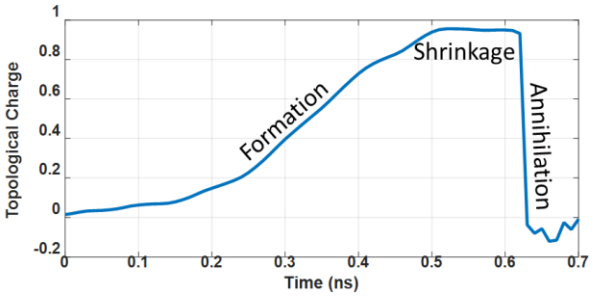

Figure 4-4 Evolution of topological charge during the switching, Reprinted with permission from [1], Copyright (2018), American Chemical Society.

To analyze the evolution of magnetic energies of the system during the switching process, different energies along with magnetic configurations of different states visited are shown in *Figure 4-5*. When the anisotropy is lowered (state 1- state 3), an incomplete skyrmion forms. Increase in the anisotropy and the exchange energy is compensated by the reduction in the demagnetization energy and enables this transformation. Thereafter, the voltage pulse is withdrawn, which results in a transformation to an intermediate skyrmion

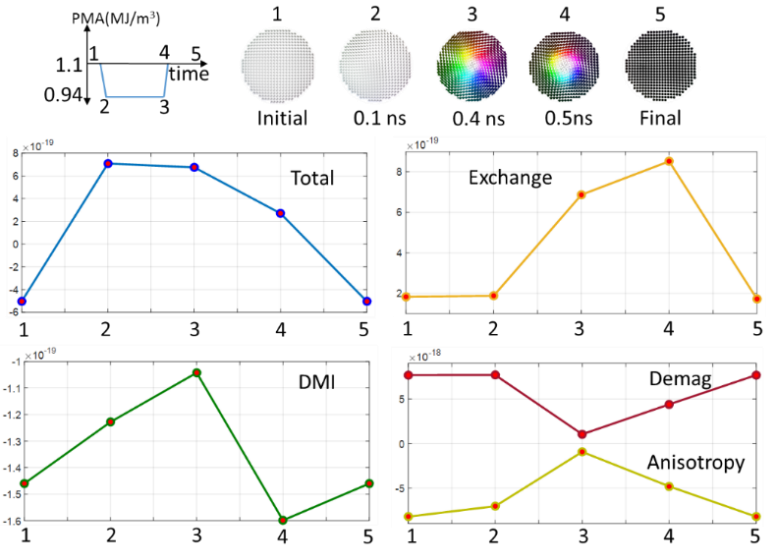

Figure 4-5 Evolution of magnetic energies during the switching. Reprinted with permission from [1], Copyright (2018), American Chemical Society.

state (state-4). The DMI energy reaches the lowest value at this state. Finally, the skyrmion annihilates which brings back the system to its initial energy state.

We show in *Figure 4-6*, magnetization dynamics of our proposed mechanism including the following:

(i) Ambient magnetic field: We consider a typical ambient field of 10 Oe in two different directions and show that the magnetization dynamics is not affected due to this ambient field (*Figure 4-6*(a)).

(ii) Perturbative spin current: With voltage control of magnetic anisotropy (VCMA) scheme, there is always some perturbative spin current. Considering the lower bound of RA product ≈ 225 ohm. μm^2 [5], (i.e. maximum perturbative current) our simulations show that the magnetization dynamics involving the skyrmion mediated switching does not deviate in the presence of this spin current.

(iii) Electric field induced modulation of DMI: Electric field induced change in DMI is calculated to be 26 fJ/(Vm) [6]. Application of 1.6 V will change the DMI parameter by ~40 μJ/m^2. We included such voltage induced modification of DMI in our simulations. We also simulated a case where the change in DMI due to electric field was considered to have same amplitude as change in PMA (100 fJ/Vm). In both cases, we show that the switching physics remains unchanged and the magnetization dynamics is negligibly affected.

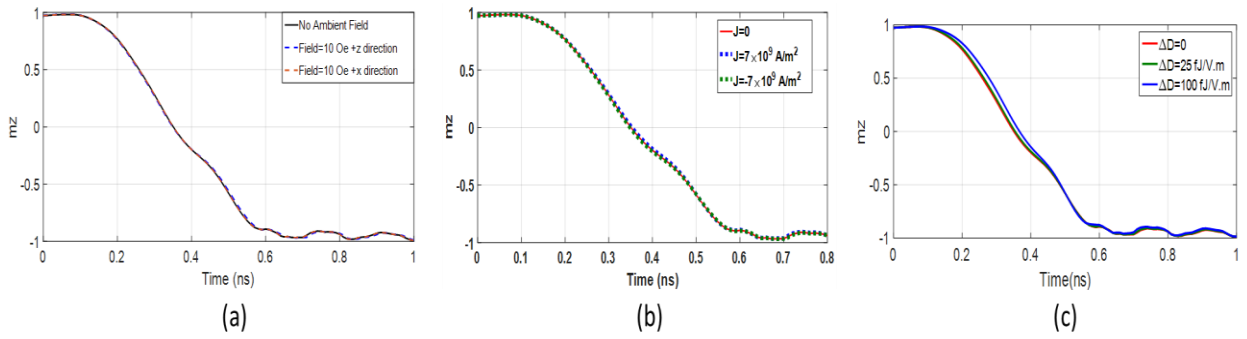

Figure 4-6 (a) Magnetization dynamics with and without considering ambient field during a switching event, pulse width=0.5 ns, (b) Magnetization dynamics with and without the perturbative spin current in addition to the VCMA. Current density was taken to be J=7×10^9 A/m2 which corresponds to resistance area product of about 225 ohm. μm^2. (c) Comparison of magnetization dynamics with and without modulation of DMI value due to application of an electric field for switching with a voltage pulse of 0.5 ns pulse width. Reprinted with permission from [1], Copyright (2018), American Chemical Society.

4.2 Switching Error Analysis under Thermal Noise:

The skyrmion mediated reversal is oscillallatory in nature but nevertheless does not involve precession. Prior precessional schemes without DMI that involve precession around a effective magnetic field, suffer

from large error rates, possibly due to incoherence in magnetization dynamics, i.e. deviation from the single domain (macrospin) state, affects the switching. However, in our scheme, we accept that the reversal mechanism is inherently incoherent and then device a way to use DMI to provide a robust and reliable pathway among the multitide of pathways available for incoherent switching. This makes our scheme physically different and potentially more robust to thermal noise than other precessional schemes for switching ferromagnets. This is corroborated by rigorously simulating the switching behavior and calculating the switching probability using various voltage pulse width in the presence of room temperature thermal noise (*Figure 4-7* (a)). An upward ferromagnetic state was relaxed for 1 ns and was subjected to voltage pulse of pulse width ranging from 0.4 ns to 1 ns. The voltage pulse is same as shown in *Figure 4-3*. Due to computational limitation only 100 events were simulated for every case. Switching is considered to be successful if m_z<-0.7 after 2 ns of pulse withdrawal. The probability shows an oscillatory behavior and between 0.48 ns to 0.68 ns all simulated events switched successfully. We picked a pulse width of 0.52 ns which is in the middle of this range and performed 10,000 successful simulations which proves the reliability of our proposed switching scheme.

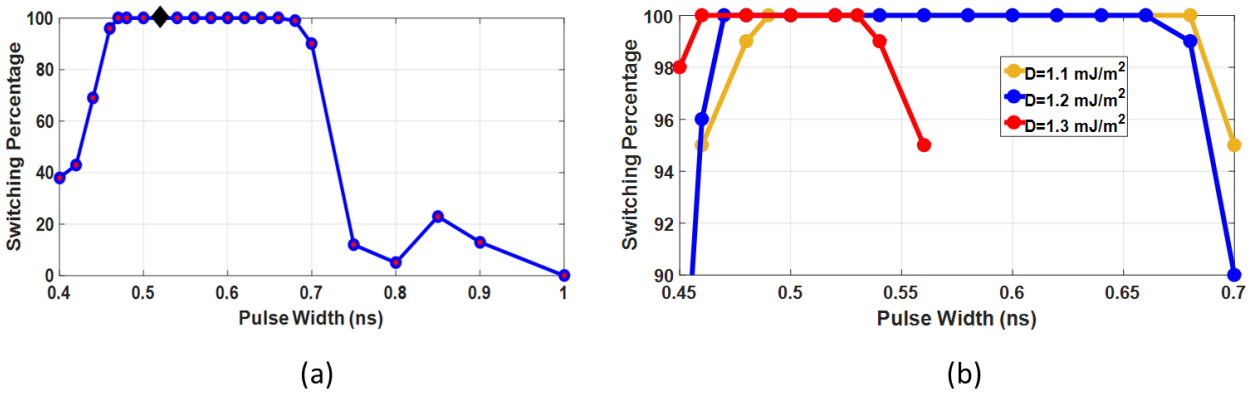

Figure 4-7 (a) Switching probability vs pulse width. The diamond shows the pulse width for which 10,000 simulations were carried out. The blue line is a guide to the eye. Thermal noise is included in the magnetization dynamics. (b) Switching probability vs. pulse width for three different DMI values, Reprinted with permission from [1], Copyright (2018), American Chemical Society.

To study the sensitivity of our approach to DMI strength, we study switching probability vs. pulse width for three different DMI values (*Figure 4-7*(b)). Increasing DMI value increases breathing frequency and shifts the probability curve to left. This gives rise to a spread in the switching probability. However, there

is considerable overlap (pulse widths between ~480 ps to 540 ps) for the three different DMI values where the switching probability is ~100%. Therefore, choosing a correct pulse width can make our scheme potentially immune to device variation.

Next, we investigate the effect of disorders. the free layer was configured to have a random grain structure of average grain size of 4 nm using Voronoi tessellation (*Figure 4-8*). Perpendicular anisotropy and DMI values were drawn from a similar Gaussian distribution with mean PMA of 1.1 MJ/m^3 and mean DMI of 1.2 mJ/m^2 with 10% standard deviation while easy axis orientation was assumed to be distributed with a 3% standard deviation. A 10% reduction of exchange coupling between grains were also considered. The switching probability of both precessional and skyrmion mediated switching were calculated (*Figure 4-9 (a, b)*). For precessional switching, an in-plane external magnetic field of 200 Oe along +x axis was employed while VCMA induced reduction in PMA was taken to be 1×10^5 J/m^3. All other parameter values were taken to be the same as skyrmion mediated switching. No DMI was considered in this case.

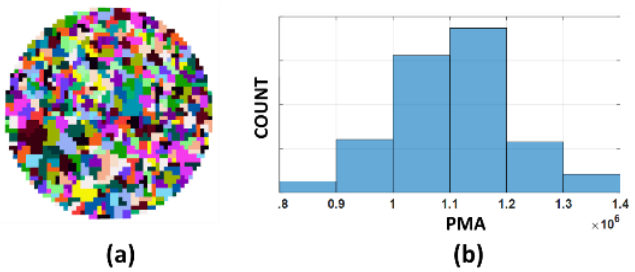

Figure 4-8 (a) Random grain orientation, (b) Gaussian distribution of PMA. Reprinted with permission from [1], Copyright (2018), American Chemical Society.

The peak switching probability is shifted as well as the switching percentage is deteriorated in both the cases, however, the deterioration is much smaller in the skyrmion mediated VCMA switching scheme. While 100% switching was achieved for pulse widths between 0.44 ns to 0.48 ns in the skyrmion mediated case with or without DMI variation, 3% WER was observed for best case precessional switching. We further simulated 1000 events for best case pulse widths. Skyrmion mediated switching showed 0 errors without considering DMI variation and 1 error considering DMI variation while precessional switching showed 54 errors. This proves that VCMA switching is more robust to disorders in the presence of room temperature thermal noise compared to precessional VCMA switching. We note that, a large defect density was

deliberately incorporated so that the switching error deteriorates to a point that 100 (and in limited cases 1000) simulations are enough to bring out the difference between the two switching schemes. For lower defect density we expect the skyrmion mediated VCMA scheme will again be much more robust than the simple precessional VCMA scheme, but the switching error is both schemes will be much lower and larger number of simulations will be needed to establish the WERs.

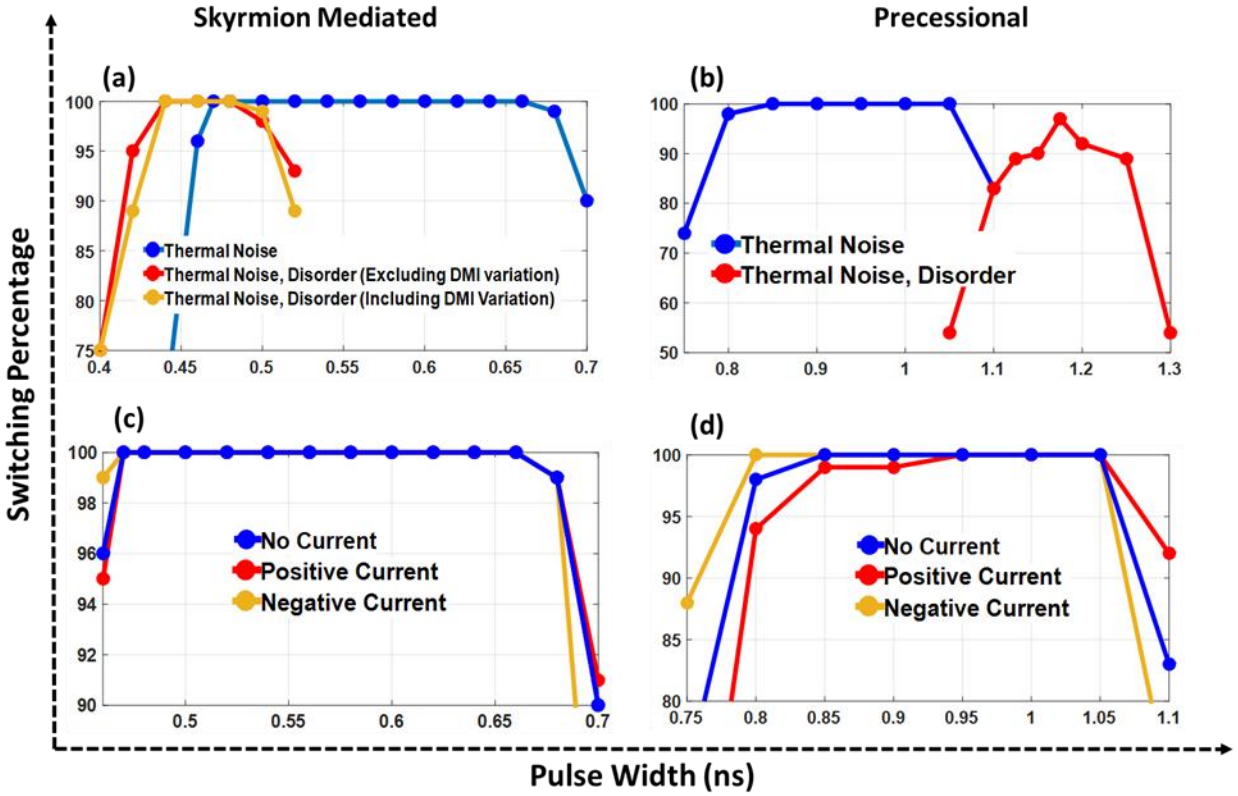

Figure 4-9 Switching probability in skyrmion mediated vs. precessional VCMA switching scheme with (a, b) disorder and (c, d) perturbative spin transfer torque. Reprinted with permission from [1], Copyright (2018), American Chemical Society.

Finally, with any "purely" voltage control of magnetic anisotropy (VCMA) scheme, there is always some perturbative spin current (although much smaller than STT switching) that can lead to switching error. Furthermore, across a wafer, the resistance area product can vary significantly (Ref. [5] estimates the variation to be in the range of 225-650 ohm.μm^2. Considering the lower bound of RA product, (i.e. maximum perturbative current) our simulations show that the magnetization dynamics involving the skyrmion mediated switching does not deviate in the presence of this spin current (*Figure 4-6*) and is therefore extremely robust to this perturbative spin current. *Figure 4-9* (c, d) shows that additional STT

does not cause further increase in WER for skyrmion mediated switching but the WER rate for the precessional switching can deteriorate significantly.

Write error rate (WER) in the conventional VCMA induced switching strongly depends on the voltage pulse duration. Peak switching probability is attained when pulse width is set to half period of magnetization precession. However, experimental studies achieved WER of only 4×10^{-3} [7], possibly due to incoherent magnetization states during the switching process that result in substantially higher error rates than predicted by single domain simulations of magnetization dynamics and presence of finite perturbative spin current. We note that the tolerable error limit for memory application can be 10^{-15} necessitating an iterative approach to lower the WER. For example, WER of 10^{-9} is achieved with 4 iterations while 10 iterations were needed to improve the WER to 10^{-17} [5]. This technique obviously consumes more energy and increases write time substantially. We evaluated the performance of our proposed method under room temperature thermal perturbation. Reliable performance with $<10^{-4}$ switching error in the pulse width between the range of 0.48 ns to 0.68 ns was found. We note that we could only run 10,000 simulations (as solving the magnetization dynamics with thermal noise takes a lot of computational time) and saw no switching error. Hence, we only claim $<10^{-4}$ switching error (which is an order magnitude better than other incoherent switching schemes in the presence of thermal noise [5]), while our scheme could be even more robust to switching in the presence of thermal noise. Our switching mechanism also performs better in the presence of disorder and perturbative spin current. This method therefore has the potential to eliminate or at least reduce the iterative write process which will consequently lower the write time and energy dissipation.

4.3 Energy Dissipation:

The modulation of the perpendicular magnetic anisotropy ΔPMA = aE, where a, and E are respectively the coefficient of electric field control of magnetic anisotropy, the applied electric field. The coefficient of electric field control of magnetic anisotropy is defined as, $a = \frac{\Delta k \times t_{free}}{\Delta V / t_{MgO}}$. Reported value of "$a$" is ≈100

$\mu J/m^2$ per V/nm. Thus, with a 1 nm thick free layer and 1 nm thick MgO layer, $1\times10^5\ J/m^3$ change in the anisotropy energy density can be obtained per volt. The required modulation of PMA can be achieved by applying a voltage pulse of 1.6 V for the proposed device configuration. These values translate into an energy dissipation of ≈ 0.6 fJ per switching cycle at a switching speed of ~2 GHz if all the energy required to charge the capacitive MgO layer (relative permittivity ≈ 7, thickness ≈ 1nm, and diameter ≈ 100 nm) is ultimately dissipated.

Previous studies showed that DMI deteriorates the thermal energy barrier of a MTJ cell [8, 9]. For the DMI value used in our simulations, the thermal energy barrier can decrease by 20%. In other words, to maintain the same thermal stability we need a K_{eff} that is 20% higher than that of a system without any DMI. Additionally, one needs to reduce the anisotropy so that the skyrmion emerges as an intermediate state. This reduction is larger than the value needed to drive the anisotropy just in plane which is required for a system without DMI. Nevertheless, the energy dissipation is not significantly different (same order of magnitude as other VCMA schemes). As such, any non-volatile memory scheme with potential to switch a bit with < 1 fJ/bit energy dissipation is extremely competitive and 2 orders of magnitude more energy efficient than spin transfer torque random access memory (STT-RAM devices).

In summary, our proposed method, is more robust to thermal noise, disorder, perturbative spin currents and does not need a bias magnetic field, unlike VCMA induced reversal of magnetization without DMI where the magnetization rotates to upward or downward ferromagnetic state with equal probability when the voltage pulse is withdrawn and precise precessional dynamics is required for switching. The key finding in this work is that the inclusion of a small DMI in the system can create an alternative pathway for skyrmion mediated incoherent reversal between two stable single domain ferromagnetic states. Therefore, deterministic magnetization reversal is possible without depending on the precessional motion of the magnetization about an in plane magnetic field.

References:

[1] D. Bhattacharya and J. Atulasimha., "Skyrmion-mediated voltage-controlled switching of ferromagnets for reliable and energy-efficient two-terminal memory," ACS applied materials & interfaces 10 (20), 17455-17462 (2018).

[2] T. Dohi, S. Kanai, A. Okada, F. Matsukura, and H. Ohno, "Effect of electric-field modulation of magnetic parameters on domain structure in MgO/CoFeB," AIP Adv. 6, no. 7(2016).

[3] A. D. Verga, "Skyrmion to ferromagnetic state transition: A description of the topological change as a finite-time singularity in the skyrmion dynamics," *Phys. Rev. B* 90, no. 17(2014).

[4] S. Rohart, J. Miltat, and A. Thiaville, "Path to collapse for an isolated Neel skyrmion," *Phys. Rev. B - Condens. Matter Mater. Phys.*, vol. 93, no. 21, 1–6(2016).

[5] C. Grezes et al, "Write Error Rate and Read Disturbance in Electric-Field-Controlled Magnetic Random-Access Memory" IEEE Magnetics Letters 8, 3102705 (2017)

[6] H. Yang, O. Boulle, V. Cros, A. Fert, and M. Chshiev, "Controlling Dzyaloshinskii-Moriya Interaction via Chirality Dependent Atomic-Layer Stacking, Insulator Capping and Electric Field" Sci. Rep. 8, 12356 (2018).

[7] Y. Shiota *et al.*, "Evaluation of write error rate for voltage-driven dynamic magnetization switching in magnetic tunnel junctions with perpendicular magnetization," *Appl. Phys. Express* 9, no. 013001(2016).

[8] P. H. Jang, K. Song, S. J. Lee, S. W. Lee, and K. J. Lee, "Detrimental effect of interfacial Dzyaloshinskii-Moriya interaction on perpendicular spin-transfer-torque magnetic random access memory," *Appl. Phys. Lett.* 107, no. 20(2015).

[9] J. Sampaio *et al.*, "Disruptive effect of Dzyaloshinskii-Moriya interaction on the magnetic memory cell performance," *Appl. Phys. Lett.* 108, no. 11(2016).

Chapter 5: Creation and annihilation of non-volatile fixed magnetic Skyrmions using voltage control of magnetic anisotropy

In this chapter, experimental manipulation of fixed magnetic skyrmions using voltage controlled magnetic anisotropy is discussed. Voltage control of skyrmions has recently been experimentally investigated. A scanning probe microscope tip was, for example, used to modify exchange interaction in an iron monolayer to create skyrmions at very low temperatures and high magnetic fields [1]. It has also been shown that room temperature skyrmion nucleation and annihilation can be achieved, by, primarily, changing the saturation magnetization due to changes in Curie temperature caused by the application of an electric field [2]. With this approach, the number of skyrmions varied as a function of electric field in a volatile manner. Room temperature creation and movement of skyrmion bubbles have also been demonstrated when domain walls are moved in an electric field-induced magnetic anisotropy gradient due to geometric effects [3]. We show that skyrmions can be stabilized in antiferromagnet/ferromagnet/oxide heterostructure films without any external magnetic field due to an exchange bias field in section 5.1. The isolated skyrmions are annihilated or formed by applying voltage pulses that increase or decrease the perpendicular magnetic anisotropy, respectively in section 5.2. We also show skyrmions can be created from chiral domains by increasing the perpendicular magnetic anisotropy of the system. Our experimental findings are corroborated using micromagnetic simulations in section 5.3. This could provide a pathway to realize of fixed skyrmion based high density and energy efficient magnetic memory devices.

5.1 Device structure and characterization:

The heterostructure used in our experiments was grown by our collaborators at UCLA. The structure is Ta (2) / IrMn (5) / CoFeB (0.52-1.21) / MgO (2.5) / Al_2O_3 (35) / ITO where the numbers represent the thicknesses in nm. The layers consisting of Ta (2) / IrMn (5) / CoFeB (0.52-1.21) / MgO (2.5) / Al_2O_3 (5) were grown on Si/SiO_2 substrates by DC and RF magnetron sputtering at room temperature, where the numbers represent the thicknesses in nm. The CoFeB layer has a wedge shape with continuously changing thickness with a gradient of 0.115 nm per 1 cm of the sample length. The samples were then patterned into

an array of Hall bar devices using standard photolithography techniques. A 30 nm Al_2O_3 gate oxide was deposited using atomic layer deposition (ALD). Finally, transparent ITO layer was fabricated as a top gate electrode to facilitate Magneto Optical Kerr Effect (MOKE) imaging. The samples were then annealed at 150° C for 30 minutes under an out-of-plane magnetic field of 6 kOe to introduce the exchange bias and enhance the perpendicular anisotropy. The dimensions of the Hall bars are $130\ \mu m \times 20\ \mu m$. All electrical and optical measurements were done at room temperature using Keithley 6221 current source, Keithley 2182A nanovoltmeter, Stanford Research Systems SR830 lock-in amplifier, and HeNe laser with 632.8 nm of wavelength. The external magnetic field is provided by an electromagnet driven by a Kepco power supply. The interface of CoFeB with the antiferromagnetic IrMn layer gives rise to DMI [4, 5]. Similar to conventional VCMA induced switching, ferromagnetic/oxide interface is used to achieve the necessary PMA as well as enable VCMA.

Across the wafer, an array of several hall bars ($130\ \mu m \times 20\ \mu m$) was fabricated by collaborators at UCLA (*Figure 5-1*(a)). The thickness of the CoFeB layer was varied across the wafer roughly between 0.52 nm to 1.21 nm. The magnetic properties of the devices, especially the PMA and the DMI, are expected to vary with the thickness of the CoFeB layer. To verify this, anomalous hall resistance due to Anomalous Hall Effect (AHE) was measured by collaborators at UCLA to estimate the magnetization component perpendicular to the film as a function of perpendicular magnetic field. This is shown in *Figure 5-1*(b), where the hysteresis loops obtained show the expected trend. For example, devices in the range of 0.87 nm - 1.1 nm CoFeB layer exhibit higher perpendicular anisotropy and abrupt switching, while devices with thickness on either side of this range showed lower perpendicular anisotropy and gradual transition during reversal. Another important observation is the presence of exchange bias field in all the devices (5-20 Oe) that emerges from the ferromagnet/antiferromagnet interface. While presence of PMA and DMI are adequate, an external bias magnetic field is generally required to stabilize skyrmions in experiments.

However, in our structure, the readily available interfacial exchange bias field eliminates this requirement thus allowing stabilization of skyrmions at zero externally applied bias magnetic field [4].

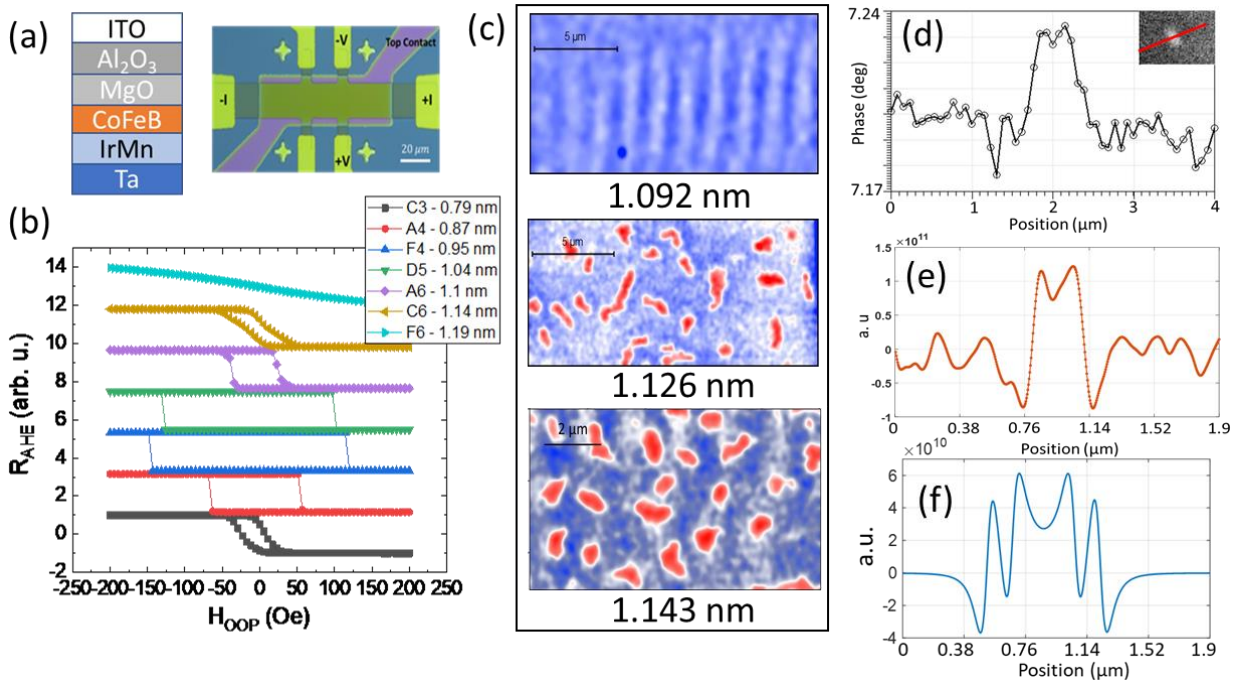

Figure 5-1 Device structure and characterization. (a) Left: Cross-section of the device. Right: Top view of the device structure: The two current contacts can be used for applying current through the stack and the voltage contacts can be used for measuring transverse voltage. For VCMA, a voltage pulse was applied between one of the two top gate contacts, and any one of the other current and voltage contacts. (b) Anomalous Hall measurements for different CoFeB thicknesses, where HOOP denotes out-of-plane magnetic field, (c) Magnetic force microscopy image showing magnetic states for different CoFeB thicknesses. At lower thickness uniform state was observed while at higher thicknesses skyrmions and a mixture of skyrmion and stripe domains were seen. (d) Skyrmion profile obtained from the raw MFM image of a skyrmion shown in the inset which was qualitatively similar to the simulated skyrmion MFM profile as shown in (e). (f) Simulated MFM profile of a classical bubble. Reprinted with permission from [17], Copyright (2020), Springer Nature.

The thickness dependence of magnetic states was imaged using Magnetic Force Microscopy (MFM). We obtained MFM image at room temperature and atmospheric pressure with Bruker Dimension Icon AFM system. We used Bruker MESP-LM low-moment probes to minimize tip-induced magnetization reorientation. To confirm there is no tip induced effects, we scanned the same area twice (scanning up and down). These two scans produced similar images (see section 5.5). Nominal cantilever frequency, lift height and scan rate were respectively 75 kHz, 40 nm and 0.2 Hz. We note that, raw MFM images were processed using a Gaussian filter to aid visualization by eliminating noise. In devices with high perpendicular anisotropy, the magnetization orientation was found to be completely out of plane (t=1.092 nm, *Figure 5-1*(c) top panel, we note that stripe like contrasts appear due to optical interference between the laser

reflected from the cantilever and the sample surface). In devices with increased thickness, we observed a mixture of stripe domains and circular domains (t=1.126 nm, *Figure 5-1*(c) middle panel) and mostly circular domains (t=1.143 nm, *Figure 5-1*(c) bottom panel).

Figure 5-1 (d) shows a phase profile extracted from the experimental MFM image of an observed domain along the line shown in the inset. This profile qualitatively matches the simulated MFM profile (*Figure 5-1*(e)) of a skyrmion stabilized in the presence of thermal noise and inhomogeneity and is fundamentally different from MFM profile of a classical bubble (*Figure 5-1*(f)) with 400 nm core diameter surrounded by a 300 nm domain wall separating the two oppositely polarized perpendicular regions. The MFM profile was simulated using micromagnetic simulation where the tip magnetization is modeled as a point monopole at the apex. We observe two side peaks that emerge due to the achiral domain wall with spins pointing in the same direction separating two perpendicular regions. We do not observe this in our MFM line scans. These give us confirmation of the presence of skyrmions in our system. The skyrmion has a collinear core at the center. The dip at the center of the MFM profile is indicative of that. Such textures are often called skyrmion bubbles. In a strict sense, spins in a skyrmion structure should rotate continuously with a single spin at the center pointing perpendicularly. However, there is no clear distinction between the skyrmion and the skyrmion bubble state and these terms are used interchangeably in the literature [6, 7]. Lastly, we note that, the observed stripe domain like states are expected to be topologically equivalent to the circular skyrmionic state. Therefore, these states are possibly elongated skyrmions or elliptically shaped skyrmions. However, to avoid confusion we call the mixed state as “skyrmions and stripe domains”.

The MFM imaging was further complemented with magneto optical Kerr effect (MOKE) imaging by our collaborators at UCLA. Skyrmions and stripe domains were clearly observed in the intermediate steps of the switching during a cycle of perpendicular magnetic field. More importantly, we show that current induced motion of these magnetic objects exhibited skyrmion Hall Effect, which is a clear indication of the topological nature of these magnetic objects. We utilize spin-orbit torques from IrMn (with a thickness of 5 nm) to drive the skyrmion motion [4]. It has been shown that IrMn has a sizable spin Hall angle [8],

allowing for a relatively large damping-like spin-orbit torque. First, we create skyrmions by scanning the external magnetic field, and then by utilizing electrical current in this system, we displace skyrmions by pulses with an amplitude of 9 mA and a duration of 5 ms. As seen in *Figure 5-2*, the direction of the current-driven skyrmion motion is not along the current direction and has a transverse component. This phenomenon is the so-called skyrmion Hall effect [9], which is a signature of magnetic skyrmions. The calculated skyrmion Hall angle is around 10.4°. These results further confirm that our observed states have a topological nature and are indeed skyrmions.

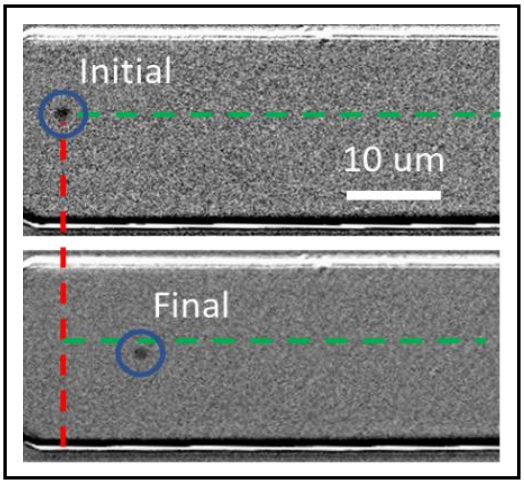

Figure 5-2 Current-driven skyrmion motion imaged using magneto-optical Kerr effect (MOKE) microscopy. Current pulse has 9 mA amplitude (corresponding to a current density of 8.3×10^6 A/cm^2 through the IrMn layer) and a duration of 5 ms. Blue circles indicate the position of skyrmions before and after the application of current pulse. Red (green) dashed line shows the initial horizontal (vertical) position of the skyrmion. At the final position, the skyrmion also shows a vertical shift in addition to the horizontal one, which is due to the skyrmion Hall effect. Reprinted with permission from [17], Copyright (2020), Springer Nature.

5.2 Manipulation of skyrmions with electric field alone in the absence of an external magnetic field:

We probe the effect of application of an electric field in the devices where skyrmions and stripe domains were observed at zero magnetic field. A voltage pulse is applied between one of the two top gate contacts, and any one of the other current and voltage contacts. Current and voltage contacts are all attached to the Hall bar, which is metallic and conductive. In this way, the electric field is dropped over the MgO and Al_2O_3. Consequently, the electron density at the ferromagnet/oxide interface is modulated, leading to a modulation in the PMA of the system. We characterize VCMA coefficient in our perpendicularly

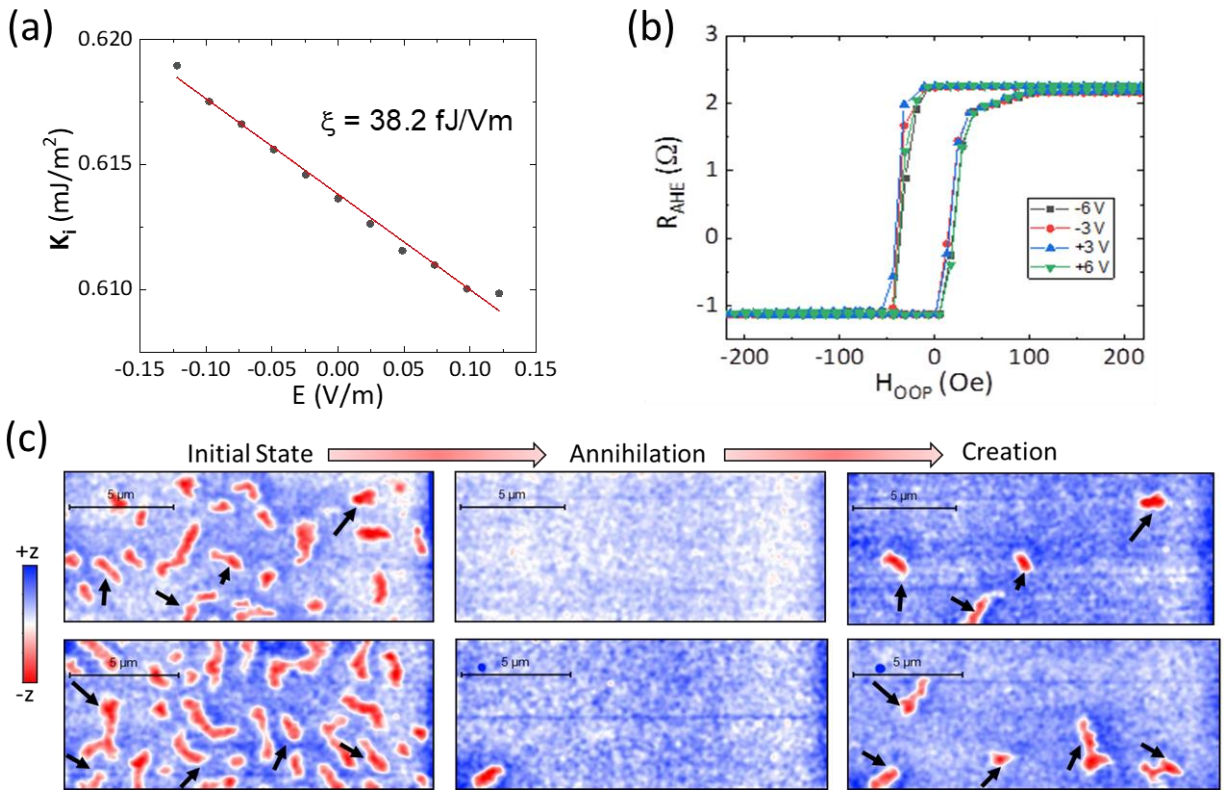

Figure 5-3 VCMA induced manipulation of skyrmions. (a) Interfacial anisotropy (Ki) as a function of the applied electric field (E) in the sample with nominal CoFeB thickness of 1.06 nm. The slope of this plot is the VCMA coefficient (ξ). (b) Anomalous Hall (AHE) measurement on a sample with CoFeB thickness of 1.08 nm and under different gate voltages. The exchange bias and the difference in AHE resistance between the two states is almost the same for all samples. (c) MFM images obtained before and after application of electric field. Scale bars are 5 μm. Left column: magnetization state before application of any electric field. Middle Column: Magnetization state obtained after applying a negative voltage pulse that increased PMA. Right Column: Magnetization state obtained after applying a positive voltage pulse that decreased PMA. Reprinted with permission from [17], Copyright (2020), Springer Nature.

magnetized samples by measuring anomalous Hall resistance as a function of an in-plane magnetic field in our Hall bar structures with top gates. We can then calculate the interfacial anisotropy using the transport data and magnetization saturation obtained from SQUID measurement ($\sim 9\times10^5 \pm 5\%$) A/m [10]. The results are shown in *Figure 5-3*(a), where interfacial anisotropy is plotted as a function of applied electric field. VCMA coefficient (ξ) is defined as the slope of this plot. The effect of voltage application is primarily limited to changing the perpendicular magnetic anisotropy of the system. In other words, applied voltage does not alter the saturation magnetization, exchange bias etc. In order to investigate the effect of the applied voltage on the exchange bias and magnetization saturation in our sample, we performed anomalous Hall

effect measurements under different applied gate voltages as shown in *Figure 5-3*(b). This measurement is performed on the sample with nominal CoFeB thickness of around 1.08 nm. We observe that the exchange bias under different bias voltages is almost the same and the negligible changes might be due to the change in interfacial properties. Furthermore, the difference in anomalous Hall resistance between the up/down states is independent of the applied voltage, which suggests that the magnetization saturation (M_s) does not change.

The oxide barrier breakdown voltage was observed to be around 8 V. In most of the cases, we applied ±7 V across the oxide barrier (unless otherwise mentioned) by using a Keithley 2636B source meter and Signatone probe station, which corresponds to an electric field of $E_{MgO} = \frac{V}{t_{MgO}+\frac{\epsilon_{MgO}}{\epsilon_{AlOx}}t_{AlOx}}$= 0.157 V/nm, using $\frac{\epsilon_{MgO}}{\epsilon_{AlOx}} = \frac{9}{7.5}$. In our system, application of a positive (negative) electric field leads to decrease (increase) of the PMA (*Figure 5-3*(a)). Before applying this electric field, we imaged the initial magnetization state of the device as shown in the left column of *Figure 5-3* (c). The initial states consist of skyrmions and stripe domains. Next, we applied -7 V between the top and the bottom electrode for 1-2 seconds to increase the PMA of the system. The voltage pulse was withdrawn and the transformation of the magnetic state due to application of this voltage pulse was imaged in the absence of an applied electric field. We observed that the skyrmions and the stripe domains were annihilated (middle column of *Figure 5-3*(c)) and the magnetization of the system reoriented in the +z direction as evidenced by the MFM image. Subsequently, we applied an opposite polarity voltage pulse (i.e. +7V) in a similar manner. Due to this, the PMA decreases and DMI prevails over PMA. This is expected to be a favorable condition for formation of spin spiral states. Indeed, some skyrmions and stripe domains reappear as can be seen in the MFM images shown in the right column of *Figure 5-3*(c). We note that all imaging was performed at zero external magnetic field and zero applied electric field. Therefore, these creation and annihilation processes were nonvolatile and were achieved without the assistance of any external bias magnetic field. Therefore, the

skyrmion state and the saturated out of plane ferromagnetic state both emerged as stable states of the system and the applied electric field can result in switching between these states.

Additionally, we observed incomplete annihilation where starting from an initial state with mostly stripe domains and some skyrmions; a negative voltage pulse could annihilate some of the skyrmions while many of the stripe domains transformed to more circular skyrmionic state as shown in *Figure 5-4*. Therefore, transformation from stripe domain to skyrmions is also achievable using VCMA. However, unlike the previous case, this transformation was found to be irreversible. In other words, application of a positive pulse could not recreate more skyrmions or transform the circular skyrmions back to original stripe domains. Possibly, when the stripe domains transform to circular skyrmions they get pinned more strongly. Therefore, subsequent application of a positive pulse (i.e. reduction of PMA) did not affect them substantially. Transformation from chiral domain to skyrmions were previously observed experimentally by using a current pulse [11, 12]. Theoretically, chopping skyrmions from chiral domain was proposed using strain using anisotropy modulation [13]. Here, we demonstrate the feasibility of such transformation by employing VCMA.

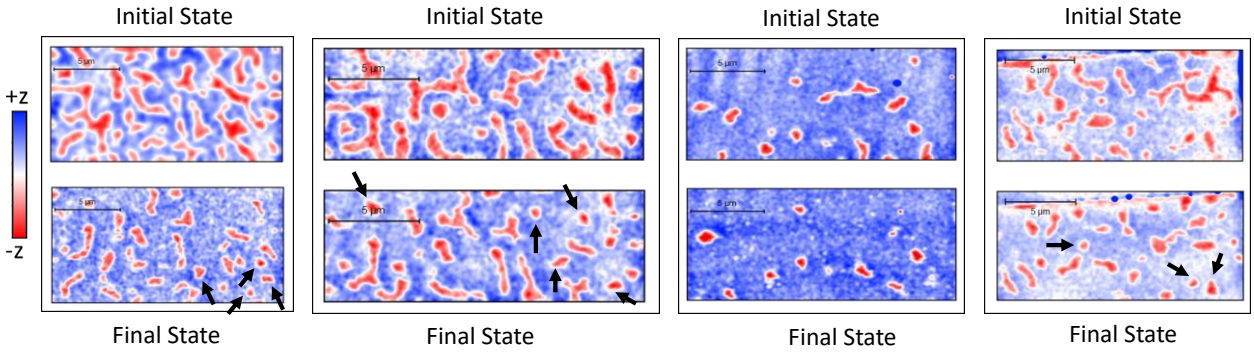

Figure 5-4 Incomplete annihilation that shows stripe domain to skyrmion transformation. Initial states are shown in the top panel and final state is shown in the bottom panel. Arrows mark some of the created skyrmions due to application of a negative voltage pulse. Scale bars are 5μm. Reprinted with permission from [17], Copyright (2020), Springer Nature.

All these different observations can be satisfactorily explained if we consider pinning sites in the thin film stack. The CoFeB and the IrMn films are polycrystalline in nature, which could lead to intergranular variation of PMA, DMI and exchange bias. Pinning sites could also exist due to inhomogeneity in film thickness and presence of material defects etc. We observed the size and shape of the skyrmions vary widely

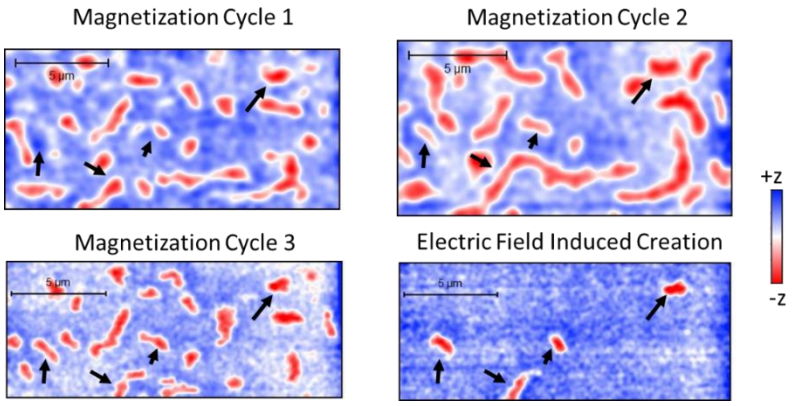

Figure 5-5 Skyrmions/stripe domains at almost exact position in different magnetization cycle and after electric field induced creation. Reprinted with permission from [17], Copyright (2020), Springer Nature.

(*Figure 5-1*(c)) which indicate the existence of inhomogeneity. Due to corresponding non-uniformity of magnetic parameters across the film, the stripe domains and the skyrmions have a propensity to occupy the same location (e.g. emerge roughly at the same position in successive magnetization cycles as shown in *Figure 5-5*). Similarly, skyrmions created by VCMA appear at the same initial location that they occupied before annihilation as indicated by the arrows in the *Figure 5-5*. The same skyrmions were also present at the same location in all the magnetization cycles *Figure 5-5*. Finally, due to the pinning sites, fewer skyrmions were created by VCMA compared to the initial state (prior to annihilation) as shown in *Figure 5-3*(c). In the next section, we establish the validity of these explanations using micromagnetic simulation.

5.3 Simulations for manipulation of skyrmions with electric field:

We perform micromagnetic simulation to show the voltage-controlled creation and annihilation process of skyrmions. Material parameters used in the simulation: saturation Magnetization (Ms)= 9.3×10^5 A/m (measured by SQUID= 9×10^5 ±5% A/m), Perpendicular Anisotropy Constant (Ku_1) = 5.8×10^5 J/m^3 (*Figure 5-3*a), Exchange Bias=15 Oe (*Figure 5-1*b), Exchange Constant (A)=8 pJ/m [14], DMI Parameter (D)=135 µJ/m^2 [4], Gilbert Damping (α)=0.01. For simplicity, we incorporate the effect of inhomogeneity by varying only the perpendicular anisotropy. We simulated a 3.8 µm × 3.8 µm rectangular geometry with 1.1 nm thickness and divided it into regions of average 100 nm size using Voronoi tessellation with a gaussian PMA distribution with 1% standard deviation. Left column of *Figure 5-6* (a) shows the PMA distribution in different regions across the film. Usually, grain size in CoFeB is in the order of 5-10 nm. However,

regions of such dimensions were not sufficient to pin skyrmions and consequently corresponding simulations did not reproduce all the experimentally observed scenarios. Ultimately, there can be many causes of inhomogeneity besides intergranular variations. Regions in the film (comprised of many grains) can have exchange bias, PMA, DMI that are clearly different from surrounding areas, particularly in IrMn/CoFeB interfaces. Additionally, there can be material defects in the sample acting as pinning sites. Thus, our systematic study of effect of spatial dimensions of the inhomogeneity indicates that regions that are on average ~100 nm and higher are most effective in pinning skyrmions.

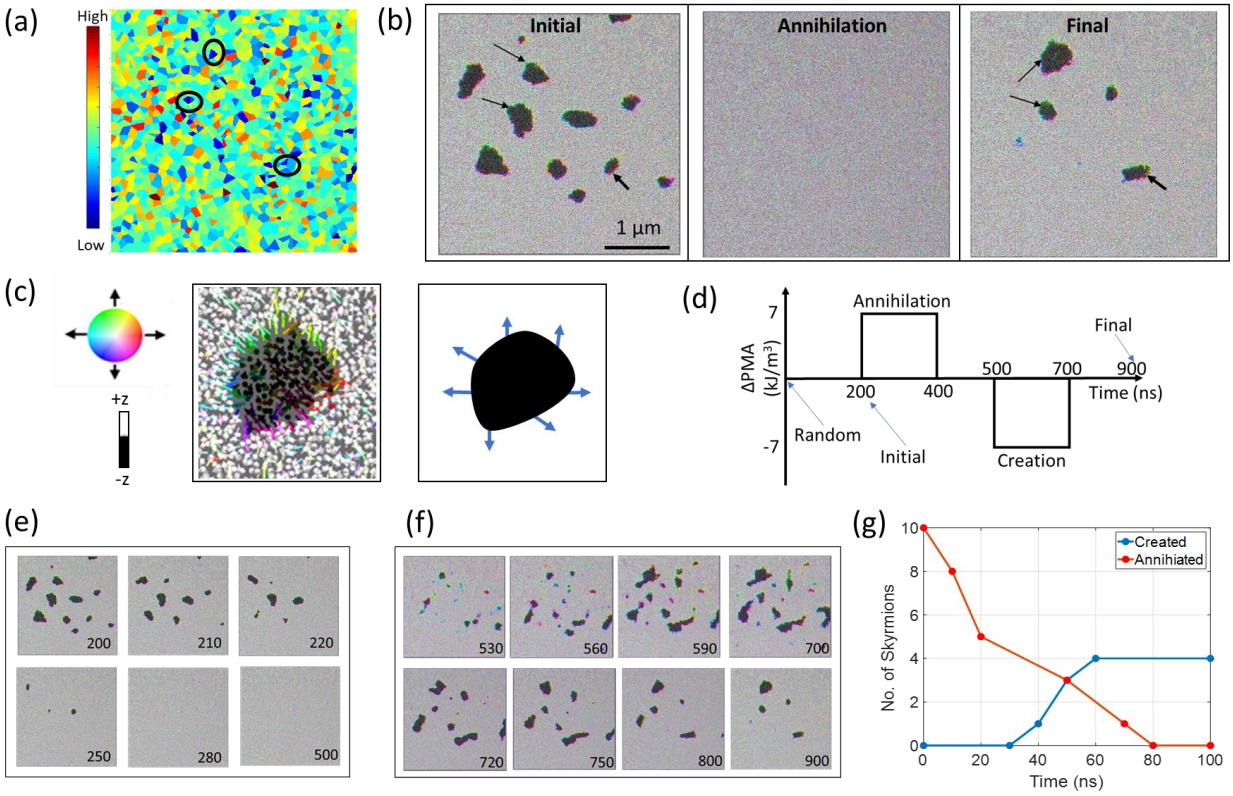

Figure 5-6 Micromagnetic simulation of voltage control of skyrmions. (a) Simulated system with different regions having a gaussian PMA distribution. The blue regions correspond to lower anisotropy and these act as pinning sites. (b) Overview of the creation and annihilation process. Left column shows equilibrium magnetic state obtained by finding the equilibrium state starting from a random magnetic state. Middle Figure shows the annihilated state while the right figure shows created skyrmions. Arrows show that the skyrmion located at the same pinning site before annihilation and after creation. These pinning sites corresponds to the low anisotropy (blue) regions marked by circles in (a). (c) Zoomed view of a skyrmion (left) with Neel like spin spiral, (d) Temporal PMA variation used in the simulation. (e) Annihilation process of skyrmion. (f) Creation process of skyrmions. The numbers represent time corresponding to the pulse shown in (d), (g) Pulse time dependence of skyrmion creation and annihilation process. Reprinted with permission from [17], Copyright (2020), Springer Nature.

As previously discussed, applied voltage does not alter the saturation magnetization, exchange bias. There are recent reports of DMI modulation by applying an electric field [15]. However, these changes in DMI

are relatively small and do not affect the magnetization dynamics significantly [16]. Therefore, we only consider the change in PMA as a consequence of voltage application which is considered to be the same in all the regions. VCMA coefficient in 1.06 nm CoFeB was measured to be 38.2 fJ/Vm (*Figure 5-3* (a)). Therefore, electric field of 0.157 V/nm can cause 5.5×10^3 J/m^3 change in anisotropy energy density. In our simulations, we considered a change of 7×10^3 J/m^3 in anisotropy density, which is close to the estimated change in anisotropy energy density.

Figure 5-6 (b) shows the overview of the switching process. The initial magnetic state (*Figure 5-6* (b), left column) was obtained by finding the equilibrium magnetization orientation starting from a random magnetization state. During this initialization, a labyrinth like state is first formed which then transforms into many skyrmions and stripe domains. Most of these skyrmions remain pinned due to prevalence of pinning sites of varying strength across the film. These skyrmions were annihilated when PMA was increased and a ferromagnetic state was formed (*Figure 5-6* (b), middle column). Lastly, when PMA was reduced dome skyrmions were created at the same initial location that they occupied before annihilation (marked by arrows in the *Figure 5-6* (b)). We found that these locations are the low anisotropy regions of the film which act as pinning sites to the skyrmions. *Figure 5-6* (c) shows zoomed in view of a skyrmion. We observe that the skyrmion is Neel like. This is expected as the heterostructure fabricated has interfacial DMI.

Next, we analyze the dynamics of the switching process. As large pulse times (several seconds) were used in the experiment, we ran the simulations with long enough pulse time (200 ns) beyond which increasing pulse time makes no difference. The pulse used in our simulation is shown in *Figure 5-6* (d) where increase (decrease) of PMA correspond to a negative (positive) voltage. *Figure 5-6* (e) shows the annihilation process starting from the initial state. Due to increase of PMA, skyrmions start to shrink and ultimately annihilates. At t=280 ns, all the skyrmions are annihilated and a ferromagnetic state is reached. This ferromagnetic state persists when the PMA is restored to the original value (t=400-500 ns). *Figure 5-6* (f) shows the creation process starting from a ferromagnetic state. Due to PMA reduction, domains start to

nucleate at regions of low PMA. Domain growth slows down over time and almost entirely stops at t=700 ns. When the PMA is restored to the initial value, some of these domains start to annihilate. However, after 200 ns (t=900 ns), 4 skyrmions still persist. Clearly, number of created skyrmions are fewer than the initial state. This is because, starting from a ferromagnetic state, domains nucleate only at very strong pinning sites when PMA is reduced. However, when skyrmions are formed from a labyrinth like state (which is observed in our initialization process), many skyrmions can interact with comparatively lower strength pinning sites and remain pinned there. This explains the creation of fewer skyrmions compared to the initial state. It was previously shown using a magnetic field, more skyrmions can be created from a labyrinth domain state than from a single domain saturated state due to non-uniformity [4] which is consistent with our simulation and experimental observations. Finally, we explore the pulse time dependence of skyrmion creation and annihilation process. We show in *Figure 5-6* (g), the switching can be controlled by varying the pulse time and 80 ns is enough for both annihilation as well as creation of skyrmions.

5.4 Estimation of energy dissipation:

We estimate the total energy dissipation considering all the energy required to charge the capacitive oxide layer is ultimately dissipated. The capacitance of the 130 µm × 20 µm area with 35 nm Al_2O_3 layer and 2.5 nm MgO layer is C= 4.66×10^{-12} F (relative permittivity of 9 and 7.5 respectively). Therefore, total energy dissipation= $\frac{1}{2}CV^2$= 109 pJ as V=7 V. Initially, the density of chiral objects (Skyrmions and stripe domains) observed in our devices was 0.183 μm^{-2}. Therefore, the total number of such objects in a 130 µm× 20 µm area is expected to be around 660. Thus, the energy required to annihilate each object (skyrmion or stripe domain) on an average =166 fJ. On the other hand, number of created Skyrmions is fewer than the initial condition with a density of 0.03 μm^{-2}. This translates into average energy dissipation to create a skyrmion = 995 fJ. We note that the oxide barrier was grown thicker compared to a patterned MTJ to avoid pinholes. In a scaled device, MgO thickness will usually be 1.5 nm. That will provide a reduction in the energy dissipation by a factor of 25 and the energy dissipated will be much lower (~6.6 fJ for annihilation, ~40 fJ for creation). Furthermore, interface optimization can lead to a higher VCMA co-efficient. For example, a

VCMA co-efficient of 100 μJ/m^2 per V/nm [10] can reduce the energy dissipation to ~1 fJ for annihilation, ~6 fJ for creation. Finally, these proof-of-concept experiments were performed with large skyrmions. If skyrmion diameter is ~100 nm, the energy dissipated could potentially be much smaller than 1 fJ/skyrmion creation or annihilation event.

5.5 Additional images

To confirm there is no tip induced effects, we scanned the same area twice (scanning up and down). These two scans produced similar images as shown in *Figure 5-7* indicating that tip induced changes to the magnetic state of the films in minimal.

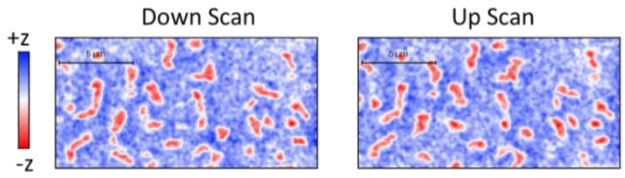

Figure 5-7 MFM image of the same location scanning up and down. Reprinted with permission from [17], Copyright (2020), Springer Nature.

Many of the magnetic force microscopy (MFM) images and some in the supplement have been presented after performing some image processing. The raw MFM images that correspond to these processed images are presented below.

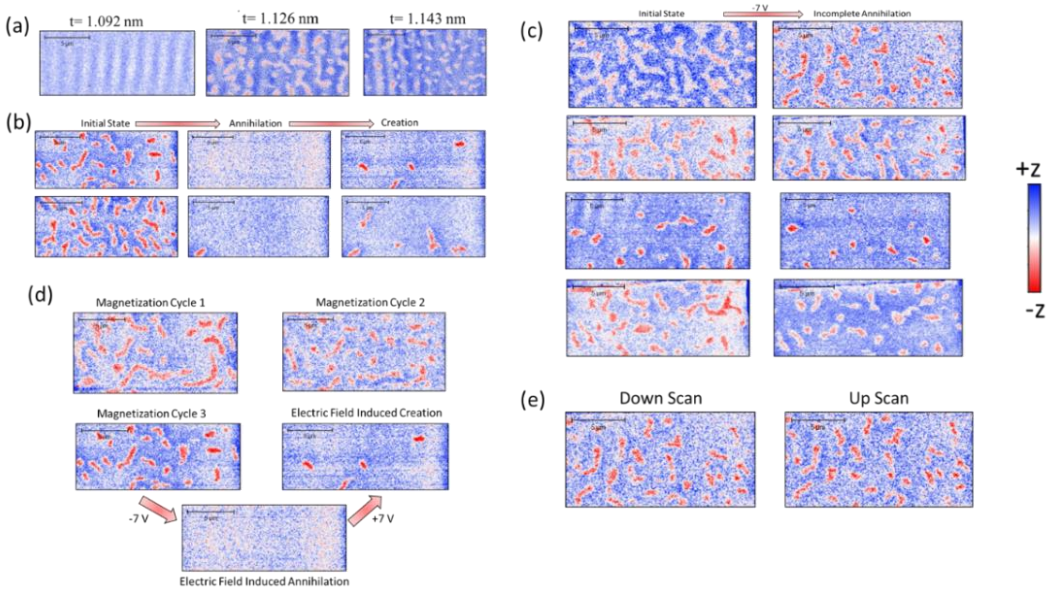

Figure 5-8 RAW MFM image corresponding to the following figures in the main or supplemental section: (a) Fig. 1(c), (b) Fig. 3(b), (c) Fig. 4, (d) Fig. 5, (e) Fig. 7. Reprinted with permission from [17], Copyright (2020), Springer Nature.

In summary, we have reported experimental control of fixed magnetic skyrmions using VCMA. In particular, we showed that skyrmions can be stabilized without applying any external magnetic field and can be annihilated and recreated by applying voltages of opposite polarity. We also showed that skyrmions can be created from chiral domain states. This control is non-volatile and depends on the pinning sites across the device. Our experimental observations were corroborated using micromagnetic analysis. The electric field control of magnetic skyrmions could lead to the development of energy efficient high-density magnetic memory devices.

References:

[1] P. J. Hsu, A. Kubetzka, A. Finco, N. Romming, K Von Bergmann and R. Wiesendanger, "Electric-field-driven switching of individual magnetic skyrmions," *Nat. Nanotechnol.* 12**,** 123–6(2017).

[2] M. Schott, A. Bernand-Mantel, L. Ranno, S. Pizzini, J. Vogel, H. Béa, C. Baraduc, S. Auffret, G. Gaudin and D. Givord, "The Skyrmion Switch: Turning Magnetic Skyrmion Bubbles on and off with an Electric Field," *Nano Lett.* 17**,** 3006–12 (2017).

[3] C. Ma, X. Zhang, Y. Yamada, J. Xia, M. Ezawa, W. Jiang, Y. Zhou, A. Morisako and X. Liu, "Electric Field-Induced Creation and Directional Motion of Domain Walls and Skyrmion Bubbles," *Nano Lett.* 19 (1), 353–361(2019).

[4] G. Yu, A. Jenkins, X. Ma, S. A. Razavi, C. He, G. Yin, Q. Shao, Q. L. He, H. Wu, W. Li, W. Jiang, X. Han,X. Li, A. C. Bleszynski Jayich, P. K. Amiri and K. L. Wang K L, "Room-Temperature Skyrmions in an Antiferromagnet-Based Heterostructure," *Nano Lett.* 18, 980–6 (2018).

[5] X. Ma, G. Yu, S. A. Razavi, S. S. Sasaki, X. Li, K. Hao, S. H. Tolbert, K. L. Wang and X. Li, "Dzyaloshinskii-Moriya Interaction across an Antiferromagnet-Ferromagnet Interface," *Phys. Rev. Lett.* 119, 027202 (2017).

[6] W. Jiang, X. Zhang, G. Yu, W. Zhang, X. Wang, M. Benjamin Jungfleisch, J. E. Pearson, X. Cheng, O. Heinonen, L. L Wang, Y. Zhou, A. Hoffmann and S. G. E. Te Velthuis, "Direct observation of the skyrmion Hall effect," *Nat. Phys.* 13, 162–9 (2017).

[7] O. Boulle et al., “Room-temperature chiral magnetic skyrmions in ultrathin magnetic nanostructures,” *Nat. Nanotech.*, 11, p. 449 (2016).

[8] D. Wu, G. Yu, C.-T. Chen, S.A. Razavi, Q. Shao, X. Li, B. Zhao, K.L. Wong, C. He, Z. Zhang, P.K. Amiri, and K.L. Wang, “Spin-orbit torques in perpendicularly magnetized Ir22Mn78/Co20Fe60B20/MgO multilayer,” *Appl. Phys. Lett.*, 109(22), 222401(2016).

[9] W. Jiang, X. Zhang, G. Yu, W. Zhang, X. Wang, M. Benjamin Jungfleisch, J. E. Pearson, X. Cheng, O. Heinonen, K. L. Wang, Y. Zhou, A. Hoffmann and S. G. E. Te Velthuis, “Direct observation of the skyrmion Hall effect,” *Nat. Phys.* 13, 162–9 (2017).

[10] X. Li, K. Fitzell, D. Wu, C.T. Karaba, A. Buditama, G. Yu, K.L. Wong, N. Altieri, C. Grezes, N. Kioussis, S. Tolbert, Z. Zhang, J.P. Chang, P.K. Amiri, and K.L. Wang, “Enhancement of voltage-controlled magnetic anisotropy through precise control of Mg insertion thickness at CoFeB|MgO interface,” *Appl. Phys. Lett.*, 110(5), 052401(2017).

[11] W. Jiang, P. Upadhyaya, W. Zhang, G. Yu, M. B. Jungfleisch, F. Y. Fradin, J. E. Pearson, Y. Tserkovnyak, K. L. Wang, O. Heinonen, S. G. E. Te Velthuis and A. Hoffmann, “Blowing magnetic skyrmion bubbles,” *Science* 349, 283–6(2015).

[12] G. Yu, P. Upadhyaya, Q. Shao, H. Wu, G. Yin, X. Li, C. He, W. Jiang, X. Han, P. K. Amiri and K. L. Wang, “Room-temperature skyrmion shift device for memory application,” *Nano Lett.* 17, 261–8(2017).

[13] Y. Liu, N. Lei, W. Zhao, W. Liu, A. Ruotolo, H. B. Braun and Y. Zhou, “Chopping skyrmions from magnetic chiral domains with uniaxial stress in magnetic nanowire,” *Appl. Phys. Lett.* 111, 022406 (2017).

[14] M. Yamanouchi, A. Jander, P. Dhagat P, S. Ikeda, F. Matsukura, and H. Ohno, “Domain Structure in CoFeB Thin Films with Perpendicular Magnetic Anisotropy,” *IEEE MAGNETICS LETTERS* 2, 3000304 (2011).

[15] H. Yang, O. Boulle, V. Cros, A. Fert and M. Chshiev, “Controlling Dzyaloshinskii-Moriya Interaction via Chirality Dependent Layer Stacking, Insulator Capping and Electric Field,” *Sci. Rep.*,

8, 12356(2018).

[16] D. Bhattacharya and J. Atulasimha, “Skyrmion-Mediated Voltage-Controlled Switching of Ferromagnets for Reliable and Energy-Efficient Two-Terminal Memory,” *ACS Appl. Mater. Interfaces* 10, 17455–62(2018).

[17] D. Bhattacharya, S. A. Razavi, H. Wu, B. Dai, K. L. Wang, J. Atulasimha, Creation and annihilation of non-volatile fixed magnetic skyrmions using voltage control of magnetic anisotropy, Nature Electronics, 1-7 (2020).

Chapter 6: Conclusion

In the previous chapters, we discussed different strategies to implement fixed skyrmion based memory devices that are controlled by an electric field. We will conclude this dissertation outlining future research directions that can utilize our proposed methods to build efficient nanomagnetic devices. In section 6.1, we discuss our preliminary results on skyrmion switching in a nanodisk. In section 6.2, we analyze the feasibility of scaling skyrmion based memory device simulating MTJ free layer of different lateral dimensions. In section 6.3, we discuss the possibility of utilizing voltage induced skyrmion dynamics to design neuromorphic computing elements. Finally, we will end this dissertation with concluding remarks in section 6.4.

6.1 Skyrmion switching in a confined geometry:

In chapter 3 and chapter 4, we theoretically demonstrated that switching of skyrmions in a nanodisk can be used as magnetic memory devices. As a proof of concept experiment, we showed switching of skyrmions in a thin film heterostructure. However, in a film, complete reversal of skyrmion cannot be achieved by applying an electric field. Skyrmion confinement is required to reverse the core as the boundary plays a

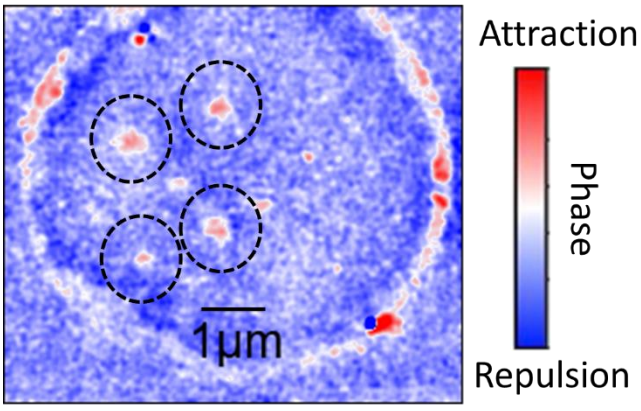

Figure 6-1 Skyrmions confined in a nanodisk under externally applied magnetic field of 10 Oe and V=1300 mV

central role in the reversal process. Therefore, to demonstrate skyrmion reversal experimentally, we are currently performing experiments on MTJ like circular magnetic dots consisting of Ta/CoFeB/MgO layers. These dots are 3-8 μm in diameter. *Figure 6-1* shows two such nanodots imaged using magnetic force microscopy (MFM). The skyrmions are 300-500 nm in size. Therefore, the boundary effect is small on

these skyrmions. However, we have observed annihilation and creation of skyrmion of skyrmion while imaging the nanodot under applied electric field. Further characterization is necessary to unambiguously prove this. Moreover, fabrication of smaller nanodots is necessary to increase confinement effect and demonstrate reversal of skyrmion core.

6.2 Scaling of skyrmion-mediated memory devices:

In chapter 4, we have shown skyrmion mediated switching of ferromagnets in a nanomagnet of lateral dimension 100 nm. To be competitive with the current miniaturization trend in Spin Transfer Torque Random Access Memory (STTRAM), further downscaling is required. In this section, we theoretically investigate the feasibility of downscaling the skyrmion mediated switching scheme by studying three MTJs of different sizes, 100nm, 50 nm and 20 nm respectively. We observe that with the reduction in lateral dimension, high perpendicular magnetic anisotropy, high DMI and a larger VCMA coefficient are required for successful operation of the device (Section 6.2.1). We also present switching error statistics in the presence of thermal noise using these material parameters. In Section 6.2.2, we discuss future directions towards downscaling the proposed device.

6.2.1 Required material parameters:

We simulate the magnetization dynamics of the free layer of the MTJs of diameter 100 nm, 50 nm and 20 nm, which were discretized into 64×64×1, 32×32×1 and 16×16×1 cells respectively to keep the lateral (in-plane) discretization similar to the extent possible. We start with an initial ferromagnetic state. Next, when the PMA is reduced (voltage applied), we need to form an intermediate skyrmion state to provide a robust pathway for magnetization reversal to the opposite ferromagnetic state when the PMA is restored (voltage withdrawn). We varied the perpendicular anisotropy (K_{u1}) and the DMI parameter (D) to fulfill these requirements. The rationale behind choosing different anisotropy and DMI values is discussed below.

Firstly, to form the intermediate skyrmion state, we need a sizeable DMI. Moreover, reduction of lateral dimension requires higher DMI to form an intermediate skyrmion state. However, to maintain an initial

ferromagnetic state, the DMI value must be less than the critical value ($D_{crit} = \frac{4}{\pi}\sqrt{AK_{EFF}}$, where $K_{EFF} = K_{u1} - \frac{1}{2}\mu_0 M_s^2$) at the corresponding initial PMA value. Here, K_{EFF} is the effective perpendicular anisotropy and the D_{crit} (critical DMI) value signifies a threshold beyond which a metastable skyrmion can be formed in the system. Energy barrier between two ferromagnetic states reduces due to the presence of DMI. To incorporate this reduction, we have estimated the energy barrier with K_{eff} from the phenomenological equation $K_{eff} = (K_{u1} - \frac{1}{2}\mu_0 M_s^2 - \frac{D^2\pi^2}{16A})$. The perpendicular anisotropy is determined from the thermal stability factor $K_{eff}V/k_BT$, which was considered to be approximately around 50 for all three MTJs. Therefore, with reduction of lateral dimension, required DMI increases and consequently the uniaxial anisotropy K_{u1} needs to be increased to ensure thermal stability with an energy barrier of ~50 k_BT. Optimized material parameters are listed in Table I considering application of voltage pulse (ΔV) of 2.0 V across 1 nm thick MgO layer for all three MTJs. Exchange stiffness A=25 pJ/m, Saturation Magnetization $M_s=1.3\times10^6$ A/m, Gilbert damping α=0.01 were used for all cases.

Table 6-1 Required parameters

MTJs	Osc. Freq. (GHz)	K_i ($\mu J/m^2$)	ΔK_i ($\mu J/m^2$)	VCMA Coeff. (fJ/Vm)	D_{crit} (mJ/m^2)	D (mJ/m^2)
100 nm	~1	1332	204	102	1.42	1.2
50 nm	~8	1044	504	252	5.25	4.5
20 nm	~60	3798	3138	1569	14.61	13.0

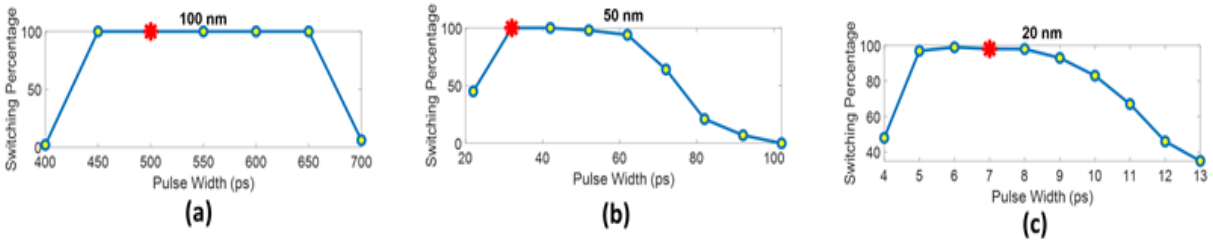

Figure 6-2 Switching probability vs. pulse width of (a) 100nm (b) 50nm and (c) 20 nm nanomagnets. [For studying the switching percentage for different pulse widths, the simulations were run for 100 times for most points. For one point in each sub-figure, the simulations were run 1000 times. Thus, points marked as 100% with a star (indicate a better than 99.9% switch for 100 nm and 50 nm lateral dimension as there are no failure for 1000 runs). However, for 20 nm case, 19 failures in 1000 runs at pulse width of 7 ps indicate ~98% switching]. Reprinted with permission from [1], Copyright (2020), IEEE.

Using these material parameters, switching error was found to be >99.5% in the 100 nm and 50 nm cases and ~98% in the 20 nm case (*Figure 6-2*). Additionally, the breathing frequency of skyrmions in the downscaled nanomagnets is high leading to switching frequency ~1 GHz, ~10 GHz, ~100 GHz for 100 nm, 50 nm and 20 nm respectively. Thus, as one scales to lateral dimension to 50 nm, faster, energy efficient and less error prone switching can be achieved.

6.2.2 Route to downscaling:

In summary, our simulations show that switching remains robust when scaling down to 50 nm lateral dimensions in the presence of thermal noise with appropriate choice of feasible material parameters based on experimentally reported values of VCMA coefficient (370 fJ/Vm) [2], PMA (3700 μJ/m^2) [3] and DMI (~3mJ/m^2) [4-6]. Similarly, while downscaling to 20 nm, thermally robust switching can be achieved provided material parameters with large VCMA [7], DMI [8, 9] and PMA [3, 6] are chosen. However, among these three parameters only PMA has been experimentally reported [3], while DMI and VCMA values (for the 20 nm nanomagnet simulation) have only been theoretically predicted [7-9] to date but not experimentally demonstrated. This is an important challenge in scaling from 50 to 20 nm which requires optimization of material system and interfaces. For aggressive scaling to 20 nm and below, ferrimagnet systems (rather than ferromagnets) could potentially offer a thermally robust skyrmion mediated switching route with experimentally demonstrated material parameters due to small stray fields and low DMI and PMA requirement to form skyrmions [10, 11].

6.3 Resonate and Fire neuron with fixed skyrmions

Nanomagnetic devices are one of the promising alternatives to implement neuromorphic computing and other non-von-Neumann like architectures due to their low energy consumption, nonlinear dynamics, and non-volatility [12–20]. Among artificial neurons, most emulate the behavior of (leaky) integrate and fire type neurons where the firing frequency depends only on the strength of the stimulus [21]. However, in the brain, many “resonate-and-fire” neurons also feature damped or sustained subthreshold oscillation [22-25] of membrane potential and therefore show sensitivity towards the timing of stimulus. [26]. Artificial

"resonate-and-fire" neurons could also be useful in neural networks where computation involves synchronized oscillation of spin torque nano-oscillators (SNTOs) for pattern recognition [27].

In this section, we show the implementation of an artificial resonate-and-fire neuron by utilizing the magnetization dynamics of a fixed magnetic skyrmion in the free layer of a magnetic tunnel junction. The next subsection (6.3.1) describes device structure. This is followed by a discussion of damped skyrmion core oscillation (section 6.3.2), resonant behavior and application of the "resonate and fire" functionality for detection of phase and frequency synchronization (section 6.3.3).

6.3.1 Device Structure

Our proposed device is an MTJ structure in which the circular free layer hosts a fixed skyrmion. The anisotropy can be modulated via voltage control of magnetic anisotropy in the device shown in *Figure 6-3*

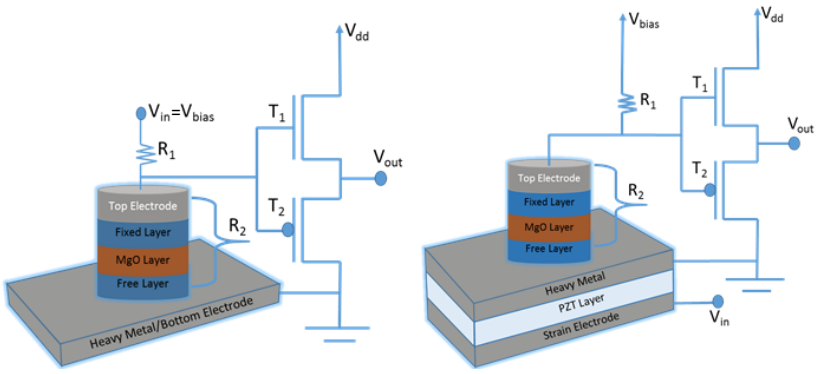

Figure 6-3 (a) Proposed device structure operated with voltage control of magnetic anisotropy (VCMA) (b) MTJ structure stacked on PZT layer for strain control of magnetic anisotropy. Reprinted with permission from [29], Copyright (2018), American Physical Society.

(a) and voltage generated strain in the device shown in *Figure 6-3* (b). Modulation of perpendicular anisotropy in the system induces breathing of skyrmions. which mimics the subthreshold damped oscillations of resonate and fire neurons. The electrical resistance of the MTJ layer (R_2) changes during this breathing. A voltage divider consisting of a fixed resistor and the voltage controlled MTJ resistance can be used to drive a CMOS buffer from OFF to ON state as shown in Fig 6.3 and generate a firing pulse if the skyrmion core size increases beyond a threshold. Throughout this section we set a threshold value of average magnetization along the z-axis $m_{z\_threshold}$=0.8, magnetization is almost antiparallel to the free layer).

For $m_{z\_free} > m_{z\_threshold}$, we consider the CMOS buffer to be in the 'ON' or "high" state and "OFF" or "low" otherwise.

6.3.2 Damped Oscillatory Behavior of Skyrmions

We simulated the magnetization dynamics in a 100 nm diameter nanodisk with thickness of 1 nm. Our geometry was discretized into 1× 1× 1 nm^3 cells. The parameter values used were: Saturation Magnetization (M_{sat})=1× 10^6 A/m, Exchange Constant (A_{ex})=2× 10^{-11} J/m, Perpendicular Anisotropy Constant (K_{u1}) = 6×10^5 J/m^3, Gilbert Damping (α)= 0.03. The ground magnetization state was found to be a skyrmion. A triangular input spike of ΔPMA=1×10^5 J/m^3 was applied with 50 ps rise and 50 ps fall time. The momentary change in anisotropy causes the core of the skyrmions to expand and oscillate about the equilibrium state. The oscillatory behavior can be seen from the net magnetization curve in *Figure 6-4* (a). This imitates the subthreshold neuron oscillation of a resonant neuron. The breathing frequency was found to be a strong function of interfacial parameters PMA and DMI as shown in *Figure 6-4* (b)).

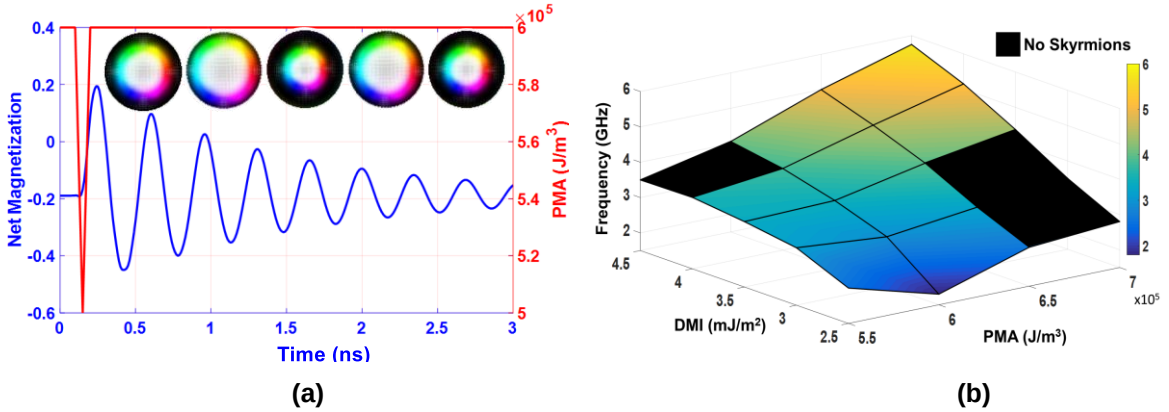

Figure 6-4 (a) Damped oscillation of a fixed skyrmion's core due to stimulation with a single pulse [Red color line: Input spike, Blue color line: Output average magnetization along the perpendicular direction (z-axis) (b) Modulation of breathing frequency by varying the interfacial parameters. Reprinted with permission from [29], Copyright (2018), American Physical Society.

6.3.3 Resonant behavior of Skyrmions

Appropriate frequency triangular/sinusoidal inputs can result in firing due to resonance. Sinusoids of different frequencies with peak to peak ΔPMA=0.96×10^5 J/m^3 were used as inputs in *Figure 6-5*. Strongest firing (4 spikes over 6 ns) was found around 2.86 GHz (time period of 0.35 ns) input frequency. Higher frequency (3 GHz or time period of 0.33 ns) and lower frequency (2.5 GHz or time period of 0.4 ns) resulted

in weaker spiking behavior (less than 4 spikes over the same 6 ns). Further deviation in frequency from resonance: 3.3 GHz (time period of 0.3 ns) and 2.38 GHz (time period of 0.42 ns) resulted in no spiking behavior at all.

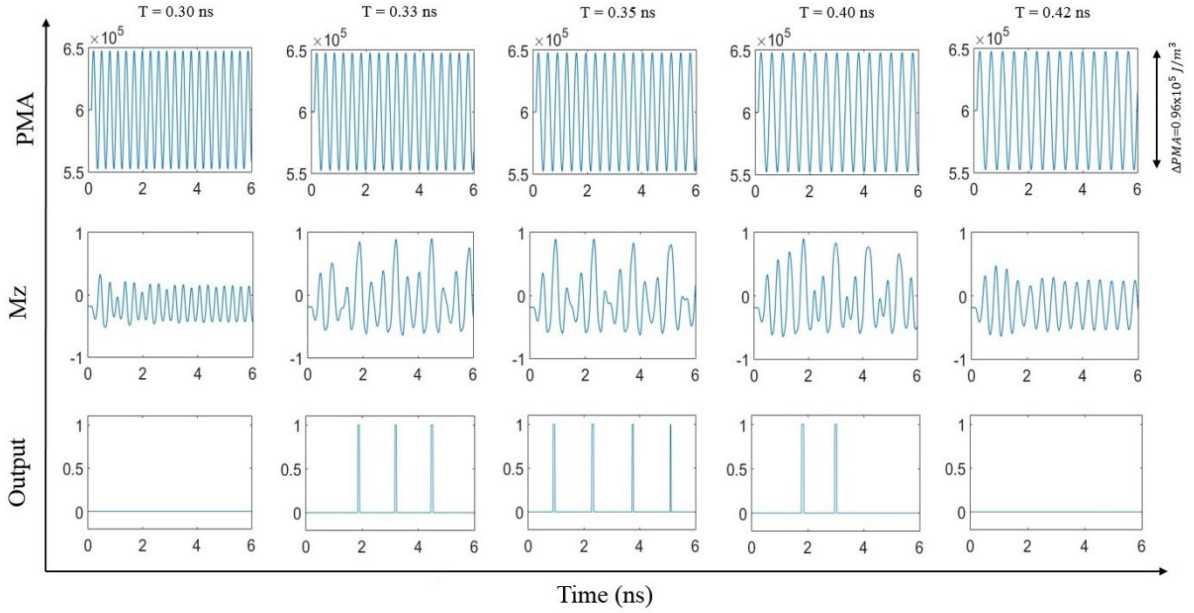

Figure 6-5 Resonant behavior with sinusoidal input. Reprinted with permission from [29], Copyright (2018), American Physical Society

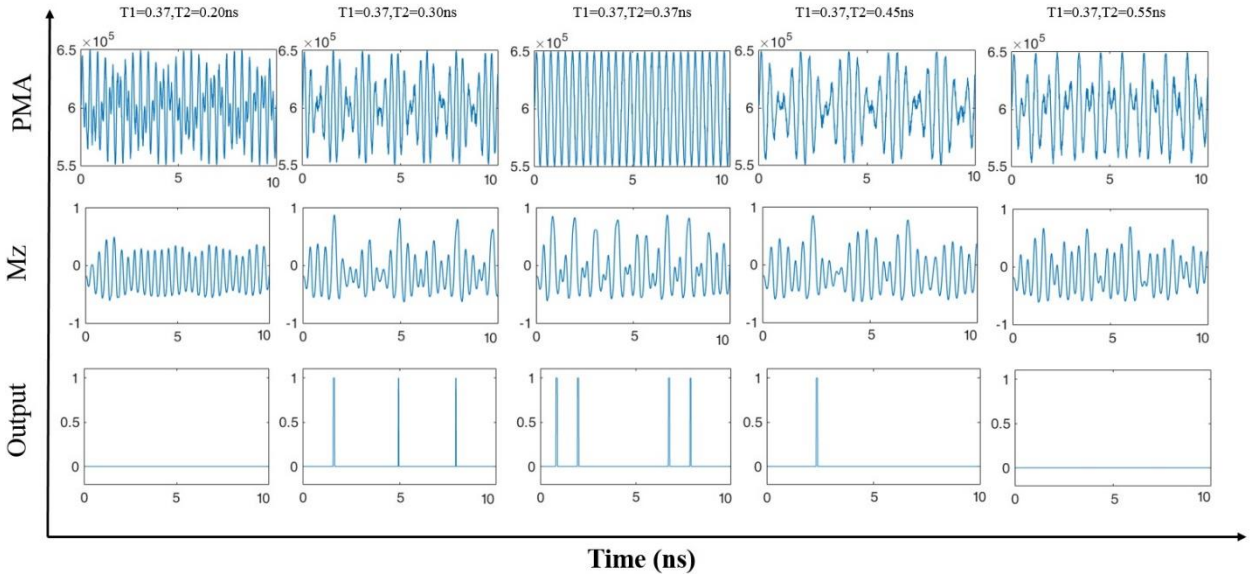

Figure 6-6 Frequency synchronization detection. Reprinted with permission from [29], Copyright (2018), American Physical Society.

Our proposed device (single voltage-controlled oscillator) can be used to detect the relative degree of phase and frequency synchronization of the outputs of two coupled STNOs (and, in general, any coupled oscillators). In *Figure 6-6*, we show frequency synchronization detection between two signals have different frequency but have no phase difference at t=0. When both frequencies are equal (2.7 GHz) 4 spikes are produced in 10 ns; when mismatched by ~20% (e.g. the 3.33 GHz and 2.22 GHz cases), less than 4 spikes are produced in 10 ns and finally with significant deviation (e.g. 5 GHz and 1.82 GHz) no output spike is produced. The number of output spikes over a given time window can provide an estimate of the degree of synchronization.

In conclusion, we studied novel nonlinear resonant dynamics of the core of a fixed skyrmion. The total energy requirement will be ~ 1 femto-Joule/spiking event. CMOS implementation of a resonate-and-fire neuron leads to an energy consumption per firing event in the range of pico-Joules, an area of many micrometer square and resonant frequency of a few 10s of Hz [28]. In fact, the proposed hybrid skyrmion-MTJ and CMOS buffer implementation of the resonate and fire neuron, is capable of resonant frequencies ~few GHz and is potentially 3 orders of magnitude more energy efficient/spiking event and potentially has 2 orders of magnitude higher density than that the all CMOS implementation [28].

6.4 Concluding Remarks:

In conclusion, we theoretically demonstrated skyrmion creation, annihilation and reversal using voltage control of magnetic anisotropy. We also experimentally demonstrated skyrmion creation and annihilation experimentally. These could result in energy efficient fixed skyrmion based memory devices. To accomplish this, experiments with skyrmions in confined geometry are required. Initial study also shows that, scaling of the proposed memory device will need further material optimization. These could be performed in future to establish voltage controlled fixed skyrmion based memory devices. Furthermore, voltage control of skyrmions has potential to be implemented in neuromorphic devices and nanomagnetic oscillators.

Therefore, this dissertation provides the foundation to implement voltage controlled-nanomagnetic memory and neuromorphic devices based on fixed magnetic skyrmions that are potentially very energy efficient, dense and fast.

REFERENCES

[1]. M. M. Rajib, W. A. Misba, D. Bhattacharya, F. Garcia-Sanchez and J. Atulasimha, "Dynamic Skyrmion-Mediated Switching of Perpendicular MTJs: Feasibility analysis of Scaling to 20 nm with Thermal Noise" arXiv:2003.12904, IEEE Trans. Of Elec. Devices (2020).

[2] A. Kozio-Rachwa, T. Nozaki, K. Freindl, J. Korecki, S. Yuasa and Y. Suzuki, "Enhancement of perpendicular magnetic anisotropy and its electric field-induced change through interface engineering in Cr/Fe/MgO," Sci. Re., Vol. 7(1), 5993(2017).

[3] T. Nozaki, A. Kozio-Rachwa, M. Tsujikawa, Y. Shiota, X. Xu, T. Ohkubo, T. Tsukahara, S. Miwa et al., "Highly efficient voltage control of spin and enhanced interfacial perpendicular magnetic anisotropy in iridium-doped Fe/MgO magnetic tunnel junctions," NPG Asia Materials 9(12), e451(2017).

[4] A. Samardak, A. Kolesnikov, M. Stebliy, L. Chebotkevich, A. Sadonikov, S. Nikitov, A. Talapatra, J. Mohanty, A. Ognev, "Enhanced interfacial Dzyaloshinskii-Moriya interaction and isolated skyrmions in the inversion-symmetry-broken Ru/Co/W/Ru films," Appl. Phys. Lett. 112(19), 192406(2018).

[5] A. Cao, X. Zhang, B. Koopmans, S. Peng, Y. Zhang, Z. Wang, S. Yan, H. Yang and W. Zhao, "Tuning the Dzyaloshinskii-Moriya interaction in Pt/Co/MgO heterostructures through the MgO thickness," Nanoscale, 10, 12062(2018).

[6] A. Cao, R. Chen, X. Wang, X. Zhang, S. Lu, S. Yan, B. Koopmans and W. Zhao, "Enhanced interfacial Dzyaloshinskii-Moriya interactions in annealed Pt/Co/MgO structures," Nanotechnology 31, 155705(2020).

[7] Sohee Kwon, Q. Sun, F. Mahfouzi, Kang L. Wang, P. K. Amiri and N. Kioussis, “Voltage-controlled magnetic anisotropy in heterostructures with atomically thin heavy metals,” Physical Review Applied 12(4), 044075(2019).

[8] H. Yang, A. Thiaville, S. Rohart, A. Fert and M. Chshiev, “Anatomy of Dzyaloshinskii-Moriya Interaction at Co/Pt interfaces,” Physical review letters 115(26), 267210(2015).

[9] H. Yang, O. Boulle, V. Cros, A. Fert and M. Chshiev, “Controlling Dzyaloshinskii-Moriya interaction via chirality dependent atomic-layer stacking, insulator capping and electric field,” Scientific Reports, Vol. 8(1), 1-7(2018).

[10] K. Tanaka, S. Miwa, Y. Shiota, N. Mizuochi, T. Shinjo, Y. Suzuki, “Large voltage-induced magnetic anisotropy field change in ferrimagnetic FeGd,” Applied Physics Express 8(7), 073007, (2015).

[11] L. Caretta, M. Mann, F. Buttner, K. Ueda, B. Pfau et. al., “Fast current-driven domain walls and small skyrmions in a compensated ferrimagnet,” Nature Nanotech 13(12), 1154–1160(2018).

[12] J. Grollier, D. Querlioz and M. D. Stiles, “Spintronic Nanodevices for Bioinspired Computing,” Proc. IEEE 104, 2024–39(2016).

[13] M. A. Azam, D. Bhattacharya, D. Querlioz, C. A. Ross, J. Atulasimha, “Voltage control of domain walls in magnetic nanowires for energy-efficient neuromorphic devices,” Nanotechnology 31 (14), 145201 (2020).

[14] A. Sengupta and K. Roy, “Encoding neural and synaptic functionalities in electron spin: A pathway to efficient neuromorphic computing,” Appl. Phys. Rev. 4(2017).

[15] A. K. Biswas, J. Atulasimha and S. Bandyopadhyay, “Straintronic spin-neuron,” Nanotechnology 26(28), 285201(2015).

[16] K. Y. Camsari, S. Salahuddin and S. Datta, “Implementing p-bits with Embedded MTJ,” IEEE Electron Device Lett. 38, 1767–70(2017).

[17] M. R. Pufall, W. H. Rippard, G. Csaba, D. E. Nikonov, G. I. Bourianoff and W. Porod, “Physical Implementation of Coherently Coupled Oscillator Networks,” IEEE J. Explor. Solid-State Comput. Devices Circuits 1, 76–84(2015).

[18] S. Fukami, W. A. Borders, A. Kurenkov, C. Zhang, S. DuttaGupta S and H. Ohno, “Use of analog spintronics device in performing neuro-morphic computing functions,” Fifth Berkeley Symposium on Energy Efficient Electronic Systems & Steep Transistors Workshop (E3S) (IEEE) pp 1–3(2017).

[19] R. Khymyn, I. Lisenkov, J. Voorheis, O. Sulymenko, O. Prokopenko, V. Tiberkevich, J. Akerman and A. Slavin, “Ultra-fast artificial neuron: generation of picosecond-duration spikes in a current-driven antiferromagnetic auto-oscillator,” Scientific Reports 8, 15727 (2018).

[20] D. Vodenicarevic, N. Locatelli, F. Abreu Araujo, J. Grollier and D. Querlioz, “A Nanotechnology-Ready Computing Scheme based on a Weakly Coupled Oscillator Network,” Sci. Rep. 7(2017).

[21] L. F. Abbott, “Lapicque’s introduction of the integrate-and-fire model neuron (1907),” Brain Res. Bull. 50 303–4(1999).

[22] B. Hutcheon, R. M. Miura and E. Puil, “Subthreshold membrane resonance in neocortical neurons,” J. Neurophysiol. 76 683–97(1996).

[23] R. R. Llinas, A. A. Grace and Y. Yarom 1991, “In vitro neurons in mammalian cortical layer 4 exhibit intrinsic oscillatory activity in the 10- to 50-Hz frequency range,” Proc. Natl. Acad. Sci. 88 897–901(1991).

[24] C. Pedroarena and R. Llinás, “Dendritic calcium conductances generate high-frequency oscillation in thalamocortical neurons,” Proc. Natl. Acad. Sci. U. S. A. 94 724–8(1997).

[25] R. R. Llinás, “The intrinsic electrophysiological properties of mammalian neurons: insights into central nervous system function,” Science 242, 1654–64(1988).

[26] E. M. Izhikevich, “Resonate-and-fire neurons,” Neural Networks 14, 883–94(2001).

[27] D. E. Nikonov, G. Csaba, W. Porod, T. Shibata, D. Voils, D. Hammerstrom, I. A. Young and G. I. Bourianoff, “Coupled-Oscillator Associative Memory Array Operation for Pattern Recognition,” IEEE J. Explor. Solid-State Comput. Devices Circuits 1, 85–93(2015).

[28] J. V. Arthur and K. A. Boahen, “Silicon-neuron design: A dynamical systems approach,” IEEE Trans. Circuits Syst. I Regul. Pap. 58, 1034–43(2011).

[29] M. A. Azam, D. Bhattacharya, D. Querlioz and J. Atulasimha, “Resonate and fire neuron with fixed magnetic skyrmions”, Journal of Applied Physics 124 (15), 152122 (2018).

A1: Micromagnetic Codes

Code Used in Chapter 4:

```
//DEFINE STRUCTURE
SetMesh(50, 50, 1, 2e-09, 2e-09, 1e-09, 0, 0, 0)
SetGeom(Circle(10e-08))
//MATERIAL PARAMETERS
Aex = 2.5e-11
alpha = 0.01
Msat=1.3e6
//MEAN VALUE OF PMA AND DMI
Ku := 11e5
D:=0.0012
Temp=300 //TEMPERATURE
FixDt=2.5e-13 //FIXED TIMESTEP
//RANDOM GRAIN ORIENTATION
grainSize := 4e-9
randomSeed := 123
maxRegion := 25
ext_makegrains(grainSize, maxRegion, randomSeed)
defregion(25, circle(10e-8).inverse())
//INTERGRANULAR VARIATION OF DMI AND PMA
for i:=0; i<maxRegion; i++{
j:=randnorm()
Ku1.SetRegion(i, ku+ku*j*0.1)
Dind.SetRegion(i, D+D*j*0.1)
}
//INTERGRANULAR VARIATION OF PMA AXIS
for i:=0; i<maxRegion; i++{
```

```
anisU.Setregion(i,vector(0.03*randnorm(), 0.03*randnorm(),0.9+0.9*0.03*randnorm()))
}
//REDUCTION OF EXCHANGE INTERACTION BETWEEN GRAINS
for i:=0; i<maxRegion; i++{
for j:=i+1; j<maxRegion; j++{
ext_ScaleExchange(i, j, 0.9)
}
}
//LOOP TO CALCULATE WER FOR 0.5 ns PULSE
for l:=1; l<=100; l++{
ThermSeed(l)
m=uniform(0.01,0.01,0.99) //INITIAL ORIENTATION
steps(4000)
//0.1ns ramp
for k:=1; k<=400; k++ {
for i:=0; i<maxRegion; i++{
Ku1.SetRegion(i, ku1.getregion(i)-400) //corresponds to PMA reduction of 1.6e5 J/m3
}
S-6
steps(1)}
//0.3ns dwell
steps(1200)
//0.1ns ramp
for k:=1; k<=400; k++ {
for i:=0; i<maxRegion; i++{
Ku1.SetRegion(i, ku1.getregion(i)+400) //restoration of PMA
}
steps(1)}
steps(8000)
```

```
}
//STT PARAMETERS
fixedlayer=vector (0, 0, 1)
pol = 0.4
Lambda=1.000
EpsilonPrime=0.0002
```

Code Used in Chapter 5:

```
//Geometry
SetMesh(1000, 1000, 1, 3.8e-09, 3.8e-09, 1.1e-09, 0, 0, 0)
SetGeom(rect(3800e-9,3800e-9))
//Material Parameters
Aex = 8e-12
alpha = 0.01
anisU = vector(0, 0, 1)
Msat=9.3e5
Dind=0.000135
//Exchange Bias
B_ext=vector(0,0,0.0015)
//ThermalNoise
Temp=300
fixdt=8e-13
ThermSeed(125)
//Inhomogeneity
grainSize := 100e-9
randomSeed := 123
maxRegion := 255
ext_makegrains(grainSize, maxRegion, randomSeed)
ku:=5.8e5
```

```
for i:=0; i<maxRegion; i++{
j:=randnorm()
Ku1.SetRegion(i, ku+j*0.01*Ku)
}
//Initialization
m=randommag()
run (200e-9)
//Annihilate
for i:=0; i<maxRegion; i++{
Ku1.SetRegion(i, Ku1.getregion(i)+7e3)
}
run (200e-9)
for i:=0; i<maxRegion; i++{
Ku1.SetRegion(i, Ku1.getregion(i)-7e3)
}
run (100e-9)
//Create
for i:=0; i<maxRegion; i++{
Ku1.SetRegion(i, Ku1.getregion(i)-7e3)
}
run (200e-9)
for i:=0; i<maxRegion; i++{
Ku1.SetRegion(i, Ku1.getregion(i)+7e3)
}
run (200e-9)
```

A2: List of Journals

1. Voltage controlled core reversal of fixed magnetic skyrmions without a magnetic field, **D. Bhattacharya**, M. Al-Rashid, and J. Atulasimha, *Sci. Rep.*, vol. 6, p. 31272 (2016).

2. Energy efficient and fast reversal of a fixed skyrmion two-terminal memory with spin current assisted by voltage controlled magnetic anisotropy, **D. Bhattacharya**, M. Al-Rashid, and J. Atulasimha, *Nanotechnology*, 28, 425201 (2017).

3. Skyrmion mediated voltage controlled switching of ferromagnets for reliable and energy efficient 2-terminal memory, **D Bhattacharya**, J Atulasimha, *ACS Applied Materials and Interfaces, 10 (20), 17455–17462 (2018).*

4. Creation and annihilation of nonvolatile magnetic skyrmions using voltage control of magnetic anisotropy, **D. Bhattacharya**, S. Razavi, H. Wu, B. Dai K.L. Wang, J. Atulasimha, *Nature Electronics 2020.*

5. Voltage Induced Strain Control of Magnetization: Computing and Other Applications, **D. Bhattacharya**, J. Atulasimha and S. Bandyopadhyay, *Multifunctional Materials, 10.1088 (2019*).

6. Incoherent magnetization dynamics in strain mediated switching of magnetostrictive nanomagnets, **D. Bhattacharya**, M. Al-Rashid, N. D'Souza, S. Bandyopadhyay, and J. Atulasimha, *Nanotechnology*, 28(1), 015202 (2016).

7. Dynamic Skyrmion-Mediated Switching of Perpendicular MTJs: Feasibility of Scaling to 20 nm with Thermal Noise, MM Rajib, WA Misba, **D. Bhattacharya**, F Garcia-Sanchez, J Atulasimha, *IEEE Transaction of Electron Devices (2020).*

8. Resonate and Fire Neuron with Fixed Magnetic Skyrmions, Md. Ali Azam, **D. Bhattacharya,** D. Querlioz and J. Atulasimha, *Journal of Applied Physics 124, 152122 (2018).*

9. Acoustic-wave-induced magnetization switching of magnetostrictive nanomagnets from single-domain to nonvolatile vortex states, V. Sampath, N. D'Souza, **D. Bhattacharya**, G. M. Atkinson, S. Bandyopadhyay and J. Atulasimha, *Nano Letters* 16 (9), 5681-5687, (2016).

10. Effect of Nanomagnet Geometry on Reliability, Energy Dissipation, and Clock Speed in Strain-Clocked DC-NML, M. Al-Rashid, **D. Bhattacharya**, S. Bandyopadhyay, and J. Atulasimha, *IEEE Trans. of Electron Devices, vol. 62, no. 9, pp. 2978– 2986 (2015).*

11. Resonant Acoustic Wave Assisted Spin-Transfer-Torque Switching of Nanomagnets, A. Roe, **D Bhattacharya**, J Atulasimha, *Applied Physics Letters 115, 112405 (2019).*

12. Polarized Neutron Reflectometry Study of Depth Dependent Magnetization Variation in Co Thin Film on a PMN-PT Substrate, M. Al-Rashid, **D. Bhattacharya**, A. Grutter, B Kirby and J. Atulasimha *Journal of Applied Physics 124, 113903 (2018)*.

13. Acoustic Wave Induced FMR Assisted Spin-Torque Switching of Perpendicular MTJs with Anisotropy Variation, WA Misba, M Rajib, **D. Bhattacharya**, J Atulasimha, *Physical Review Applied 14, 014088 (2020).*

14. Energy-efficient switching of nanomagnets for computing: Straintronics and other methodologies, N. D'Souza, A. Biswas, H. Ahmad, M. Fashami, M. Al-Rashid, V. Sampath, **D. Bhattacharya**, A Abeed, J. Atulasimha and S. Bandyopadhyay, *Nanotechnology 29, 44 (2018)*.

15. Voltage control of domain walls in magnetic nanowires for energy efficient neuromorphic devices, Md. Ali Azam, **D. Bhattacharya,** D. Querlioz, C. A. Ross and J. Atulasimha, *Nanotechnology 31, 145201 (2020).*

A3: List of Conference proceedings (Selected)

1. **Invited Talk:** Energy efficient switching of fixed magnetic skyrmions with an electric field for nanomagnetic computing devices, **D. Bhattacharya**, MM Al-Rashid, J Atulasimha, *SPIE Optics+Photonics, San Diego, CA, 2017.*

2. An energy efficient memory device based on fixed magnetic skyrmions switched with an electric field, **D. Bhattacharya**, MM Al-Rashid, J Atulasimha, *Device Research Conference (DRC), 74th Annual, 1-2, Newark, DE, 2016.*

3. Voltage controlled reversal of fixed magnetic skyrmions, **D. Bhattacharya**, MM Al-Rashid, J Atulasimha, *61st Annual Conference on Magnetism and Magnetic Materials, New Orleans, LA, 2016*.

4. Switching fixed skyrmions with electrical field in the presence of thermal noise, **D. Bhattacharya**, MM Al-Rashid, J Atulasimha, *APS March Meeting, New Orleans, LA 2017.*

5. Robust Pathway for Voltage Controlled Switching of Ferromagnets Via an Intermediate Skyrmion State, **D. Bhattacharya**, J Atulasimha, *APS March Meeting, Los Angeles, CA, 2018.*

6. Fixed Magnetic Skyrmion Based Resonate and Fire Neurons, MA Azam, **D. Bhattacharya**, D Querlioz, J Atulasimha, *APS March Meeting, Los Angeles, CA, 2018.*